From the Department of Neuroscience
Karolinska Institutet, Stockholm, Sweden

BACTERIAL SENSORS AND CONTROLLERS BASED ON ORGANIC BIOELECTRONICS

Karen Butina

Karolinska Institutet

Stockholm 2021

Published by Karolinska Institutet.
Printed by Universitetsservice US-AB, 2021

ISBN **978-91-8016-049-0**
Cover illustration: Delvin Flisek

Bacterial sensors and controllers based on organic bioelectronics

THESIS FOR DOCTORAL DEGREE (Ph.D.)

By

Karen Butina

The thesis will be defended in public at Karolinska Institutet, Stockholm, 5th of February 2021 at 9:00 am.

Principal Supervisor:
Prof. Agneta Richter-Dahlfors
Karolinska Institutet
AIMES
Department of Neuroscience

Co-supervisors:
Prof. K. Peter R. Nilsson
Linköping University
Department of Physics,
Chemistry and Biology

Susanne Löffler, PhD
Karolinska Institutet
AIMES
Department of Neuroscience

Opponent:
Tatsuro Goda, PhD
Toyo University
Department of Biomedical Engineering

Examination Board:
Prof. Staffan Svärd
Uppsala University
Department of Cell and Molecular Biology

Madeleine Ramstedt, PhD
Umeå University
Department of Chemistry

Prof. Fredrik Almqvist
Umeå University
Department of Chemistry

To Johan and Johan.

Your friendship made it worthwhile.

POPULAR SCIENCE SUMMARY OF THE THESIS

Bacteria are forming a big part of our body and are necessary for our well-being since they help us digest certain foods and keep our skin healthy. However, they can also be very harmful and make us sick. This can happen if we get some "bad" bacteria, but also if the good ones enter places they should not – for example our bloodstream. If we get an infection, our doctor prescribes antibiotics to kill the bacteria – but they do not always work. This is because we use antibiotics too much and some bacteria are finding ways to defy their attack, i.e., they are becoming resistant. To slow down this process we need to use less antibiotics. The best way to achieve this would be to prevent an infection in the first place – this would alleviate the need for antibiotic consumption. If an infection occurs nonetheless, it is important to quickly become aware of it and identify the culprit. This knowledge is crucial for doctors, so they know which antibiotic to use, instead of using many of them and hoping one will work. In this thesis, we aimed to find new ways for detection as well as identification of bacteria and studied the working mechanism of one of the oldest antimicrobial agents: copper.

In Paper I, we developed a sensor for electrochemical detection of bacteria in liquid samples. The sensor is made of a conducting polymer, a type of material that looks like plastic but can transport electrons, similar to what metals can do. As bacteria grow, they can donate electrons to this polymer, which can easily be measured. Different species of bacteria could be detected on the sensor and we have shown that we can use this technology to determine if bacteria are present in urine samples.

In Paper II, we used a more colourful approach to spot the presence of bacteria: fluorescence. Together with our collaborators, we developed a class of molecules that we call optotracers. We found that an optotracer named HS-167 could be used to detect *Staphylococcus aureus*, a pathogenic bacterium. HS-167 bound to the cell envelope, the outermost layer of *Staphylococcus aureus*. A very useful characteristic of this optotracer is that it switches on the fluorescence when it binds to the bacterium, while it does not fluoresce when unbound. This makes it easy for us to see if *Staphylococcus aureus* is in a sample and we envision for optotracers to be developed for use in diagnostics. To do this, we need to first get a good understanding of how they work. In Paper III we tested many different optotracers to find out which are most suitable for detection of *Staphylococcus aureus* and why. This knowledge will aid us in design of new optotracers for the future.

In Paper IV, we turn our attention to copper, a metal whose antimicrobial effects have been known for millennia. The aim of our study was to understand how are the antimicrobial properties of copper influenced by human skin contact. To simulate touch, we applied artificial sweat, that is very similar to regular human sweat. Artificial sweat deposition led to enhanced corrosion, which was reflected in altered colour of copper surfaces. We found that corrosion does not impair the antimicrobial properties of copper, since all bacteria died in contact with corroded and non-corroded copper surfaces within 10 – 15 minutes. This is important for the applicability of copper as an antimicrobial surface, since it means that even if it is visually altered, it is still effective.

ABSTRACT

Bacterial infections and contaminations are worldwide problems, leading to morbidity and mortality, food waste and economic losses in a variety of industries. The situation is aggravated by the increased occurrence of antibiotic-resistant strains, identified by the WHO as one of the biggest threats to development, food security and public health today. The solution to this problem is complex and requires efforts from several different layers of the society, and different disciplines. The knowledge about microbiology has greatly advanced in the last decades and several powerful methods were introduced. However, in most clinical microbiology laboratories, culture-based techniques are still standard practice, representing a bottleneck in the diagnostic workflow. In this thesis, we prototype novel methods to detect and identify bacteria, aiming to reduce the time and workload for future microbiology research and diagnostics. Furthermore, a new methodology is devised to evaluate antimicrobial surface properties for relevant high-touch surfaces.

In Paper I, we investigated whether conducting polymers can be applied for label-free electrochemical detection of bacteria. Employing a poly(3,4-ethylenedioxythiophene): polystyrenesulfonate (PEDOT:PSS)-based two-electrode sensor we demonstrated that potentiometric detection and quantification of *Salmonella* Enteritidis is possible within 15 min, without any sample pre-treatment. We show that the reduction of PEDOT:PSS electrode occurs by low molecular weight species secreted by *Salmonella* Enteritidis. To evaluate the genericity of the sensor, several uropathogenic strains were tested and we found that they could all be detected using the sensor. In its current form, the sensor is a prototype, and we aim to improve its sensitivity and introduce specificity. Electroactivity was shown to be a rather common characteristic of bacteria and consequentially, electrochemical methods for detection and characterization of microbes are gaining momentum. We envision that this field will provide novel diagnostic devices but also contribute to discoveries in basic science.

Luminescent conjugated oligothiophenes, called optotracers, have previously been applied in microbiology to visualize extracellular matrix components in biofilms of *Salmonella* and *Escherichia coli*. In Paper II, we investigated the use of optotracers for detection and visualization of *Staphylococcus aureus (S. aureus)*. We show that the optotracer HS-167 selectively binds to *Staphylococci* and can be used for fluorometric detection and quantification of *S. aureus*, as well as for staining and visualization using confocal microscopy. HS-167 displays an on-switch of fluorescence upon binding and it does not affect bacterial growth, which enabled us to develop a high-throughput assay where the fluorescence was plotted against bacterial density, measured as an increase in turbidity. The resulting slope was a quantifiable variable that we employed to compare binding of HS-167 to different species and strains. Diverse approaches collectively pointed to the cell envelope as the target for HS-167 binding. Finally, we showed that binding is highly dependent on the environmental conditions and those can be adjusted to tune the selectivity of HS-167.

To improve optotracer design for detection of *S. aureus*, a better insight into the structure-function relationship is needed. In Paper III, we set out to establish a structured approach to optotracer screening that would enable us to compare optotracer performance. As we compared a library of ten different optotracers, we identified the length to be positively

correlated and the total negative charge to be negatively correlated with the ability to detect *S. aureus*. A balance between the two was necessary to achieve the highest signal while maintaining selectivity. Selected optotracers were added to *S. aureus* and visualized under the confocal microscope. All localized in the cell envelope of the bacterium, as was previously observed for HS-167 (Paper II). We foresee that further insight into the binding mechanism will enable targeted optotracer design, and together with optimized assay conditions, specific detection of different bacterial species.

Copper is known to possess antimicrobial properties, yet studies have reported discrepant results on its efficacy, especially in the clinical settings. Disagreeing results were ascribed to the lack of a standardized approach to evaluate the antimicrobial properties of copper surfaces. In Paper IV, we establish a multifaceted approach to address the effect of human touch, which we simulate by applying artificial sweat, on surface corrosion and antimicrobial properties of copper. We found that artificial sweat accelerates corrosion, leading to changes in surface appearance and wettability. Corrosion did not negatively affect the antimicrobial properties of copper as these surfaces killed bacteria within minutes, regardless of ageing or corrosion product formation. The antimicrobial effect is ascribed in part to copper ions released from the surface and in part to direct surface contact. To further validate the results of this study, other bacterial species need to be tested. Since high touch surfaces are likely to collect a lot of microbes over time, it would be of interest to determine how the bacterial load affects the antimicrobial properties.

LIST OF SCIENTIFIC PAPERS

I. **Butina, K**., Löffler, S., Rhen, M., & Richter-Dahlfors, A. (2019). Electrochemical sensing of bacteria via secreted redox active compounds using conducting polymers. *Sensors and Actuators B: Chemical*, *297*, 1-8.

II. **Butina, K**., Tomac, A., Choong, F. X., Shirani, H., Nilsson, K. P. R., Löffler, S., & Richter-Dahlfors, A. (2020). Optotracing for selective fluorescence-based detection, visualization and quantification of live *S. aureus* in real-time. *NPJ biofilms and microbiomes*, *6*(1), 1-12.

III. **Butina, K**., Lantz, L., Choong, F. X., Tomac, A., Shirani, H., Löffler, S., Nilsson, K. P. R., Richter-Dahlfors A. Structural properties dictating selective optotracer binding to *S. aureus. Manuscript*.

IV. Chang, T., Sepati, M., Herting, G., Leygraf, C., Kuttuva Rajarao, G., **Butina, K**., Richter-Dahlfors, A., Blomberg, E., Odnevall Wallinder, I. A novel methodology to study antimicrobial properties of high-touch surfaces used for indoor hygiene applications - a study on Cu metal. *Manuscript submitted for publication.*

CONTENTS

LIST OF ABBREVIATIONS

A	Absorbance
AMP	Antimicrobial peptide
AST	Antibiotic susceptibility testing
ASW	Artificial sweat
ATP	Adenosine triphosphate
BATH	Bacterial adhesion to hydrocarbons
B. subtilis	*Bacillus subtilis*
CE	Counter electrode
CFU	Colony forming units
CP	Conducting polymer
D-A-D	Donor-acceptor-donor
DNA	Deoxyribonucleic acid
EET	Extracellular electron transfer
E. coli	*Escherichia coli*
E. faecalis	*Enterococcus faecalis*
FAD	Flavin adenine dinucleotide
GC	Glassy carbon
GFP	Green fluorescent protein
HOMO	Highest occupied molecular orbital
LCO, LCP	Luminescent conjugated oligo-, polythiophenes
LMW	Low molecular weight
LOD	Limit of detection
LPS	Lipopolysaccharide
LTA	Lipoteichoic acid
LUMO	Lowest unoccupied molecular orbital
MALDI-TOF	Matrix-assisted laser desorption ionization time of flight
MRSA	Methicillin resistant *Staphylococcus aureus*
MS	Mass Spectrometry
NAD	Nicotinamide adenine dinucleotide
NGS	Next-generation sequencing
OD	Optical density
PBS	Phosphate buffered saline

PCR	Polymerase chain reaction
P(EDOT)	Poly(3,4-ethylenedioxythiophene)
PGN	Peptidoglycan
PI	Propidium iodide
PPy	Polypyrrole
P. aeruginosa	*Pseudomonas aeruginosa*
PSS	Polystyrene sulfonate
QCM	Quartz crystal microbalance
RE	Reference electrode
RFU	Relative fluorescence units
RNA	Ribonucleic acid
S. aureus	*Staphylococcus aureus*
S. epidermidis	*Staphylococcus epidermidis*
SEM	Scanning electron microscopy
S. Enteritidis	*Salmonella* Enteritidis
SWV	Square wave voltammetry
TSB	Tryptic soy broth
WE	Working electrode
WT	Wild type
WTA	Wall teichoic acid

1 INTRODUCTION

Bacterial pathogens have evolved with humans from our very beginnings and are ever since causing disease and death. *Helicobacter pylori*, which infects human stomachs, has been around for approximately 100000 years, similar to anatomically modern humans. *Mycobacterium tuberculosis* has been found on skeletons from 6000 years ago and *Yersinia pestis* has spread globally on several occasions within the last 5000 years, leading to plague pandemics[1]. The existence of microorganisms was postulated already in the 6th century BC by Jainism and the causality between ”yet unseen organisms” and disease was suggested by a Roman scholar in the 1st century AD[2]. In 1546, Girolamo Fracastoro, an Italian physician, poet and scholar, made the correct assumption that diseases were caused by seed-like entities that can be transmitted[2]. Bacteria were observed for the first time by Antoni van Leeuwenhoek in the late 17th century, but it took another 200 years before Louis Pasteur proved the germ theory[3]. Even before Pasteur, a Hungarian physician Ignaz Semmelweiss understood that childbed fever was introduced from the physician (often coming from the morgue!) handling the mother. He urged his colleagues to wash hands with a chlorine solution to reduce the incidence of infection[4]. The causal relationship between bacteria and human disease was established by Robert Koch in the late 19th century[3]. In 1929, Alexander Fleming discovered penicillin and, ten years later, Howard Florey and colleagues developed a process for large scale production of penicillin, which became available to the general public after the end of WWII[3]. This prompted the pharmaceutical companies to search for and develop more antibiotics, revolutionizing the treatment of infectious disease[3]. Today, treating infections is becoming increasingly challenging due to the continuous emergence of antibiotic-resistant strains of bacteria[5]. The development of novel antibacterial compounds is challenging, especially for gram-negative bacteria[6]. The burden of infectious disease is highest in low and middle-income countries[7] and is associated with poverty and poor infrastructure[8]. In European countries, healthcare-associated infections lead to significant morbidity and mortality and represent a high burden for healthcare systems[9]. As nosocomial infections are often caused by bacterial colonization of surfaces, great efforts are invested in the development of anti-bacterial surfaces that could be used both outside (near-patient surfaces) and inside the patient (implant coatings) to prevent surface colonization and subsequent infection[10]. To make the antibiotics that we have last, it is of ultimate importance to develop and employ methods for rapid pathogen identification enabling targeted antibiotic prescription[11]. Moreover, rapid detection of bacterial contaminations would contribute to lowering the risk for infection and therefore limit the overuse of antibiotics[12].

To address the challenges stated above, academic research is of importance. In this thesis we show how can organic bioelectronics, fluorescent tracers and copper all contribute to the common goal of gaining control over bacteria. The term *organic bioelectronics* has been introduced by Richter-Dahlfors and Berggren in their seminal review[13] in 2007 and since then, the field has greatly expanded. Prof. Richter-Dahlfors´group has focused heavily on the implementation of organic bioelectronics in microbiology and infection research[14–17] and within the scope of this thesis we have contributed to further development of this field by employing conjugated polymers to electrochemically detect and quantify bacteria in solution[18]. Next to their electrochemical properties, conjugated oligo- and polythiophenes are widely used due to their favourable optical properties. Together with Prof. Nilsson from

Linköping University, Prof. Richter-Dahlfors´ group has developed optotracers, i.e., luminescent conjugated oligothiophene based fluorescent tracer molecules, for use in microbiology. Optotracers enabled real-time biofilm monitoring in *Salmonella*[19] and were used to develop a biofilm diagnostic assay to detect extracellular matrix components of uropathogenic *Escherichia coli* (*E. coli*)[20]. In this thesis, optotracing was further developed for the detection and visualization of gram-positive bacteria, focusing on *Staphylococci*[21]. A follow-up study was performed to investigate the structural requirements of optotracers necessary for selective detection of *Staphylococcus aureus* (*S. aureus*). In the final study, we focus on infection prevention, as we establish a novel methodology for characterizing antimicrobial properties of copper.

2 LITERATURE REVIEW

2.1 A BRIEF INTRODUCTION OF BACTERIA

Bacteria and Archaea are the two phylogenetic domains of prokaryotes. All known pathogenic prokaryotes are bacteria, which is why they have been more extensively studied compared to archaea. Bacteria are further divided into several groups (i.e., phyla). The biggest phylum is *Proteobacteria*, to which some important pathogens from the *Salmonella*, *Rickettsia*, *Neisseria* and *Escherichia* genera belong. The second biggest phylum is gram-positive bacteria (see the explanation for Gram staining below), to which pathogenic *Streptococci* and *Staphylococci* belong, as well as the antibiotic-producing *Streptomyces*[3].

2.1.1 Morphology and structure

The most common shapes of bacterial cells are round (cocci), cylindrical (rods) and spiral (spirochaetes). *Staphylococci* and *Streptococci* are examples of cocci, while *Escherichia* and *Salmonella* are examples of rods[3]. The great majority of bacteria are small in size relative to eukaryotic cells, and typically have a volume of ~0.4–3 μm^3, even though examples of much larger and much smaller bacteria are known[22]. This comes with the advantage of a high surface to volume ratio, supporting nutrient exchange[3]. In contrast to eukaryotic cells, bacteria do not contain organelles and their cytoplasm is a gel-like solution containing ribosomes, granules or inclusions, proteins (e.g. enzymes) and RNA, energy-rich compounds, metabolites and various inorganic ions[3,23]. In general, a single copy of a circular chromosome is present and occasionally extrachromosomal DNA elements (plasmids), which typically provide fitness advantages, such as resistance to antibiotics[3,23]. The cytoplasmic membrane encloses the cytoplasm. It is responsible for energy generation and conservation, regulation of the flow of nutrients and metabolic products in and out of the cell, translocation of envelope macromolecules and transmembrane signalling[24]. It is composed of similar amounts of proteins and phospholipids, the former being either tightly or loosely bound to the membrane[24]. Respiratory chain dehydrogenases, cytochrome oxidases and quinones are present in the membrane[25] as well as adenosine triphosphate (ATP) synthases[26], several active and passive transporters and other proteins[24]. Outside of the cytoplasmic membrane, bacteria have a cell wall. Depending on the composition of the cell wall, bacteria are divided into two large groups: gram-positive and gram-negative (**Figure 1**). This division is based on the Gram stain, a method developed by the Danish scientist Hans Christian Gram and published in 1884[27]. Bacteria with thick cell walls retain the crystal violet dye after decolourization with ethanol and are therefore termed gram-positive bacteria. Those that have thinner cell walls, and do not retain the dye, are called gram-negative bacteria[3,27].

The outermost layer of the gram-negative bacteria is the outer membrane, that functions as a selective barrier, protecting the cell from harmful compounds in the environment[28]. It is an asymmetrical bilayer; the inner side consists of phospholipids and the outer side of lipopolysaccharides (LPS)[28]. The proteins of the outer membrane can be divided into lipoproteins (not transmembrane proteins) and β-barrel proteins (transmembrane proteins)[29]. Not much is known about the functions of the former, while the latter are mostly porins (OmpC, OmpF) and gated channels[29]. LPS are composed of three covalently linked chemical structures: lipid A, core polysaccharide and O-antigen[30]. While LPS comprise

approximately 10 – 15 % of the total molecules in the outer membrane, they are occupying 75 % of the surface area[31]. LPS molecules are negatively charged and amphiphilic, presenting a barrier to negatively charged and/or hydrophobic molecules[31]. LPS toxicity is mainly attributed to lipid A, composed of a diglucosamine backbone with ester-linked and amide-linked long-chain fatty acids[32]. The O-antigens are composed of many oligosaccharide units repeats, therefore hydrophilic, and are commonly used for serotyping due to their high variability[33]. Below the outer membrane, there is a thin layer of peptidoglycan (PGN). PGN determines the cell shape and prevents cell lysis due to turgor pressure while enabling growth by insertion of new material in the existing layer[34]. It is composed of linear glycan strands, made of alternating N-acetylglucosamine and N-acetylmuramic acid residues, cross-linked by short peptides[35,36]. In gram-negatives, the PGN layer is only a few nanometers thick and is composed of a single or a few layers of poorly ordered but mostly circumferential glycans of mean length around 20 – 40 nm that lie parallel to the cytoplasmic membrane[37,38]. The periplasm is an oxidative environment[39] between the inner (plasma) and outer membrane[29]. It is denser than the cytoplasm and used by the cell to keep potentially harmful enzymes such as RNAse and alkaline phosphatase safely separated[29]. Braun lipoprotein, numerically the most abundant protein in *E. coli*, is providing a covalent connection between the outer membrane and the PGN[40,41].

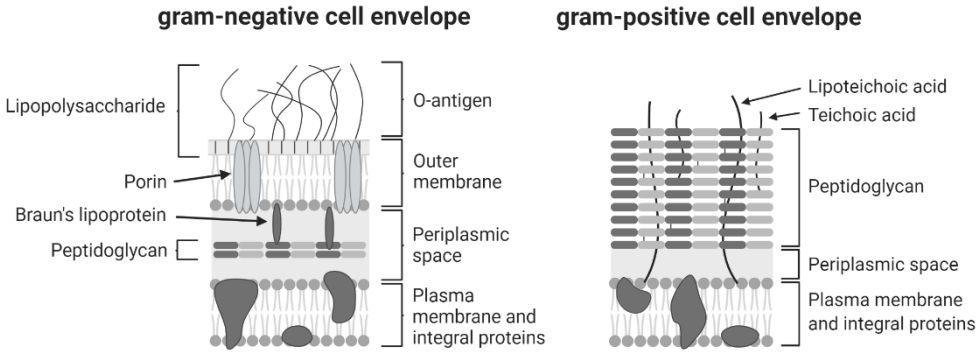

Figure 1: Schematic representation of gram-positive and gram-negative cell envelope. Adapted with permission after an image of Karen Steward, Technology Networks. Created with BioRender.com

The outermost layer of gram-positive bacteria is a cell wall composed of a thick PGN layer, including teichoic acids, surface proteins and optionally capsular polysaccharides[3]. Unmodified glycan strands of gram-positive bacteria are the same as those of gram-negative, however, modifications that arise during PGN maturation result in that the mature PGN is different[42]. The crosslinking of PGN in most gram-positive bacteria involves an interpeptide bridge, while it is direct in the case of gram-negative bacteria[36]. In *S. aureus* the intrapeptide bridge consists of 5 glycine residues[36]. The average length of glycan strands in *S. aureus* is 18 disaccharide units, while in *Bacillus subtilis (B. subtilis)* it is 50 – 250[36]. The thickness of PGN layer in both species was reported to be between 15 and 30 nm[36]. The PGN orientation was shown to be species and location dependent[43]. The outer surface of both species was composed of less dense, randomly ordered PGN, while the PGN was denser at the inner surface and circumferential for *B. subtilis*, but not for *S. aureus*[43]. Surface proteins can be roughly separated in three groups: *i)* those that bind via their N-terminal region (lipoproteins), *ii)* those that bind by charge or hydrophobic interactions and *iii)* those that anchor at their C-terminal ends through

an LPxTG motif[44]. The LPxTG proteins are anchored to the PGN via sortase[45] and their deposition on the cell wall is dynamic, linked to several cellular processes[46]. *S. aureus* can express up to 24 different LPxTG proteins, while coagulase-negative *Staphylococci* express less[47]. Teichoic acids include lipoteichoic acids (LTAs), which are anchored to the plasma membrane via a glycolipid, and wall teichoic acids (WTAs) that are covalently bound to PGN[48]. They have zwitterionic properties, as negative charges from the phosphate groups are balanced with the free amino groups, commonly contained in D-alanine residues on the repeating units[49,50]. WTAs are made of a disaccharide linkage unit and a phosphodiester-linked polyol repeat unit[49,51]. Their structures differ between species and often even between clonal groups[50]. *S. aureus* WTAs are made of repeating ribitol phosphate (Rbo-P) and/or glycerol phosphate (Gro-P) units, while *Staphylococcus epidermidis* (*S. epidermidis*) only contains Gro-P repeats[50]. It has been shown that WTAs are dispensable for the viability of *S. aureus* and *B. subtilis*[49], yet these cells display a range of defects[48]. LTAs are alditol phosphate containing polymers, linked to the cytoplasmic membrane via a lipid anchor[52] and their structures are typically less diverse than those of WTAs[50]. Five structural types of LTAs have been described[52,53], of which Type I is most common (found in *B. subtilis, S. aureus, Enterococcus faecalis (E. faecalis), Listeria mnocytogenes, Streptococcus pyogenes, Streptococcus agalacticae*)[53]. Type I LTAs consist of glycerol-phosphate (Gro-P) repeats, that are, in the case of laboratory-grown *Staphylococci,* modified with D-alanine esters and N-acetylglucosamine[53]. LTAs are generally considered indispensable, yet *S. aureus* mutants containing 87% less glycolipid, due to shorter chains, were viable but had reduced autolytic activity and were unable to form biofilms on plastic[54]. Further, a recent study showed that LTAs become dispensable in *S. aureus* lacking ClpX chaperone[55]. Some of the gram-positive bacteria have S-layers, composed of a single protein that encompasses the cell, and polysaccharide capsules[29,56]. Capsular polysaccharides are highly conserved in clinical isolates and therefore promising targets for vaccines[57], however, some of the most virulent strains of *S. aureus*, such as the MRSA strain USA300 do not have a capsule[58].

2.1.2 Metabolism

Metabolism is divided into catabolism (= energy generation) and anabolism (= energy consumption, biosynthesis). Based on their catabolism, bacteria are divided into phototrophs, chemolithotrophs and chemoorganotrophs. The central processes for energy generation are oxidation-reduction (= redox) processes. Energy is conserved by the synthesis of energy-rich compounds, the most abundant being ATP. ATP is synthesized by substrate level phosphorylation and by oxidative phosphorylation. In substrate level phosphorylation, ATP is made by using the energy released during the conversion of an organic molecule from one form to another. In oxidative phosphorylation, the electrons are removed from the substrate and passed down an electron transport chain to reach the final electron acceptor (i.e., O_2 in aerobic respiration). The energy released in the transfer process is used for proton expulsion and the generation of a proton motive force. This is in turn used to fuel ATP synthase which generates ATP. All pathogenic bacteria are chemoorganotrophs and their metabolism is typically driven by fermentation or respiration. In the presence of glucose, the initial step of fermentation and respiration is glycolysis (most commonly Embden-Meyerhoff pathway), which yields two pyruvate molecules from one glucose molecule. During this process, two net ATP molecules are produced and the electron carriers (i.e., nicotinamide adenine dinucleotide, NAD^+) are reduced. If the microorganism is incapable of respiration or there is no suitable electron

acceptor available, fermentation products are formed as a result of NADH + H^+ reoxidation. In respiration, products of glycolysis are transferred to the tricarboxylic acid cycle, where they are completely oxidized. NADH and flavin adenine dinucleotide ($FADH_2$) are oxidized as they transfer the electrons (and protons) from the tricarboxylic acid cycle intermediates to the cytoplasmic membrane, where they are passed along the electron transport chain. NADH dehydrogenase, flavoproteins, iron-sulfur proteins, cytochromes and quinones are oriented in such a way that electrons can be separated from protons. The energy generated during the electron transfer is used for proton expulsion and the generation of proton motive force which in turn fuels ATP synthesis and several other processes[3].

Over a century ago it was discovered that bacteria can transfer electrons also to external electron acceptors[59]. Similar to electron carriers that can transfer electrons between different intracellular compartments, there are also electron carriers (usually termed electron shuttles) that can transport electrons between the cell and an extracellular electron acceptor/donor[60,61]. The most studied bacteria in relation to extracellular electron transfer (EET) are dissimilatory metal-reducing bacteria. These bacteria reduce metals by using them as terminal electron acceptors and have an important influence in geochemistry[62]. Besides electron transfer using electron shuttles, dissimilatory metal-reducing bacteria perform also direct contact respiration and respiration via different extensions (i.e., nanowires)[61]. The two most studied bacteria are *Geobacter sulfurreducens* and *Shewanella oneidensis*. *Geobacter* employs nanowires composed of polymerized cytochrome OmcS[63], while the predominant mode in *Shewanella* is electron shuttling[64]. Moreover, the use of electron shuttles has also been indicated in *Klebsiella pneumoniae*[65], *Lactococcus lactis*[66], *Sphingomonas xenophaga*[67], *Bacillus megaterium*[68] *and E. faecalis*[69,70]. Recently, *Listeria monocytogenes* was shown to perform EET via soluble flavins[71]. An 8-gene locus was identified to code for an NADH dehydrogenase, that channels the electrons to a membrane-localized quinone pool, segregating aerobic respiration from EET, and a surface associated flavoprotein, the extracellular component of the EET apparatus[71]. Orthologs of the EET genes were shown to be present in hundreds of species from the Firmicutes phylum[71]. This finding has caused a great excitement in the research community as it clearly implied that EET shall not be seen as a special mechanism employed by dissimilatory metal-reducing bacteria, but rather as a general mechanism present in a plethora of microbes[72]. In line with that, it was found that hundreds of species of *Proteobacteria* and *Actinobacteria* contain phenazine biosynthetic clusters, indicating that they might have a physiological function[73]. It has been suggested that redox-active molecules could be employed under oxygen limiting conditions to aid in NAD^+ regeneration and reduce the formation of fermentation products[74,75].

2.2 MICROBIOLOGY AND MICROBIAL DIAGNOSTICS TOOLBOX

In the late 19th and early 20th century, different stains for bacteria became available, namely Gram stain, acid-fast stain and Albert stain[76] and the first strain collections of pathogens were made[1]. This was also the time when the enrichment culture technique was established to isolate different types of microorganisms depending on their metabolism[3]. Over time, these approaches were complemented by selective growth media and serological tests, as well as species-specific biochemical tests[77]. In the 1980s and 1990s, DNA amplification-based molecular diagnostics became widely used in research and clinical microbiology laboratories[76].

Today, clinical microbiology workflow is still heavily dependent on culture to promote growth and/or to isolate species from clinical samples. Gram stain is often initially

used to give the clinician preliminary information about the pathogens present in the specimen and to estimate the specimen quality and suitability for culture, yet discrepancies between stain and culture were shown to occur 5 % of the time[78]. For urine cultures, a dipstick analysis is usually performed as an initial step. While being able to rule out an infection, the dipstick was shown not to be reliable for confirming an infection[79]. Molecular biology techniques such as regular and quantitative PCR[80] and fluorescence in situ hybridization (FISH)[81] are commonly used in diagnostic laboratories for pathogen identification. Immunoassays enable fast confirmation of the presence of a specific pathogen and several are commercially available[82].

2.2.1 Contemporary techniques in microbiology

In recent decades microbiology has been revolutionized by the introduction of novel technologies and big-data approaches that are starting to replace the slow and laborious manual procedures[83]. Two of the most pronounced examples of such technologies are the implementation of Matrix-Assisted Laser Desorption Ionization Time of Flight Mass Spectrometry (MALDI-TOF MS) and next-generation sequencing (NGS) in microbiology and microbial diagnostics[84].

Mass spectrometry has been initially proposed for the analysis of bacteria already in the early 70s[85,86]. Since 2009, MALDI-TOF MS has been increasingly used in microbiology and diagnostics[84,87,88]. In this technique, the sample is embedded in an organic polymer matrix, which is vaporized via laser irradiation. Ionized sample molecules are accelerated through the electric field until they reach the detector. The time of flight is used to calculate ion masses, i.e., mass-to-charge ratios [m/z][89]. For analyzing microbial samples, the majority of the read-out comes from basic ribosomal proteins, which is advantageous as they are not generally influenced by the culture conditions[90]. An advantage of MALDI-TOF MS is its speed – a sample is analyzed in a few minutes. However, a pre-culturing step is necessary as $10^5 – 10^7$ bacterial cells are typically required, depending on the procedure and the chemical treatment applied[91]. A significant drawback of MALDI-TOF MS is that only pure cultures can be analyzed[90]. There is very active research on the use of MALDI-TOF for determining the antibiotic resistance profile of pathogens and but as of now, only very few methods are in clinical use[92].

Since 2001, the cost of sequencing has dropped from 5292.39 USD to 0.008 USD for one Mbp[93], mainly due to technological advancements in sequencing technology. There are several different approaches used: sequencing by ligation (SOLiD, BGISEQ), sequencing by synthesis (Illumina, Qiagen), single-molecule real-time long reads (Pacific Biosciences, Oxford Nanopore) and synthetic long reads (Illumina, 10x Genomics)[94]. NGS has become an invaluable tool in microbiology as it enables sequencing of non-culturable species in environmental samples[95] such as bacterial communities in river[96] and marine[97] environments. NGS is increasingly being used in microbial diagnostic laboratories where it is applied for 16S rRNA gene sequencing to identify pathogens, while the metagenomic approaches are applied to characterize them, e.g. determine the presence of virulence and antimicrobial resistance genes[98]. It has been suggested that the introduction of genomics in the clinical microbiology laboratory marks the beginning of a new era as whole genome sequencing might replace laborious phenotypic characterization and susceptibility testing[98]. Besides, the development of MinION (Oxford Nanopore Technologies, Oxford, UK) enabled NGS in a point-of-care device[99].

MS and NGS are extremely powerful but they require skilled personnel, equipped facilities and, often, sample pre-culturing and pre-processing. While infectious diseases are a global issue, the highest incidence and disease burden are observed in developing countries, where access to such facilities is less likely[8]. Furthermore, even in developed countries, sample transport from remote regions to centralized laboratories with adequate facilities can be problematic[84]. To this end, there has been a strong push to develop on-site sensors and sensing technologies to enable timely detection of bacteria outside of the laboratory[100].

2.2.2 Sensors for bacterial detection

An ideal (bio)sensor has been described by Ahmed *et al.*[100] to have the sensitivity of fewer than 10^3 bacteria/mL, specificity to distinguish between different serotypes, operate in physiological fluids, provide the end readout in 10 min, to be compact and portable so that it can be used as a point-of-care device, to be stable at room temperatures across the world (10 – 45 °C) for months, to require minimal sample processing and to be so easy to use that a patient can perform the test on his/her own without the need of a trained specialist.

Most of the sensors employed for detection of bacteria contain a biological component (enzyme, DNA, whole cell, etc.) that recognizes the analyte and produces a signal, a signal transducer (electrode, piezoelectric material, pH electrode, photodetector etc.), signal processing module (signal amplification, filtering, etc.) and a reader device that produces an output understandable to the user[100]. These sensors are termed biosensors[100]. Importantly, there are also non-biological recognition elements that can be employed such as cellularly or molecularly imprinted polymers, which are produced to mimic their natural counterpart[101]. These sensors are not classified as biosensors and correspond better to the definition of the chemical sensor[102].

2.2.2.1 Recognition elements

To achieve recognition of unlabeled, whole bacterial cells, several different ligands have been employed. Most common are antibodies, antimicrobial peptides (AMPs), sugars and lectins, phages or phage peptides and aptamers[103]. Antibodies exhibit high specificity towards their targets[104], however, they are expensive to produce and difficult to store, as they are sensitive to chemical, enzymatic and physical damage[105]. An alternative to antibodies that has not yet been widely explored are nanobodies, which lack the light chain and are easier to produce and purify[106]. AMPs are stable[107], but their selectivity is limited[108] and they can lead to cell lysis[109]. Lectins to bind bacterial carbohydrates or carbohydrates to bind bacterial lectins can be used in either combination and recently a lectin based surface plasmon resonance biosensor has been reported to detect *E. coli* O157:H7 in food samples[110]. The immobilization of lectins (and other proteins) on a sensor can be difficult, while carbohydrates are promising due to their chemical stability which enables straightforward manufacture[103]. Differential affinity to various mono- and disaccharides has been used for identification of different *E. coli* strains on a polypyrrole (PPy) coated gold chip using a modified surface plasmon resonance technique[111]. Further, using alpha-mannoside immobilized on a gold chip based on self-assembled monolayer chemistry, an impedimetric sensor for detection and quantification of *E. coli* ORN178 was reported[112]. Phages are stable in a wide range of environments and can be very specific, however, obtaining a correct orientation of the phage on the biosensor surface is challenging[103]. It has been indirectly shown that the orientation of phages upon adsorption can be controlled

using an electric field, as virions are in fact particles with permanent dipole[113]. Besides orientation, a limitation of phage use is also their large size and possible retention of lytic activity that can complicate the assay readout[103,114]. To address both issues, phage receptor binding proteins, phage molecules with high affinity to host cell structures, can be used instead of the whole phages[114]. Aptamers are single stranded DNA[115] or RNA[116] that originate from in vitro selection and are optimized for their affinity towards a specific target[117,118]. Aptamers are promising candidates for bacterial diagnostics[119] and have been used as recognition elements in sensors for detection of bacteria[120,121].

Molecularly and cellularly imprinted polymers are the major synthetic recognition elements used in bacterial sensing applications. They are made of a polymer matrix containing cavities corresponding to a target analyte[122]. These materials are created by using analyte molecules or cells as templates, around which the monomers are polymerized, followed by template removal[122,123]. Different organic and inorganic polymers can be employed, such as polystyrene, polyvinylpyrrolidone, PPy, 3-aminophenol and 3-aminophenylboronic acid, polydimethylsiloxane, polydopamine, polyurethane and Epon1002F[123]. The process of imprinting can occasionally damage the template (e.g. a bacterial cell) due to employment of organic solvents, extreme pH, high temperature etc.. In such cases, a surrogate template can be used instead[122]. Analyte recognition occurs through structure fitting and reversible covalent bond formation or non-covalent interactions such as coulombic and hydrophobic interactions, hydrogen bonding, metal ion coordination complex formation, π-π stacking and van der Waals forces[122]. In an innovative approach, bacteria were used as doping agents for PPy and were electrochemically polymerized on a quartz crystal microbalance (QCM) chip. Overoxidation was used to remove the template bacteria out of the polymer[124]. For detection of sulfate-reducing bacteria, a mixture of reduced graphene sheets and chitosan was electrodeposited on indium tin oxide and another layer of chitosan was deposited on top to facilitate imprinting. The binding of sulfate-reducing bacteria could be detected by measuring impedance in the presence of $Fe(CN)_6$[125]. Another example of an impedimetric biosensor employing $Fe(CN)_6$ was developed for the detection of *S. epidermidis*. 3-aminophenylboronic acid (3-APBA) was used for the electrochemical fabrication of the cellularly imprinted polymer. Boronic acid group specifically interacts with cis-diol (present in TAs and PGN), allowing the formation of a polymeric matrix with structural and chemical recognition[126].

2.2.2.2 Signal transduction

(Bio)sensors can broadly be divided into three different classes, based on the transduction method employed: *i)* optical, *ii)* mechanical and *iii)* electrochemical sensors[100].

Optical biosensors inspired by conventional immunoassays are fluorescence-based and have high sensitivity[127]. Yet, the obvious drawbacks are the need for expensive reagents and specialized, non-portable equipment. The latter can be replaced with optical fibres[100,127]. Optical fibres are also used in non-fluorescence based biosensors, as these fibres respond to changes in the evanescent field due to analyte-binding induced alterations in refractive index at the surface[128]. Other types of optical sensors use surface plasmon resonance, optical waveguides (optical fibres belong here too), optical resonators and photonic crystals[129]. Surface plasmon resonance systems are based on polarized light passing through a glass prism that contains bioreceptor functionalized gold surface. Change in refractive index occurs upon analyte binding, altering the deflection of polarized light exiting the prism[100]. This technique has been applied for detection of several different pathogens,

e.g. *Salmonella* spp*, Streptococcus pneumoniae*, *Cronobacter* spp, *Chlamydia trachomatis* and *Neisseria gonorrhoeae*[130].

Mechanical biosensors are based on piezoelectric materials or employ cantilever technology. QCM measures the changes in mass per unit/area via measuring the frequency variation of the (piezoelectric) quartz crystal. It can operate in vacuum, gas or liquid and has been applied to detect different *E. coli*[131,132] and *Salmonella* strains[133]. Cantilever sensors came from atomic force microscopy and are typically functionalized with biorecognition molecules[134–136].

Electrochemical sensors include potentiometric, impedimetric and amperometric sensors[100]. While they appear in many different configurations, the basics of electrochemical sensing can be understood in the context of a three-electrode electrochemical cell. The cell contains a working electrode (WE), a reference electrode (RE) and a counter electrode (CE). The WE is the part of the sensor where the reaction of interest occurs and is measured. If the method of choice is potentiometry, the potential difference between the WE and the RE is measured (CE is often not needed in this setup) and in case of amperometry, the current flowing between the WE and the CE is measured, while the potential on the WE is kept stable in relation to the RE[137]. Impedance is a measure of resistance of the circuit to the electron flow; as it is not limited to an ideal resistor it does not only include a resistive component but also capacitive and inductive components. A commonly used technique is electrochemical impedance spectroscopy, where an alternating potential is applied to the electrochemical cell, at different frequencies, and the current response is measured. Importantly, to fully understand impedance measurements one often fits the data to electrochemical circuit models[138]. Ultrasensitive potentiometric sensors for detection of *Salmonella* Typhimurium[120] and *E. coli*[139] were fabricated using aptamers immobilized on single-wall carbon nanotubes. Further, a potentiometric sensor for *S. aureus* with 1 CFU/mL sensitivity was developed by immobilizing aptamers on graphene[140]. An amperometric immunosensor made of antibodies immobilized on carbon electrodes for detection of *Streptococcus agalacticae* with the sensitivity of 10 CFU/mL and detection time of 90 min was reported[141]. Impedance microbiology took off in 1970s and was based on that the solution resistance of bacterial growth media decreased when bacterial growth increased, while the capacitance increased simultaneously[142]. Modern impedimetric biosensors function by analyte-bioreceptor interaction that causes a change in capacitance and resistance at the surface of the WE[100]. A microfluidic chip with immobilized AMPs on gold was developed to detect 10^5 CFU/mL of *Streptococcus mutans* and *Pseudomonas aeruginosa* (*P. aeruginosa*) in less than half an hour[143]. Similar results were reached in another microfluidic device, a label-free sensor composed of circular interdigitated microelectrodes that made use of specific resonance frequency to detect *S. epidermidis*[144]. As mentioned above, impedimetric sensors are commonly employed for the detection of bacteria in imprinted polymers[125,126].

2.3 CONJUGATED OLIGO- AND POLYMERS

In 2000, Alan MacDiarmid, Hideki Shirakawa and Alan Heeger were awarded the Nobel prize in chemistry for the discovery of conjugated (or conducting) polymers (CPs). Iodine doped polyacetylene, the first CP synthesized in 1977, was soon replaced by other, mainly aromatic CPs, that were more stable and easier to process. Among the most used and studied CPs today are PPy, polythiophene, poly(3,4-ethylenedioxythiophene) (PEDOT) and polyaniline[145].

PEDOT and PPy are most commonly used in medical applications[146]. The term organic bioelectronics, coined in 2007[13], is today employed as an umbrella term for the applications of organic electronics in biology[13,147].

2.3.1 Conjugated polymers in solid form

The first CP reported, polyacetylene, had a very high conductivity but was air-sensitive and not processable[148]. In search of more stable systems, derivatives of polythiophenes appeared most promising and PEDOT was a breakthrough in the field as it was stable and conductive[149]. Processability was improved significantly upon doping with polystyrene sulfonate (PSS)[150] and still today PEDOT:PSS (**Figure 2**) is among the most popular formulations.

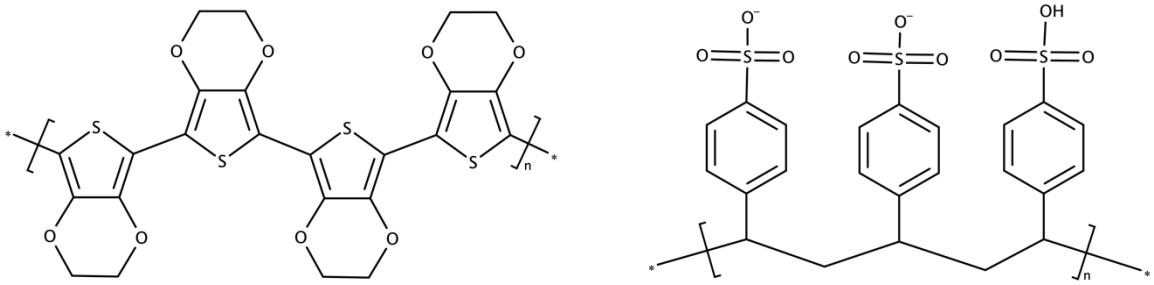

Figure 2: PEDOT (left) : and PSS (right).

2.3.1.1 Electronic conductivity

The conductivity of a material depends on its electronic structure. Metals, known to be good conductors, are usually located in the first, second and third group of the periodic system, meaning that they have few valence electrons. The ionization energy is low, i.e., the valence electrons are not tightly bound to their respective nuclei and can easily be detached. A simplified representation of a metal solid is one of positive nuclei embedded in a sea of electrons. When potential is applied to a piece of metal, the electrons can move around easily – i.e., electric current flows. In insulators, on the opposite, electrons are tightly bound to their nuclei and not willing to move. The electrons shared between atoms in covalent bonds are in σ (coaxially symmetric) and π (non-coaxially symmetric) molecular orbitals. The σ and π molecular orbitals have their non-bonding counterparts, σ∗ and π∗. In insulating polymers, such as polystyrene, carbon is sp^3 hybridized, forming 4 σ bonds in a tetrahedral structure. In CPs, the carbon atoms are sp^2p_z hybridized, i.e., each carbon forms 3 σ and 1 π bond, and the backbone consists of alternating single and double bonds. The overlap of p_z orbitals along the backbone enables delocalization of electrons along the chain, i.e., gives them space to move around. As the number of delocalized electrons in π orbitals is equal to the number of carbon atoms, the energy levels split up when chain length increases, eventually forming energy bands. The highest occupied molecular orbital (HOMO) is the top of the π band (= valence band), while the lowest unoccupied molecular orbital (LUMO) is the bottom on the π* band (= conduction band) and the energy between them is termed the bandgap. In their pristine state, CPs are semiconductors, and to make them conductive, charge carriers must be introduced[151]. This is achieved by a process called doping, which can be chemical[152] or electrochemical[153,154] (depending on the synthesis) and results in oxidation (p-doping) or reduction (n-doping) of the polymer backbone. PEDOT is typically p-doped and its optical properties change significantly depending on the doping level. In its pristine state, it is dark blue and when oxidized it becomes

transparent[155]. Charge introduction causes local distortion of the electronic and geometric configuration of the polymer, creating a quasiparticle called polaron. Polarons must be compensated by counterions[151]. These can be small ions, polyions or bigger charged molecules and have been shown to greatly affect the polymerization process, structure and function of the synthesized materials[156]. Long-distance charge travel – where charges need to travel beyond a single polymer chain - occurs through charge hopping[157]. The conductivity of PEDOT based films has been improved significantly by the addition of dimethyl sulfate[158], polyethylene glycol[159], other additives[160], and by solvent treatment[161,162]. Most of these treatments result in lowering the amount of PSS in the film and a conformational change of PEDOT chains from coil to a linear or expanded coil confirmation that happens during thermal annealing[155]. CPs backbones have low redox potentials in aqueous electrolytes, enabling reversible redox switching of the material[17]. Redox switching has been shown to affect hydrophobicity of PEDOT:Tos composites[163] but not of PEDOT:PSS[164]. Importantly, PEDOT is widely used in electrochemistry due to its electrocatalytic properties and electrocatalysis of several biologically relevant electroactive molecules has been described, for example ascorbic acid[165,166], cysteine[167] and NADH[168].

2.3.1.2 Ionic conductivity

Compared to metals and inorganic semiconductors, CPs are not so densely packed, allowing the ions to move efficiently within the polymer film[169,170]. The ability of CPs to conduct both, ions and electrons, provides them with the capacity to translate between ionic and electronic signals, making them suitable to function at the interface between biology and electronics[17,169,170]. Upon electronic switching, ions attempt to compensate the charges – small ions diffuse in/out of the polymer, while polyions cannot diffuse out and charge compensation must occur through an inflow of ions from the bulk electrolyte[17]. The inflow of hydrated ions can also cause polymer swelling, observed in PEDOT[170,171] and PPy[172]. Ion mobility within PEDOT:PSS films was shown to be comparable to that in bulk water, wherefrom the authors suggested that large water channels are formed in the PSS rich phase, extending into smaller channels in the PEDOT:PSS. In agreement with these findings, the addition of 3-glycidoxypropyltrimethoxysilane (GOPS) significantly reduced swelling and ion mobility[170].

2.3.1.3 Synthesis & functionalization

CPs are synthesized by oxidative polymerization of monomers, which can be chemical[173] or electrochemical[174]. Chemical synthesis is the method of choice in industry, as it enables large scale production[155,175]. The method has been optimized for PEDOT over the last decades to achieve conductivities up to 1000 Scm^{-1} [155] and different grades are commercially available. The advantages of electrochemical synthesis are its simplicity and the possibility to entrap charged molecules in the film during polymerization[145], however it is limited to the use of conducting substrates. PPy can likewise be chemically or electrochemically polymerized in a variety of different solvents, including aqueous solutions[176]. Photo-induced polymerization of PPy has also been reported[177]. Chemically polymerized CPs in solutions can be drop casted, spin-coated[178] or printed[179] on a variety of different substrates. Patterning of CP films can be performed using several different lithographic techniques: soft lithography, e-beam or ion-beam lithography, photolithography, dip-pen nanolithography and others[180].

When employing CPs in biosensors and other devices, functionalization with a biorecognition molecule is often necessary. There are four major strategies available to do this:

i) physical adsorption, *ii)* electrochemical entrapment, *iii)* covalent attachment, *iv)* affinity-based interactions[181]. Physical adsorption is based on electrostatic, van der Waals and hydrophobic interactions and is usually simple to perform but such composites are less stable compared to other methods[181]. Electrochemical entrapment occurs during electropolymerisation, where the molecule to be entrapped is present in the electrolyte, together with the monomer units. This strategy is commonly used for enzyme entrapment. Examples are glucose oxidase entrapped in a PEDOT film on a platinum electrode[182] and ascorbate oxidase in PEDOT/(multiwall carbon nanotube) composite films[183]. The same technique was applied to entrap whole bacteria in PPy films[184]. A promising alternative to electrochemical entrapment, especially applicable to smaller non-charged molecules, is the supercritical CO_2 mediated incorporation of targets into PEDOT:PSS films[185]. The main drawback with any entrapment technique is that the molecule availability is limited since it is buried in the polymer[181]. Covalent attachment, where linkers of desirable lengths can be employed, enables better target availability and has a smaller effect on the film itself since the binding is performed after film polymerisation[181]. Click chemistry[186], a simple organic chemistry approach for covalent bonding in physiological conditions, has been used to covalently bind proteins to carboxymethylated dextrans in the spin-coated PEDOT:PSS films[187]. Using another approach, PEDOT:PSS with poly(vinyl alcohol) was spin-coated and 3-glycidoxypropyltrimethoxysilane (GOPS) was subsequently used as a silanizing agent to bind amino groups on proteins and peptides[188]. EDOT moieties can be functionalized to enable direct coupling of compounds with the CP. EDOT and EDOT-MeOH monomers were electropolymerized in the presence of PSS and subsequent silanization with (3-Aminopropyl)-triethoxysilane (APTES) was performed to bind silver nanoparticles to the polymer[15]. In a similar approach, EDOT and EDOT with an oxylamine moiety (EDOTOA) were copolymerized in the presence of PSS and receptors for human influenza A virus were introduced by covalent binding to oxylamine moieties[189].

2.3.2 Soluble conjugated oligo- and polymers

CPs can be rendered soluble in organic and/or polar solvents by incorporation of side chains. It has been shown that these functionalized CPs can exhibit an optical response to temperature, pressure or solvent changes due to the modification of main chain confirmation[190]. These materials as well as their oligomeric counterparts, i.e., conjugated oligomers, have been developed towards applications in sensing, imaging and therapy[191] and several have already been used for detection of bacteria[192–194].

2.3.2.1 Evolution of luminescent conjugated oligo- and polythiophenes

The chemical formula of a thiophene is C_4H_4S and the carbon and sulfur atoms together form a ring. Carbons are sp^2p^z hybridized, forming 3 σ and one π bond. Sulphur forms only 2 σ bonds, leaving one lone pair of electrons. It has 2 electrons in a p orbital, and they overlap with the p electrons from the carbon atoms. In a planar chain of thiophenes, the electrons are shared by all thiophene units, leading to an extended conjugation length. If the backbone twists, the conjugation is disrupted, and the absorption/excitation and emission spectra are blue-shifted (i.e., shifted towards shorter wavelengths)[195].

After initial publications, where luminescent conjugated polythiophenes were employed for DNA[196] and peptide[197] detection, the development of luminescent conjugated oligo- and polythiophenes (LCO, LCP) was for a decade directed mainly towards amyloid detection and spectral differentiation. In 2005, an anionic polythiophene, PTAA, was reported

that demonstrated spectral changes in the presence of native and amyloid bovine insulin – absorption and emission spectra were blue-shifted in the presence of native insulin and red-shifted (i.e., towards longer wavelengths) in the presence of amyloids[198]. The fluorescence intensity of PTAA decreased in the presence of fibrils, presumably due to aggregation[198]. PTAA could be used for histological staining of amyloid deposits in tissue sections, offering an alternative to commonly used amyloid dyes such as Congo Red and Thioflavin T[199]. A zwitterionic PONT displayed a blue-shifted absorption and emission spectra and an increased emission intensity when mixed with amyloid fibrils. The spectral alterations were ascribed to a twisted conformation and better separation of polymer chains, respectively[200]. As several LCPs were compared, it became evident that the lower the degree of side-chain substitution, the higher the interchain interaction and aggregation, and correspondingly, the larger the spectral shift upon binding to fibrils[201]. Spectral separation of distinct conformational states of amyloid-beta (Aβ) within the plaque was enabled by LCPs[202]. In 2009, the synthesis of three pentameric LCOs was reported and for the first time enabled amyloid staining under physiological conditions[203]. Enhanced fluorescence intensity and spectral substructures of the LCOs bound to amyloids were said to be associated with a conformationally restricted backbone and arise from the vibrational sublevels of the excited state. Moreover, two pentamers, namely p-FTAA and p-HTAA were also shown to cross the blood brain barrier and successfully stain plaques in mouse brains, which was not possible with LCPs[203]. Further, p-FTAA was found to spectrally discriminate between amyloid plaques and neurofibrillary tangles and detect *non*-thioflavinophilic prefibrillar assemblies[203]. It was next found, that for detecting *non*-thioflavinophilic protein assemblies of Aβ1-42 and for spectral separation of Aβ and neurofibrillary tangles the length should be between 5 and 7 thiophenes, carboxyl groups extending the conjugated backbone[204] and that the conformational freedom of the backbone is important[205]. The spacing of anionic groups on tetrameric LCOs was found to be crucial for them to distinguish different stages of plaque formation[206]. To expand and enrich the LCO collection available, a new set of pentameric molecules with distinct central heterocyclic moieties was synthesized[207]. Of special interest were the donor-acceptor-donor (D-A-D) configured LCOs, which had nearly no fluorescence in the unbound state[207]. The D-A-D configuration resulted in two excitation peaks – one corresponding to π–π* transition and the other to D-A transition[207]. Recently, two heptameric variants with the same backbone, including a D-A-D motif, and a different number of charged groups were reported (LL-1, 4 charged groups; LL-3, 6 charged groups)[208]. Interestingly, LL-1 and LL-3 had very similar absorbance spectra, but strikingly different fluorescence spectra. The absorption of the unbound LCOs seemed to be predominantly corresponding to π-π* transition while only LL-3 showed excitation spectrum corresponding to the π-π* transition[208]. LL-3 was superior to all other LCOs tested in this work for spectral discrimination of different pathologies[208]. This truly emphasizes the importance of coordinating different structural features to achieve the desired functionality.

Initial work in the field of microbiology has been sparked by the idea that the LCOs could be used to visualize bacterial amyloids in the extracellular matrix of biofilms. This turned out to be very successful as not only amyloids but also cellulose could be visualized within a biofilm and their spectral signatures differed[19]. Importantly, this technology led to the development of a rapid diagnostic test for biofilm-related urinary tract infections[20]. The field subsequently broadened to include polysaccharide detection and discrimination in numerous

settings[209–211]. As the application areas of the LCOs expanded, they assumed a new name – optotracers – which they will be referred to in the continuation of this thesis.

2.3.2.2 Basic principles of luminescence

Luminescence is defined as the emission of light not caused by heating. It comprises of luminous effects caused by a transition of an electron from an excited (= higher energy) state to a state with a lower energy. The state with the lowest energy is called the ground state and is the most stable state to be in for an electron. It is only upon absorption of energy that the electron can transition to a higher energy state. As the electron falls back down to the ground state, the energy can be released in the form of emitted photons. Depending on the excitation source, several different types of luminescence exist such as chemiluminescence by a chemical reaction, photoluminescence from photon excitation and electroluminescence by electric current[212].

Electroluminescence of CPs was first reported in 1990[213] and today CPs are used for organic light-emitting diodes (OLED), referred also as P-OLEDs or PLEDs. Several different CPs were used, including polyphenylene vinylene, polyfluorene and polythiophene[214]. Derivatives were synthesized to achieve the desired colour of emitted light and improve efficiency[214]. In a PLED, a CP film is placed between an anode and a cathode, where the anode is typically a transparent material (e.g. indium tin oxide) and the cathode is a metal[215]. When the voltage is applied between the two layers, the electrons are injected in LUMO from the cathode and the electrons are withdrawn from HOMO by the anode (i.e., holes are injected)[216]. Formation of an electron-hole pair results in photon emission and re-establishment of the ground state[216].

Photoluminescence is further divided into fluorescence and phosphorescence, the difference between them being the duration of luminescence. For a molecule to fluoresce or phosphoresce it needs to be able to absorb light (i.e., photons) and use it to excite an electron from its ground state into an excited state. The excitation of an electron occurs very fast (10^{-15} s) and depending on the energy absorbed the electron is excited to one of the many different vibrational levels that exist within the excited state. Since the excited state is very unstable, the electrons return to the ground state, dissipating energy during the process via radiative and non-radiative processes. First, vibrational relaxation occurs so that the electron drops to the lowest vibrational level of the excited state and during this process energy is dissipated as heat (i.e., non-radiative process). At energy levels higher than the first excited state, vibrational and electronic energy levels overlap. This makes it possible for an electron to go from a lower vibrational state in a higher electronic state to a higher vibrational state in a lower electronic state – a process termed internal conversion, also a non-radiative process (**Figure 3a**)[212].

In phosphorescence, an intersystem crossing occurs, and an excited electron goes from a singlet excited state (S_1) to a triplet excited state (T_1), inverting its spin in the process. From the triplet state, the electron can return to the ground state via radiative transition, but it needs to invert its spin again and therefore the process is very slow, compared to fluorescence[212].

In fluorescence, the electron relaxes from the lowest excited state to the ground state by a radiative process, i.e. the energy is dissipated by photons. These photons have lower energy than the photons used for photoexcitation and the difference between energies (i.e., wavelengths of absorbed and emitted light) depends on the amount of energy dissipated in non-radiative processes. The shift between the wavelengths of excitation and emission

light is termed the Stokes shift. In a transition from the excited state, the electron can land at different vibrational levels of the ground state – this is why an emission spectrum is observed and not just a single peak (**Figure 3b**). The emission spectrum is independent of the excitation wavelength. The intensity of emission is determined by the molecular structure and the environment and is expressed as a quantum yield or quantum efficiency. This is effectively the ratio of molecules that fluoresce to the total number of molecules excited[212,217]. The molecules exhibiting fluorescence are typically, but not necessarily, aromatic compounds with low π-π* transitions. The higher the number of rings and the degree of condensation, the higher the quantum yield[212]. Several other molecular features, such as side group substitutions etc. also influence the quantum yield but will not be discussed in detail here. In conjugated oligo- and polymers, the fluorescence most often occurs as a consequence of π*-π transition, i.e., LUMO to HOMO transition. To decrease the bandgap, two different organic semiconductors with slightly offset HOMO and LUMO levels can be combined. The electron is then transferred between the HOMO of the donor and the LUMO of the acceptor, requiring less energy[218].

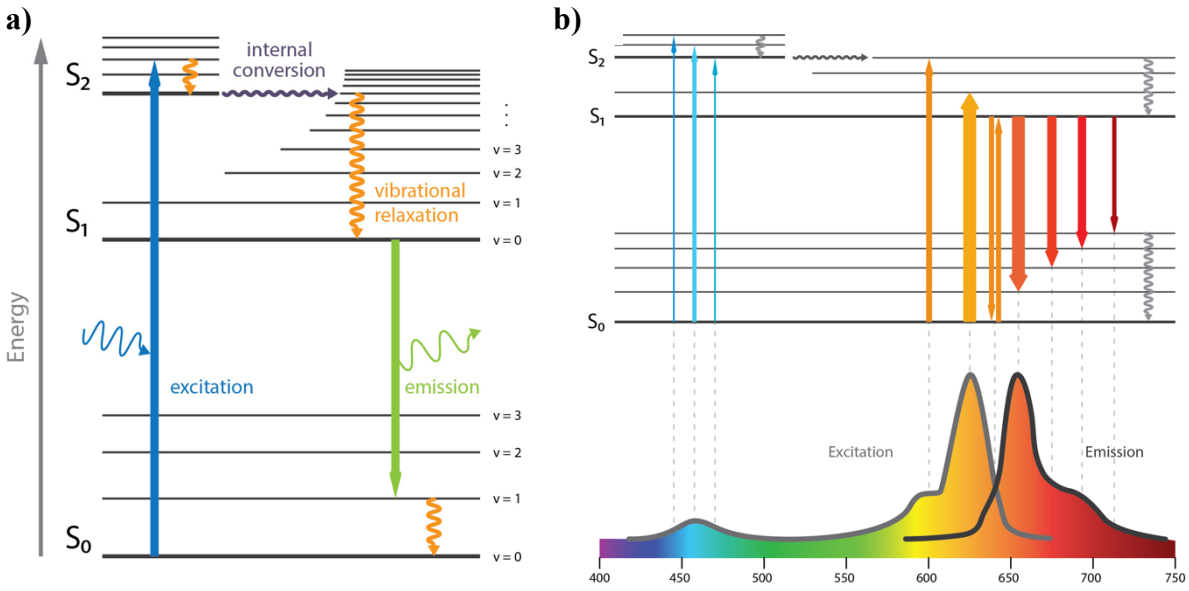

Figure 3: Simplified Jablonski diagrams. **a)** Upon photon absorption, the electron is excited to a higher energy level (excited state). Through non-radiative processes (internal conversion, vibrational relaxation), it descends to the lowest level of the excited state. From there the electron relaxes to the ground state via a radiative process, emitting light. **b)** Fluorescence spectra of a fluorophore reflect the likelihood by which excitation and emission occur at certain wavelengths. Images are the courtesy of Hartmut B.F. Pohl, Enzo Life Sciences.

2.4 PREVENTING BACTERIAL GROWTH ON SURFACES

To prevent or at least limit the spread of infection, prevention of bacterial colonization of surfaces is crucial. Roughly, there are three main approaches to antibacterial surfaces: *i)* antibacterial agent release surfaces, *ii)* anti-adhesion surfaces and *iii)* contact killing surfaces[10].

2.4.1 Antibacterial agent release surfaces

A broad range of antibacterial compounds have been used in release based systems; antibiotics, AMPs, metals and halogens, enzymes, organic cationic and non-cationic compounds, nitric oxide and titanium oxide[10]. Different matrices for entrapment of these compounds have been used, most commonly natural (chitosan, collagen, alginate, cellulose) and synthetic polymers (polyethylene glycol, polyurethane, polyamide etc.) and silica[219]. Release of antibacterial agents can be passively controlled by changing the size, charge and other properties of the bacterial agent or the viscosity, porosity and other parameters of the surface matrix[10,219–221]. Active control of antibacterial agent release is enabled by stimuli responsive materials; recent examples include surfaces where antibacterial agents are released upon contact with bacteria[10,219,222,223]. Limited amount of antibacterial agents available in the surface, hijacking long term use but also promoting the development of antimicrobial resistance, as well as cytotoxicity and inflammatory responses, are the main issues of this technology[10]. Yet, the use of quorum sensing inhibitors[224] and AMPs[225] instead of antibiotics, as well as making use of collateral sensitivity[226] to create multimodal surfaces, are just some of the promising strategies for the future.

2.4.2 Anti-adhesion surfaces

Anti-adhesion surfaces aim to prevent bacterial adhesion by hindering the physicochemical interactions of bacteria with the surface[10] or inducing mechanical damage to bacterial cell envelope[227]. The mode of action is usually mechanical, whereby the nanostructure of the surface plays a crucial role[219]. Many anti-bacterial and anti-fouling surfaces have been inspired from nanotopologies found in nature[228,229], such as shark skin[230], lotus leaf[231], gecko skin[232] and cicada wings[233]. Graphene has been widely employed in the generation of anti-adhesion surfaces[227,234], however the mechanisms behind its action are yet to be elucidated[235]. Poly(ethylene glycol) is commonly used as an antifouling surface agent, however, it is becoming increasingly replaced with zwitterionic polymers of different designs that have shown increased antibacterial or even antimicrobial properties[236]. A significant reduction in attachment, motility and biofilm formation of *P. aeruginosa* was observed on negatively charged and zwitterionic surfaces compared to positively charged surfaces[237]. The redox state of the surface can also influence biofilm formation - the formation of *Salmonella* Typhimurium biofilm on oxidized CP surfaces was much higher than the formation of biofilm on the reduced surfaces of the same material[14].

2.4.3 Contact killing

To avoid the problem of limited antibacterial agent available for release, the antibacterial agents can be covalently anchored to the surface[238]. As the antibacterial agents are immobilized on the surface, they are less likely to have access to intracellular compartments of bacteria and should preferably interact with the cell envelope[239,240]. Commonly used antibacterial agents for surface immobilization are AMPs[239,241–243] and enzymes[239,244,245], ammonium salts and polyamines[240]. Recently, quorum sensing agonists and antagonists were attached to the glass surfaces with

long poly(ethylene glycol) linkers and were shown to successfully modulate the expression of biofilm formation and dispersal related genes in *S. aureus*[246].

Metals have been used for their antimicrobial properties already by the early civilizations and are still used today[247]. Certain non-essential metals (e.g. Ag, Hg, Te) have bactericidal activity at very low concentrations, but many otherwise essential metals (e.g. Cr, Mn, Fe, Co, Ni, Cu) are bactericidal when present in excess[247]. Several different processes are involved in toxicity: *i)* generation of reactive oxygen species imposing oxidative stress; *ii)* metal-catalyzed oxidation of amino acids, destruction of Fe-S clusters, exchange of catalytic or structural metals, leading to protein dysfunction and loss of enzyme activity; *iii)* impaired membrane function; *iv)* interference of nutrient uptake and *v)* genotoxicity[247]. Copper (Cu) is of special interest for implementation as touch surface coating to prevent the spread of infection and it was shown to decrease hospital-acquired infections in clinical trials[248–251]. The antimicrobial efficiency of copper has been extensively studied and bactericidal effect towards gram-positive and gram-negative bacteria, viruses and fungi were demonstrated[252]. Studies based on *Enterococcus hirae,* a zoonotic bacterium seldomly found in humans[253], have shown that copper ions are crucial for bactericidal effect[254], and the same was found for *E. coli*[255]. These findings were corroborated by experiments showing that the addition of copper chelators (EDTA, bathocuproine disulfonate) leads to increased survival of *E. coli*[255,256], *E. faecalis* and *Enterococcus faecium* exposed to copper[257]. Unlike zinc or nickel, copper alternates between its two oxidation states, i.e., cuprous Cu(I) and cupric, Cu(II). In the presence of oxygen, this redox cycling leads to the generation of reactive oxygen species[255]. Indeed, the addition of catalase or superoxide dismutase increased *E. coli* survival[255]. Interestingly, anaerobiosis did not lead to longer survival times on copper surfaces, presumably due to Cu(I) accumulation[255].

Copper surfaces are subjected to corrosion. At ambient conditions, copper oxidation leads to the formation of cuprous oxide (Cu_2O), and upon prolonged exposure, cupric oxide (CuO)[258,259]. If copper is exposed to aqueous solutions, cupric oxide forms and the rate of formation is buffer (Tris, PBS) dependent[258]. Killing efficiency towards *Enterococcus hirae* for copper and cuprous oxide surfaces was similar, while it was reduced for cupric oxide surfaces[258].

It was recently shown that even at low concentrations, without affecting the growth rate, the presence of copper in growth medium leads to altered biogenesis of the cell wall in *E. coli* and *Enterococcus faecium*[260]. Copper inhibits β-lactam–insensitive LD transpeptidases leading to a reduction in all muropeptides with tripeptides and 3-3 cross-links, and the re-sensitization of β-lactam resistant strains that use LD transpeptidases in a bypass mechanism to achieve resistance[260]. This implies that copper could be useful in combination with other antimicrobial agents and further studies elucidating the interaction of copper with bacteria will enable us to fully harvest the potential of this ancient antimicrobial.

3 RESEARCH AIMS

The overarching aim of this thesis was to devise novel methods to be used for detection, identification and quantification of bacteria, as well as for the evaluation of antimicrobial surface properties. The specific aims were to:

1) Develop a conjugated polymer based potentiometric sensor for label-free electrochemical detection of bacteria.
2) Explore optotracing (i.e., the use of luminescent conjugated oligothiophenes) for direct detection and visualisation of *Staphylococcus aureus*.
3) Investigate the structural requirements for optotracer-based detection of *Staphylococcus aureus.*
4) Devise a multifaceted methodological approach to study antimicrobial properties of high touch copper surfaces.

4 METHODS

4.1 SPECTROSCOPY AND MICROSCOPY

Spectroscopy and microscopy are commonly employed optical techniques and can be used with transmitted light and fluorescence. Throughout this thesis absorbance at 600 nm (A_{600}) was employed as a proxy to estimate the bacterial cell density. To measure the absorbance of a sample, a plate reader (Biotek, USA) or a benchtop spectrophotometer were employed. Absorbance (A) is defined as $\log_{10}(I_0/I)$, where I_0 is the incident light, and I is transmitted light. It follows Beer-Lambert law, $A = c \cdot L \cdot \varepsilon$, c being the molar concentration, ε the extinction coefficient and L the pathlength. If L equals 1 cm the A_{600} is referred to as optical density (OD_{600}). Absorbance does not have real units, often AU is used as for "absorbance units".

For fluorescence spectra and single measurements, a plate reader was employed (Biotek, USA). In simple terms, the instrument contains a source of light, a sample holder and a detector. The wavelength of the incident and detected light can be selected, enabling spectral recordings. The excitation spectra are measured by exciting the sample with light of different wavelengths while collecting the emitted light at a single wavelength. On the opposite, the emission spectrum is determined by exciting the sample with a light of a certain wavelength and collecting the emitted light at different wavelengths. In the plate reader we employed, fluorescence intensity, i.e., the photons reaching the detector unit, are measured in Relative Fluorescence Units (RFU). In contrast to absorbance, which is ideally absolute, RFU is instrument-specific and cannot be compared across different instruments. To enable high throughput optotracing, kinetic measurements were performed in the plate reader at a fixed temperature (37 °C). Fluorescence and absorbance at fixed wavelengths were measured in regular intervals, which enabled us to follow bacterial growth and optotracer fluorescence simultaneously.

To perform fluorescence microscopy, laser scanning confocal microscopes were employed, i.e., Olympus FV1000 and Zeiss LSM800 at the Biomedicum Imaging Core at Karolinska Institutet. In these systems, lasers are employed as excitation light sources and a pinhole positioned before the detector limits the out of focus light enabling imaging on a single plane. Since optotracers have spectral characteristics that often differ from the commonly used fluorophores, the emission ranges were customized. Super-resolution microscopy was performed at the Advanced Light Microscopy facility at Science for Life Laboratory using Zeiss LSM880 equipped with an AiryScan detector. Instead of the pinhole and a single detector behind it, a hexagonally packed detector array is used. With the pinhole, there is a trade-off between the signal to noise ratio and the signal intensity, while this is not the case for the AiryScan detector, as each of its 32 elements acts as an individual small pinhole. Overall, AiryScan has approximately 1.7 x higher resolution compared to traditional confocal systems[261].

4.2 COMMON MICROBIOLOGICAL TECHNIQUES

4.2.1 Molecular biology

S. aureus RN4220 containing plasmids pSGFPS1, pSRFPS1 and pSFRFPS1[262] were obtained from BEI Resources. These plasmids are derived from pKK30, which is derived from a stable cryptic plasmid LAC-p01 found in USA300[263]. dfrA, coding for trimethoprim resistance, and a fluorescent protein are under the transcriptional control of a constitutive sarA-P1 promoter[262]. The plasmids from *S. aureus* RN4220 were purified using a Qiagen Plasmid miniprep kit (Qiagen, Germany). Electrocompetent cells of *S. aureus* 8325-4[264], *S. aureus* SH1000[264], *S. aureus* SH1002[264] and *S. aureus* ATCC 25923 were prepared as previously described[265]. The plasmids were inserted with electroporation, using BioRad Gene Pulser Xcell. Transformed cells were recovered from tryptic soy agar plates with trimethoprim. Plasmid stability in the absence of antibiotic selection was evaluated by fluorescence spectroscopy and microscopy. In our experience, the three plasmids were stable only in *S. aureus* SH1000 and SH1002, as reported previously[262] but not in *S. aureus* 8325-4 and *S. aureus* ATCC 25923.

As part of our work we have screened the Nebraska Transposon Mutant Library[266] and have sequenced the annotated mutants that have shown to be significantly different from the wild type as determined by 1 sample t-test ($\alpha = 0.05$). Genomic DNA was isolated using GenElute™ Bacterial Genomic DNA Kit, followed by restriction digestion with AciI and ligation with T4 DNA ligase as previously described[266]. DNA fragments around the *bursa aurealis* transposon were amplified with polymerase chain reaction (PCR) using the Buster and Martn-ermR primer set[266]. PCR reaction included 30 cycles, annealing temperature at 64.3 °C, 3 min extension time. GFX™ PCR DNA and Gel Band Purification Kit (GE Healthcare, UK) and ExoSAP-IT™ PCR Product Cleanup Reagent (ThermoFisher, Sweden) were used to purify PCR products. Buster primer was used for sequencing (Eurofins, Germany).

4.2.2 Bacterial adhesion to hydrocarbons (BATH)

While the hydrophobicity of surfaces can be determined relatively easily with contact angle measurements, the task is not so trivial when it comes to bacteria. Following the basic principle of hydrophobic substances attracting each other to escape water, the hydrophobicity of bacteria is typically evaluated by their ability to adhere to (hydrophobic) hydrocarbons[267]. In our experiments, we tested *p*-xylene and hexadecane and decided to use the latter for our assay, since it gave more consistent results. The assay was performed as previously described[267]. Sodium phosphate/citric acid buffers with pH 5.0 and 7.0 were prepared by mixing 0.1 M citric acid and 0.1 M dibasic sodium phosphate and were subsequently diluted to 20 mM. Trizma/hydrochloric acid buffers with pH 7.0 and 9.0 were prepared by equilibrating 0.1 M Trizma buffer with hydrochloric acid and were subsequently diluted to 20 mM. NaCl was added to final concentrations of 0, 150 and 500 mM. All buffers were autoclaved. Overnight cultures of bacteria were washed in designated buffers and the OD_{600} was adjusted to approximately 0.5, as we found this to be the most optimal concentration for the assay. 3 mL of the culture was transferred into an acid-washed (1 % HCl, overnight) glass tube, 0.5 mL hexadecane was added, and the samples were vortexed for 90 s. The tubes were left to stand for 20 min to allow for phase separation. Pasteur pipette was employed to recover the aqueous phase and its OD_{600} was measured. The recovery (i.e., the amount of bacteria not bound to

hexadecane) was determined as the ratio between the OD_{600} of the recovered aqueous phase and the OD_{600} of initial culture.

4.3 ELECTROCHEMISTRY

Voltammetric techniques are aimed at understanding the processes occurring at the working electrode (WE). Typically, voltammetry is employed to monitor redox processes occurring at the WE, where electrons are exchanged between the electrode and the redox species in solution, at the electrode/electrolyte interface. Besides WE, reference (RE) and counter (CE) electrode are present in a typical electrochemical cell. RE maintains a stable potential and the potential applied to the WE is measured relative to the RE. No current is flowing between the WE and the RE, that is, all current is flowing between the WE and the CE.

4.3.1 Square Wave Voltammetry (SWV)

Linear and cyclic voltammetry are commonly used in electrochemistry to characterize the redox reactions occurring at the WE. However, next to the faradaic current, charging current is added to the total current recorded by these techniques. When only small amounts of analytes are present in the solution, this can be troublesome, as the charging current can "mask" the faradaic one. Fortunately, the time scale at which the two currents occur differs – the formation of the double layer leading to charging is completed within few milliseconds, while the faradaic current is still significant after longer periods, so that the ratio of faradaic vs charging current increases for a given potential over time. If the continuous potential increase is then replaced with a staircase increase, the current can be measured at the end of each potential step, to diminish the contribution of charging current. This idea is at the core of differential pulse voltammetry, a variant of which is SWV, defined by equal time spent at baseline and pulse potential. Briefly, the potential is swept within a region in a pulsed staircase manner, i.e., at each potential, two oppositely oriented small pulses are applied, constituting the "potential cycle". In each potential cycle, forward and reverse currents are measured. The charging current in two neighbouring pulses has the same sign (i.e., plus or minus) and an almost identical amplitude. A net current is obtained by subtracting the reverse current from the forward current. The net current is higher than the forward and reverse ones and the contribution of the charging current is significantly reduced[268]. In our experiments, we used glassy carbon (GC) WE, a solid Ag/AgCl quasi RE and a platinum CE. To examine the electrocatalytic effect of PEDOT, EDOT and PSS were electropolymerized on the GC electrode. *S.* Enteritidis in M9 minimal medium was the analyte. We performed a forward scan between -0.2 and 0.7 V, with 25 mV pulse size, 25 Hz frequency and 2 mV step size.

4.4 DATA ANALYSIS

Modern techniques enable fast acquisition of substantial amounts of data that often cannot be processed easily using conventional statistics software. Some basic coding can be of great help for such instances and in this thesis, we have employed Python programming language to create algorithms to aid in data analysis.

4.4.1 Redox sensor

Raw data obtained from the two-electrode sensor described in Paper I was first baseline corrected by subtracting the first recorded value from all subsequent values and then filtered using a Savitzky-Golay[269] digital filter. To determine the earliest time point where detection

and quantification of analytes was possible, the coefficient of determination (R^2) was determined for the linear fit of potential difference (dV) versus analyte concentration at each time point during the measurement. The detection time for each analyte was the time point when R^2 was at or above 0.975 and the signal from the lowest detectable concentration was above the limit of detection (LOD = $mean_{blank}$ ± 1.645 SD_{blank}). The algorithm is available at (https://github.com/medicalnano/redoxsensor).

4.4.2 Optoplotting

To determine the correlation between fluorescence and A_{600} in time automatically, a simple script was written in Python programming language. The kinetic data (A_{600} and fluorescence) was first smoothed using a Savitzky-Golay digital filter[269]. Next, the gradient of the filtered A_{600} was calculated. The exponential phase was determined to be within the time frame corresponding to the top 10 % (for 20 hours measurements) or top 20 % (for 12 hour measurements) of the gradient. The generation time was calculated within this time frame ($n=((\log_{10}(end)-\log_{10}(beginning))/\log_{10}(2)$, $t_{gen} = t/n$). Filtered fluorescence data corresponding to the same time frame was extracted and the fluorescence vs A_{600} was plotted to generate the *optoplot*. The coefficient of determination (R^2) and the slope of the optoplot were determined by linear regression. Note that only values within the range of top 10 % or 20 % of the gradient, but not on the limit (i.e., 10^{th} or 20^{th} percentile), were included in the calculations.

4.4.3 Automated spectral plot analysis

To automatically process spectral data from optotracers, a simple script was written in Python programming language. Firstly, the aim was to characterize the peak wavelengths of the excitation and emission spectra. The spectra were first filtered using a Savitzky-Golay digital filter[269] and were then fed into a "find peaks" function available from Scipy[270] package of Python programming language. In this function, the peak is defined as the point whose two direct neighbours have a smaller amplitude. Results were manually checked to remove artefact peaks caused by noise in the data, that was not smoothed out by the digital filter.

Next, to determine the overall spectral shift, cross-correlation was employed, available as a function in Matplotlib[271] package of Python programming language. Briefly, cross-correlation is a measure of similarity between two signals at different lag positions, in our case in nm. In Matplotlib[271] cross-correlation function, the correlation with a lag *k* is defined as $\sum_n x[n+k] \cdot y*[n]$, where $y*$ is the complex conjugate of y, in our case $y*$ and y are the same since y is a real number. From this function, we were able to extract the lag where the correlation between the two spectra was best and this lag was subsequently translated to the spectral shift. Next, to quantify the overall fluorescence of optotracers in the presence or absence of bacterial cultures, we aligned the spectra according to the shift and calculated the quotient of the integrated fluorescence of the optotracer in the presence of either *S. aureus* or *S.* Enteritidis and the optotracer alone.

5 RESULTS AND DISCUSSION

5.1 PAPER I

Many bacteria are known to produce redox-active species[73] and we hypothesized that this could be used for detection of bacteria in culture media or in biological samples. In Paper I, we employed a (PEDOT:PSS)-based two-electrode cell for potentiometric detection and quantification of bacteria. PEDOT was chosen for its widely recognized electrocatalytic properties[272,273] that are ascribed to its ability to react with redox compounds[272,274] and were demonstrated for several biologically relevant substances[165–168]. The electrocatalytic effect is exhibited as a shift in overpotential necessary to drive a redox reaction on the electrode. This should not be confused with increased current output commonly observed with CPs - that is rather a consequence of their topography since the effective surface area available for the redox reaction to occur is often larger than that of a metal or semiconductor electrode of equal dimensions[156]. The two-electrode device used in this work is commercially available and was obtained from OBOE IPR AB (Sweden). PEDOT:PSS electrodes were screen printed on a polyethylene terephthalate substrate and a layer of patterned SU-8 was added on top to create liquid reservoirs on the electrodes. Between the two electrodes (i.e., the test and reference electrode) was a PEDOT:PSS channel that ended in an unpatterned region of the reference electrode (i.e., devoid of PEDOT:PSS) so that it acted as a salt bridge between the liquids. Carbon paint on the outer side of the electrodes was contacted with metallic probes to connect the sensor with a SourceMeter (Keithley 2602A, USA). The potential between the test and the reference electrode was recorded in steps of 5 s for 90 min.

To characterize our sensor, we first tested pure redox compounds, namely ascorbic acid, cysteine, and glutathione at different concentrations, dissolved in 10 g/L sodium chloride. All three compounds were shown to reduce PEDOT:PSS test electrode in a concentration-dependent manner. To evaluate the sensor performance for the different compounds, we set out to determine the upper and lower limits of detection and the earliest time point allowing reliable detection. The upper limit was defined as the highest concentration applied without saturating the sensor and the lower limit was determined to be the lowest concentration that has a signal above the limit of detection (LOD)[275]. LOD was determined to be the mean value of the blank ± 1.645 standard deviations of the blank (LOD = $MV_{blank} \pm 1.645$ x SD). To determine the linearity of the sensor response, we calculated the determination coefficient (R^2) for the linear fit of the potential difference vs analyte concentration for each time point of the measurement. The detection time was defined to be the time point when the signal for the lowest detectable analyte concentration was above the LOD (defined as the signal threshold) and when R^2 reached a threshold of 0.975 (defined as the R^2 threshold). A linear dependence of the measured potential on the applied concentration was observed for all three compounds at the detection time. In the current algorithm, we used mean values of replicates to determine the R^2 and for determining the signal threshold we employed mean values of the signal for the lowest detectable concentration. This means that the variability of the sample was not considered, and it is something we need to address in the future. Moreover, we reported the first possible point when detection and quantification are possible but not the time window, i.e., how long is the period where the signal is above the R^2 threshold and the signal threshold.

From the compounds we tested, the shortest detection time and lowest concentration were obtained for ascorbic acid. This can be a consequence of its negative charge at neutral pH and/or the fact that ascorbic acid donates two electrons upon oxidation while cysteine and glutathione donate only one. Cysteine is a zwitterion at neutral pH, and may be less attracted to positive sites in PEDOT. Glutathione had the lowest sensitivity, and its detection time was the longest. While it is negatively charged at neutral pH, the reason for these results could be its size, which affects the diffusion to and accessibility of oxidation sites on the electrode surface.

Due to the porous structure of PEDOT based films, ions can move in and out of them, which enabled the use of PEDOT based materials for ion sensing membranes[276] and as channel materials for organic electrochemical transistors[277]. To determine if the response observed with cysteine, glutathione and ascorbic acid was really due to redox activity and not a consequence of ion influx into the material, we applied serine, methionine and cystine on the sensor at the highest concentration tested for cysteine. Despite structural similarities, none of these compounds led to any potential change, indicating that the measured signal came from reducing species. This finding is supported by previous studies, reporting that the potential of PEDOT:PSS changes linearly with the logarithm of ion concentration and that the ion species do not have a major influence on the signal[276]. Moreover, redox interference was very strong in these systems and the presence of redox compounds even in small concentrations abolished the ionic response[276].

To investigate if we can detect the presence of bacteria on the sensor, we applied serial dilutions of *S*. Enteritidis in M9 minimal medium on the test electrode and measured the potential versus the reference electrolyte (**Figure 4a**). To process the data, we applied the algorithm described above, with the R^2 and the signal threshold. This identified the detection time (dV_t) to be at 13.29 min (**Figure 4b**). We found that *S*. Enteritidis can be detected and quantified on the two-electrode sensor as the amplitude of the measured potential difference was linearly correlated with the number of bacteria on the sensor. This implied that redox, rather than ionic processes are responsible for the observed signal. The signal threshold was at 6.6×10^6 CFU/sensor, while a significant difference was also observed between the 1.3×10^6 CFU/sensor and the blank.

To confirm the presence of electroactive compounds in the bacterial extracellular milieu, we performed Square Wave Voltammetry (SWV). This electrochemical technique amplifies the signal from the faradaic current by removing the signal from the charging current[268]. In our experiments, we used a glassy carbon (GC) WE, a solid Ag/AgCl quasi RE and a platinum CE. To examine the electrocatalytic effect of PEDOT, EDOT and PSS were electropolymerized on the GC electrode. The three electrodes were immersed in a culture of *S*. Enteritidis in M9 minimal medium. A forward scan between -0.2 and 0.7 V was performed. Two peaks were observed on the GC electrode, i.e., 0.118 V and 0.65 V (**Figure 4c**). Results were similar for the GC:PEDOT:PSS electrode, where an additional peak at 0.35 V was observed (**Figure 4d**). These experiments confirmed the presence of redox species in the bacterial culture and implied an electrocatalytic effect for PEDOT. The signals were however too weak to be used for the identification of redox species. To relate these findings to our two-electrode sensor, we measured the open-circuit potential of the sensor test electrode versus the solid quasi RE. The open-circuit potential was approximately 0.1 V, meaning that it is suboptimal for two out of three compounds identified to be oxidized on

GC:PEDOT:PSS WE. This is an important point and indicates that we might significantly increase the sensitivity of the sensor by biasing the test electrode.

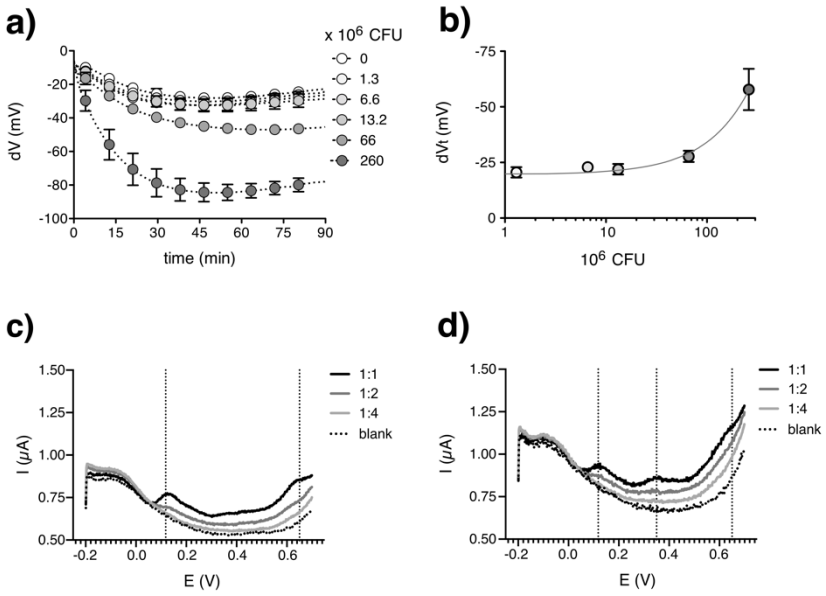

Figure 4: Detection of bacteria. **a)** Recording of potential difference over time for *S.* Enteritidis applied on the electrochemical sensor. Total number of bacterial cells in each recording is shown as colony forming units (CFU). Dotted lines represent mean values (MV) of potential difference over time ($n \geq 3$), symbols with error bars represent MV ± SD from data pruned with k = 100. **b)** Plot of the potential difference at the detection time (dV_t, 13.29 min) at each bacterial concentration from (a) shows a linear dependence ($R^2 = 0.975$) between dV_t and the number of bacteria. Symbols with error bars represent MV ± SD. **(c, d)** Square wave voltammetry using a **c)** GC electrode and **d)** GC:PEDOT:PSS electrode for recordings of an undiluted (1:1), a two-fold (1:2) and a four-fold (1:4) diluted culture of *S.* Enteritidis, with M9 minimal medium serving as blank. Dotted lines indicate peaks at 0.118 V, 0.35 V, and 0.65 V. Adapted from ref (18) with permission.

Our next quest was to identify which redox species in the bacterial cultures are causing the signal on the PEDOT:PSS sensor. To determine whether the redox activity comes from bacterial contact with PEDOT:PSS or if the presence of bacterial cells is necessary for any other reason, we removed them by filtration. To further remove enzymes and other bigger molecules, ultrafiltration with a 3 kDa cutoff was performed. When the bacterial cultures, their filtrates and ultrafiltrates were applied on the sensor, no difference could be observed between the three fractions. This indicates that the signal was caused by extracellular low molecular weight (LMW) substances. Searching the literature, we found three candidates: thiols[278], flavins[279] and NAD(P)H[280]. We knew that thiols can be detected from our sensor, as we tested cysteine and glutathione before. We could not apply flavins to the sensor, since it was not possible to obtain them in a reduced form commercially or to reduce them easily. We tested NADH and found that we can detect and quantify it on the sensor, the detection limit being 5 µM. Bacterial cultures from the exponential phase, their filtrates and ultrafiltrates were analyzed for the presence of all three compounds (i.e., thiols, flavins, NADH) but none of them appeared to be a plausible candidate. Thiols were present in bacterial cultures, filtrates and ultrafiltrates of exponential phase cultures, but their concentration was below the detection limit determined for cysteine, meaning that it is unlikely that thiols majorly contribute to the signal. NADH seemed to be absent and the amount of oxidized flavins was in the nM range. Moreover, we and others[281] have shown that

flavins bind to polyethersulfone membranes, meaning that the signal should be significantly reduced in ultrafiltrates of bacterial cultures, since flavins would not pass to the ultrafiltrate. We have not investigated this matter further in the current project but it would be of interest to apply more analytical techniques to understand what is causing the reduction of PEDOT:PSS. An option would be UV-Vis spectroscopy which can give information about the presence of peptide bonds, aromatic compounds, proteins etc. or Fourier Transform Infrared spectroscopy that provides a "molecular fingerprint". Ideally, we would separate the sample on high-performance liquid chromatography, analyze the fractions for their redox activity and then choose the relevant fractions to analyze on a mass spectrometer. It may also be possible to concentrate the sample using freeze-drying or vacuum (speedvac) in which case we might be able to reach concentrations high enough to discern peaks on a cyclic voltammogram.

Next, we aimed to investigate whether the sensor can be used to detect bacterial species other than *Salmonella*. We focused on a clinically relevant collection of species causing urinary tract infections, namely *E. coli*, *P. aeruginosa*, *S. aureus*, *Proteus mirabilis*, *E. faecalis* and *Klebsiella pneumoniae*[282]. They were grown in Luria Bertani (LB) broth until OD_{600} 0.4 and subsequently applied on the sensor. Without an exception, all caused a reduction of the PEDOT:PSS test electrode, albeit to different extents. These results are in accordance with earlier studies, reporting electroactivity in several of the tested species. EET in *E. coli* was enhanced by directed evolution and it was suggested that it occurs through hydroquinone secretion by bacteria[283]. These authors have further shown that overexpression of glycerol dehydrogenase (GldA, catalyzes NAD dependent oxidation of glycerol to dihydroxyacetone and the reverse reaction) in *E. coli* leads to electroactivity, however, the observed redox peaks did not match with those found for evolved electroactive bacteria[284]. *P. aeruginosa* is well known for its colourful redox-active metabolites pyocyanin and phenazine[73]. Quinone based electron shuttles were reported to mediate electron transfer in *Klebsiella pneumoniae*[65] and *E. faecalis*[70] and *Proteus mirabilis* has been shown to reduce azo dyes to non-toxic degradation products[285].

To test the potential diagnostic application of the sensor, we prepared urine cultures by inoculating urine from healthy volunteers with uropathogenic *E. coli*. Since the urine samples had different redox potentials, it was impossible to establish a stable baseline and to this end, we processed the sample to remove urine supernatant before applying the sample on the sensor. In this process, we also concentrated the sample to improve the effective sensitivity of the assay and could therefore detect bacteria in urine samples containing approximately 4 x 10^6 CFU/mL in 2.5 h. While this procedure was simple to perform and quick in comparison with culture-based methods, the drawback was that the sample needed to be processed in an equipped laboratory, making it impossible for this to be used in the field. In the future, this setup will be improved. One possibility would be to use the urine sample to inoculate the medium, place this on the sensor and observe the signal in time. As the bacteria would grow, the PEDOT:PSS electrode would get reduced, meaning that no blank signal is necessary and the output would rather be a relative signal change.

Currently, the sensitivity of the sensor is too poor to be used in diagnostic applications. We strongly believe that it could be improved by altering the device architecture (e.g. more exposed surface area) and by biasing the test electrode instead of keeping it at open-circuit potential. Moreover, we could employ an alternative – and possibly more sensitive electrochemical approach, such as an organic electrochemical transistor. Improving

the electrochemical detection would lead to higher sensitivity but would not improve the specificity of the sensor. In the current setting, redox-active molecules regardless of their origin can be detected. To target the sensor more towards bacteria, recognition elements need to be introduced. Several strategies have been reported for functionalization of PEDOT based surfaces. Carboxymethylated dextrans can be easily incorporated into PEDOT:PSS films and the exposed carboxyl groups enable covalent binding of proteins via amide bonds[187]. Moreover, aptamers or other molecules functionalized with azide groups can be coupled to carboxymethylated dextrans via copper-free click chemistry[286]. Silanization of PEDOT:PSS was enabled by incorporating poly(vinyl alcohol) as a handle, opening yet another possibility for covalent protein immobilization[188]. It would be of great use if the PEDOT:PSS sensor – in whatever form it would take – could be exposed to the sample and only the pathogens of interest would be immobilized. After washing, growth media can be added to the sensor and any electrochemical signal occurring would only come from the selected pathogens. Finally, 96 well plates with a three-electrode setup in each well are already commercially available, offering a platform for future multiplexing of electrochemical detection and monitoring of bacterial growth.

5.2 PAPER II

Our group has previously shown that optotracers can be used to detect and visualize the extracellular matrix in biofilms of certain gram-negative bacteria, without staining the bacterial cells themselves[19]. In contrast to gram-negative bacteria who have an outer membrane, the cell wall of gram-positive bacteria contains β-linked N-acetyl glucosamine and N-acetyl muramic acid as well as teichoic acids. We hypothesized that these polymers are plausible targets for optotracers and set out to test this in Paper II. We investigated optotracing for detection and visualization of *S. aureus*, a nosocomial pathogen of high clinical importance. The work is roughly divided into two parts – in the first part an optotracer that stains *Staphylococci* is described, while in the second part the mechanism of binding is investigated.

We started with three different pentameric optotracers: an all-thiophene based HS-84, and its structural analogues HS-163, which contains a central phenyl ring, and HS-167 which contains a central quinoxaline motif[207] (**Figure 5a, d, g**). Different from HS-84 and HS-163, HS-167 has a D-A-D structure which means it has different geometric and electronic properties. To determine if the spectral properties of optotracers change in the presence of *S. aureus,* the bacteria were resuspended in phosphate buffered saline (PBS) and added HS-84, HS-163 and HS-167, at 5 μM. As a negative control, we used *S.* Enteritidis, a gram-negative bacterium. Excitation and emission spectra (spec-plots) of these samples were compared to those of free optotracers in PBS. The spec-plots of free HS-84 and HS-163 closely resembled those of the two optotracers in the presence of bacteria. The fluorescence intensity of samples containing bacteria was slightly decreased, which can be attributed to light scattering (**Figure 5b, e**). For HS-167, no changes in the spec-plot were observed for *S.* Enteritidis relative to the free optotracer, while a marked increase in fluorescence and red-shifted excitation spectra were observed for *S. aureus* (**Figure 5h**). Using fluorescence microscopy, however, *S. aureus* appeared to be stained by all three optotracers (**Figure 5c, f, i**), yet the signal seemed strongest with HS-167. The reason for the discrepancy between the two fluorescence techniques might be that HS-84 and HS-163 bind *S. aureus* but do not undergo a conformational change, therefore the spectral signatures do not change. An alternative explanation is that the binding affinity of HS-84 and HS-163 is low and even if a minor part of the optotracer population is

bound and has altered conformation, the spectroscopic signal is masked by the predominantly unbound optotracers. To further investigate this question, serial dilutions of optotracers should be used (i.e., to increase the ratio of bound/unbound) and spectral microscopy should be performed to determine the local spectra. In summary, we identified HS-167 as the only suitable optotracer for fluorescence spectroscopy based detection of *S. aureus* and the best candidate for fluorescence microscopy.

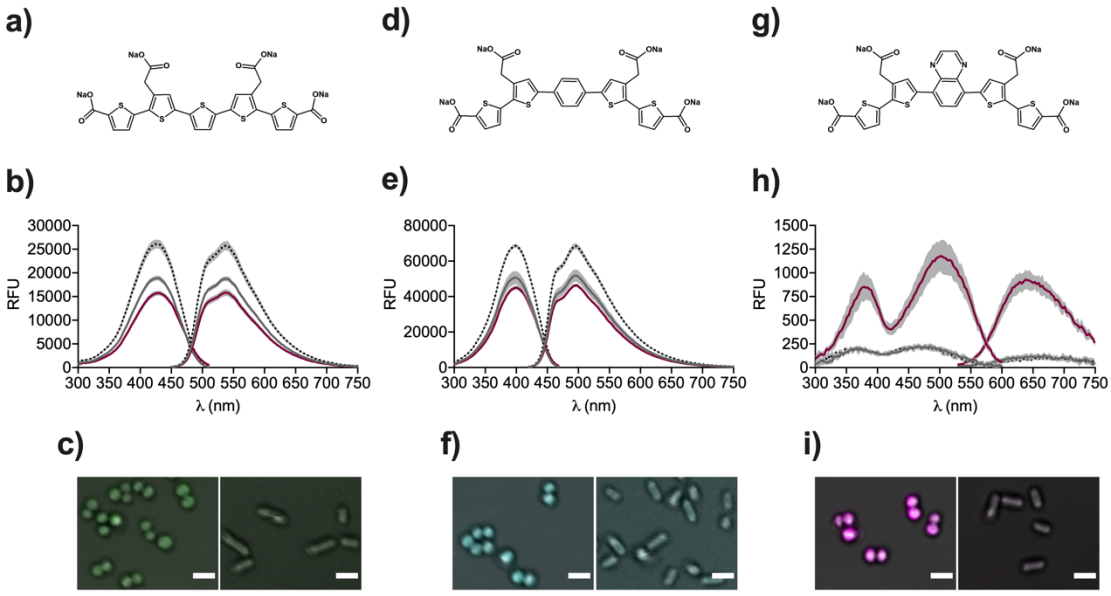

Figure 5: Fluorescence spectroscopy and microscopy using optotracers. (a, d, g) The chemical structures of **a)** HS-84, **d)** HS-163, and **g)** HS-167. **(b, e, h)** Spec-plots of **b)** HS-84, **e)** HS-163, and **h)** HS-167 in PBS (black dotted line) and when mixed with *S. aureus* (magenta) and *S.* Enteritidis (grey). Lines = mean values from n = 3-5, shaded areas = ± SD. **(c, f, i)** Merged transmitted light and pseudocoloured confocal images of *S. aureus* (left) and *S.* Enteritidis (right) mixed with **c)** HS-84 (green), **f)** HS-163 (cyan), **i)** HS-167 (magenta), in PBS. Scale bar = 2 μm.

To investigate whether HS-167 binds to other species of *Staphylococci,* we performed fluorescence spectroscopy of *S. epidermidis* with HS-167. The spectral signature was similar to that of *S. aureus*, confirming that HS-167 binds *S. epidermidis*. We performed serial dilutions of both species and visualized the relationship between fluorescence at a fixed wavelength (507 nm excitation, 625 nm emission) and absorbance at 600 nm (A_{600}). A linear relationship between fluorescence and A_{600} was observed for both species of *Staphylococci*, yet the slope values (i.e., RFU/AU) were different. While not much can be interpolated from two samples only, this experiment raised the idea, that the slope could be used to distinguish between different species of *Staphylococci*, even when they all bound HS-167.

The low fluorescence of HS-167 in its unbound state and the linear increase with bacterial density, prompted us to develop a high throughput assay for continuous monitoring of the growth and fluorescence of samples. The idea was to add HS-167 directly to the growth medium (Tryptic Soy Broth, TSB) inoculated with *S. aureus* and dispense this

in a 96 well plate. The plate was then incubated for >12 h in a plate reader at 37° C where A_{600} and fluorescence were measured continuously. Our results were unexpected - the fluorescence was not linearly dependent on the A_{600}, i.e., we could not reproduce what we observed when bacteria were resuspended in PBS. The non-linearity became more pronounced in the late exponential/ early stationary phase, and our first suspicion was biofilm formation. However, the same issue occurred when a mutant unable to form biofilm was used. We soon understood that the problem was the pH – as TSB contains glucose, bacterial metabolism leads to acidic byproduct formation, which can lower the pH of the culture for several units. Using HCl to mimic the acidification of TSB, we observed a two-fold increase in fluorescence when HS-167 was added to an acidified, compared to neutral TSB. In its original formulation, TSB is mildly buffered with di-potassium phosphate. To stabilize the pH of the medium, we increased the amount of potassium phosphate salts and termed the medium buffered TSB (bTSB). We confirmed that the growth of *S. aureus* is not affected by buffering the medium and that the pH remains stable, even when the culture enters stationary phase. With improved medium formulation, we established a workflow where samples can

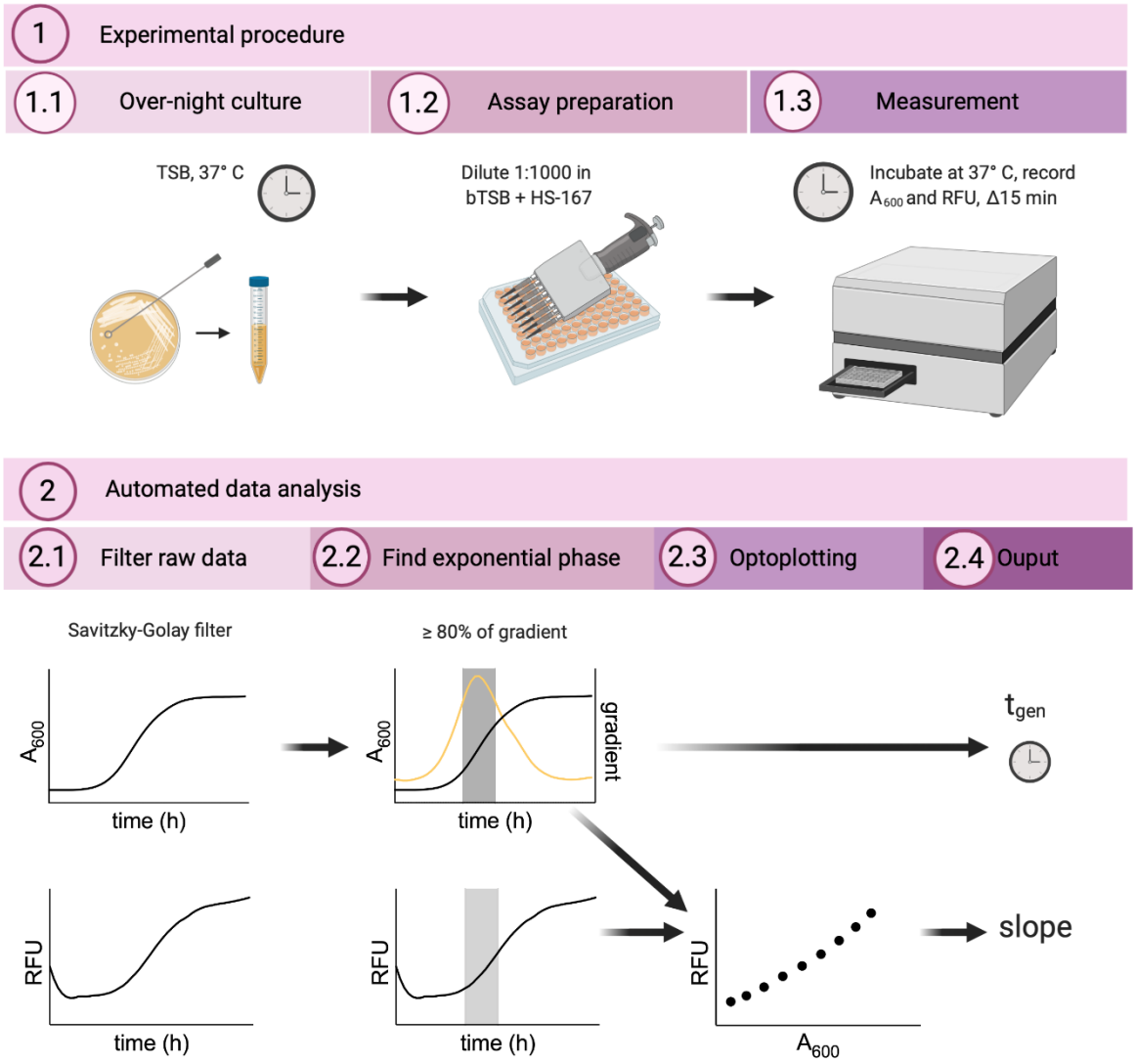

Figure 6: High-throughput optotracing for real-time monitoring of live bacterial cultures. The workflow of automated, high-throughput optotracing analysis based on real-time recordings in live bacterial cultures. The figure was created with Biorender.com

be read and analyzed with minimal efforts (**Figure 6**). The wet-lab part consists of plate preparation and incubation in the plate reader, as described above. The data extracted from the instrument is fed into a custom-made script, wherefrom the generation time and the slope (i.e., fluorescence vs A_{600}) are calculated. This workflow was tested using *S. aureus*, *S. epidermidis* and *S.* Enteritidis. We confirmed that HS-167 is non-toxic and does not affect the growth rate of any of the three species. A linear increase of fluorescence vs A_{600} was observed for *S. aureus* and *S. epidermidis*, while no increase in fluorescence was observed for *S.* Enteritidis over time. In agreement with previous observations, the slope was higher for *S. aureus* compared to *S. epidermidis*. We have hereby shown, that HS-167 is suitable for use in real-time assays of *Staphylococci* and that, if bound, its fluorescence correlates with bacterial density.

With the necessary tools at hand, we set out to test our initial hypothesis, i.e., that HS-167 binds the cell wall of *Staphylococci*. In our first approach, we screened a transposon library of *S. aureus* USA300 JE2, containing approximately 2000 strains with mutations in non-essential genes. All strains were screened using the approach described above, which allowed us to easily compare the mutants by comparing their slopes. Our first observation was that HS-167 bound to all mutants, meaning that the molecular target is a product of an essential gene, or that there are several targets, leading to redundancy. We did, however, observe differences between the slopes of the different mutants. To understand which genes contribute to altered binding of HS-167 to *S. aureus* USA300 JE2, we selected 2 mutants with the highest and 2 with the lowest slope from each of the 20 96 well plates screened. On top of these 80, we included 10 mutants with the lowest and 5 with the highest slopes from pooled plates analysis. These 95 mutants were then re-screened along with the wild type (WT). Those with mean slopes ≥ 25 % different from the WT were identified (**Figure 7a**). The first observation was that no mutants had slopes higher than the WT, i.e., we only identified mutants that exhibited lower binding. Out of 37 identified mutants, 29 were annotated and 18 of those were directly or indirectly linked to the cell envelope. Five mutants displayed ≤ 50 % binding compared to the WT, namely Δ*alr* (SAUSA300_2027), Δ*rot* (SAUSA300_1708), Δ*pknB* (SAUSA300_1113), Δ*menD* (SAUSA300_0946) and Δ*murA* (SAUSA300_2055). The gene *alr* codes for a constitutively expressed alanine racemase, which converts L-ala to D-ala for incorporation in PGN, WTA and LTA[287]. The mutant lacking this enzyme displayed the lowest binding of all tested strains. Interestingly, *alr2* (Δ*alr2*, SAUSA300_1292), an inducible homologue of *alr*[287], did not appear among the 95 candidate mutants. *Rot* (HTH-type transcriptional regulator rot; repressor of toxins) is a SarA homologue, a global regulator that negatively regulates many known virulence genes and positively regulates several cell surface proteins during the exponential phase of growth[288,289]. *Rot* translation is inhibited by RNAIII, a major effector of the *agr* system[290]. Interestingly, *rot* was shown to upregulate *dltD*, a member of the *dlt* operon that encodes proteins involved in D-alanine incorporation in the teichoic acids[288]. Recently, *agr* mediated WTA synthesis was shown to be mediated by *rot*, since Δ*rot* showed higher amounts of WTA in the cell wall, its production peaking in the stationary phase[291]. pknB (also termed Stk1) is a PASTA (penicillin-binding-protein and serine/threonine kinase-associated) kinase, having a central role in regulating metabolism and cell-wall homeostasis during stress[292]. PknB was shown to increase the expression of *dlt* operon by phosphorylating *GraR*[293] and to promote PGN synthesis[294]. Δ*pknB* strains have exhibited higher sensitivity towards beta-lactam antibiotics, making this kinase an interesting therapeutic

target[292,295]. *menD* (2-succinyl-5-enolpyruvyl-6-hydroxy-3-cyclohexene-1-carboxylate synthase) is involved in menaquinone biosynthesis and its deletion decreases the membrane potential, rendering bacteria more resistant to aminoglycosides[296]. Mutations in *menD* and *hemB* (also among the 37 mutants showing significantly lower slope than the WT) are often found in small colony variants[296]. *MurA* (UDP- N-acetylglucosamine enolpyruvyl transferase) catalyzes the reaction between UDP-N-acetylglucosamine and phosphoenolpyruvate, the first step in PGN synthesis[297]. The gene *murA* exists in two copies, *murA* and *murA2*. The mutation causing reduced binding of HS-167 was in *murA*, which is known to cause a reduction of the peptidoglycan (PGN) content of cell walls[298]. In contrast, no such effects are known for Δ*murA2*[298], which explains why this mutant (SAUSA300_2078) did not appear among the group of 95 candidate mutants. Taken together, the transposon screen did not provide us with a definite target for HS-167, but it gave a clear indication that the cell envelope plays a major role. This is in accordance with lack of binding in *S*. Enteritidis that has a differently structured cell envelope.

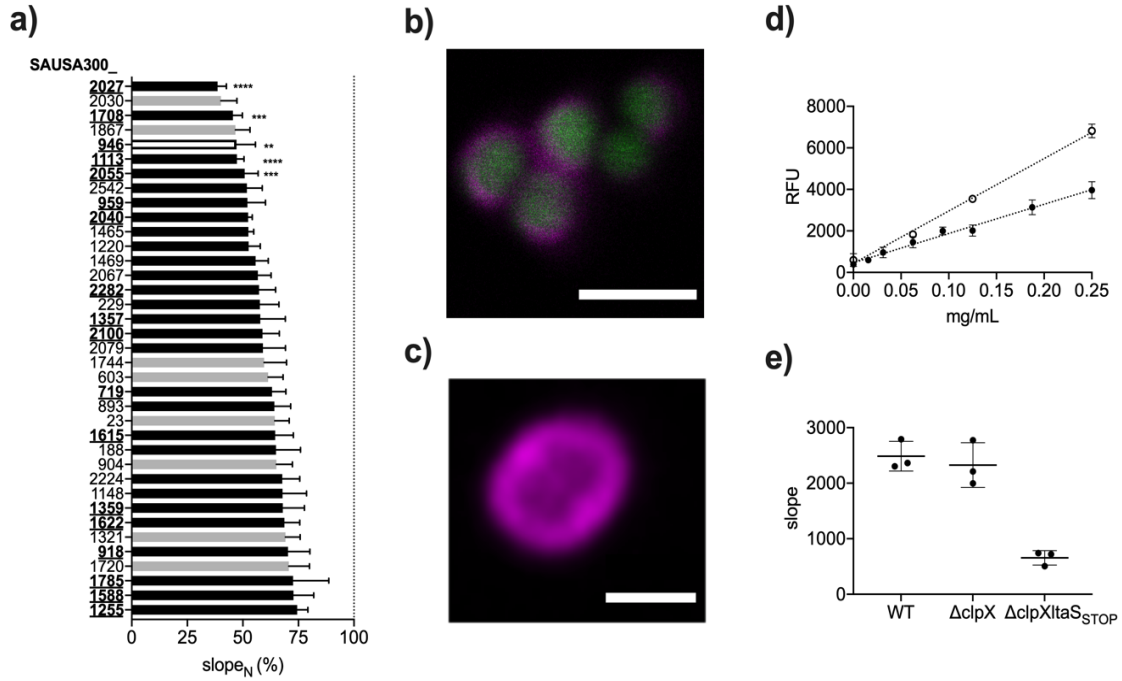

Figure 7: Identification of binding targets for HS-167 on *Staphylococci*. a) List of 37 mutants selected from the Tn library whose normalized slope (slope$_N$) differs significantly from the WT, as determined by one-sample t-tests ($p \leq 0.05$). Strains with mutations in annotated sequenced (black), non-sequenced (white) and non-annotated (grey) genes are shown. Bars show mean, error bars show + SD from n = 4. Labels of annotated genes with functions related to the cell envelope are written in bold and underlined. Annotated genes showing ≥ 50 % reduction in HS-167 binding were SAUSA300_2027 ($p<0.0001$), SAUSA300_1708 ($p=0.0001$), SAUSA300_946 ($p=0.0011$), SAUSA300_1113 ($p < 0.0001$), SAUSA300_2055 ($p = 0.0005$). **b)** Confocal microscopy of HS-167 bound to GFP-expressing *S aureus* 8325-4. Magenta = fluorescence of HS-167 bound to the cell wall, green = GFP. Scale bar = 2 μm. **c)** Airyscan image of HS-167 bound to *S. epidermidis* (magenta). Scale bar = 1 μm. **d)** Fluorescence intensity of HS-167 (10 μM in PBS) at Ex. 507 nm and Em. 625 nm, at different concentrations of PGN (black circles) (n = 3) and LTA (clear circles) (n = 2) from *S. aureus*. Circles show mean, error bars show ± SD. **e)** Slopes from *S. aureus* WT, *S. aureus* Δ*clpX* and *S. aureus* Δ*clpXltaS$_{STOP}$* at different dilutions in PBS + 10 μM HS-167. Slopes were compared by ANOVA ($F = 37.13$, $p = 0.0004$) and Tukey´s post-hoc test (*S. aureus* WT vs *S. aureus* Δ*clpXltaS$_{STOP}$* $p = 0.0006$; *S. aureus* WT vs *S. aureus* Δ*clpX* $p = 0.78$; *S. aureus* Δ*clpX* vs *S. aureus* Δ*clpXltaS$_{STOP}$* $p = 0.001$). Lines show mean, error bars show ± SD.

Next, we performed confocal and super-resolution microscopy to visualize the location of HS-167 in *S. aureus* and *S. epidermidis* (**Figure 7b, c**). Both experiments clearly showed that HS-167 locates within the cell wall and not inside the cell. Further, we tested whether HS-167 binds to isolated components of the cell wall of *S. aureus*, namely PGN and LTA, both components being indirectly identified in the transposon screen. As we prepared serial dilutions/suspensions of the two isolated compounds and added HS-167, the fluorescence increased linearly with increased concentration of PGN or LTA (**Figure 7d**). On the contrary, no comparable increase in fluorescence was observed when LPS was mixed with HS-167. These results corroborated our previous observations, however, working with isolated compounds has the drawback of *i*) limited purity and *ii*) exposure of macromolecular parts that would naturally not be exposed. To this end, we have complemented the transposon screen with a mutant in LTA synthesis, i.e., *S. aureus* 8325-4 Δ*clpXltaS*$_{STOP}$, kindly donated by Prof. Dorte Frees. While LTAs are considered essential for *S. aureus*, it was found that they become non-essential in a mutant lacking ClpX chaperone[55]. We therefore compared the slopes of *S. aureus* WT, *S. aureus* Δ*clpX* and *S. aureus* Δ*clpXltaS*$_{STOP}$ overnight cultures resuspended in PBS + HS-167. No difference in the slope was observed between Δ*clpX* and WT, which was surprising, since it was previously reported that the deletion of *clpX* in other strains of *S. aureus* resulted in increased cell wall thickness and altered appearance of the cell wall as determined by TEM analysis[299]. The Δ*clpXltaS*$_{STOP}$ strain, however, exhibited a marked decrease in slope, indicating that LTAs are not the only, but an important binding target of HS-167 (**Figure 7e**). On the other hand, it was shown for another strain that the PGN of Δ*clpXltaS*$_{STOP}$ strain had much less highly cross-linked muropeptides compared to the WT and Δ*clpX*, offering another possible explanation for reduced binding. LTA deficient cells were reported to be larger, have a thicker and more irregular cell wall and cluster more[55], which we did not account for when calculating the slope and might have influenced our results. However, since the difference between the WT and the LTA mutant is nearly 5-fold, we believe that this is not an artefact. Taking these experiments together, we were fairly convinced that HS-167 binds to PGN and LTAs in the cell wall of *S. aureus*.

The structure of PGN (except for the bridge peptide) is rather universal and several species have the same type of LTA as *S. aureus,* which lead us to assume that HS-167 will bind other gram-positive bacteria as well. To test this hypothesis, we investigated whether HS-167 binds *E. faecalis*, a gram-positive bacterium in the same class (i.e., Bacilli) as *S. aureus*. To our surprise, no binding during the exponential phase was observed when *E. faecalis* was grown in bTSB + HS-167 or when resuspended in PBS + HS-167 and examined under the microscope. We considered that the binding affinity might be different for the two gram-positives tested, due to the different microenvironment on the cell surface. To investigate this, we examined the surface properties of *S. aureus* and *E. faecalis*. Firstly, we measured the zeta potential of the two bacteria and found no difference. To double-check, we also measured the zeta potential of WT USA300 JE2 and two mutants that showed reduced binding. No difference was found there either. Next, we set out to investigate surface hydrophobicity using bacterial adhesion to hydrocarbons (BATH) assay[267]. In this assay, bacteria in a designated buffer are mixed with hexadecane and the recovery, i.e., the proportion of bacteria not bound to hexadecane is calculated. The lower the recovery, the more hydrophobic are the bacteria. In parallel with BATH, HS-167 was added to autologous samples and their fluorescence was recorded. Buffers with different salt concentrations and pH were used to alter the

hydrophobicity of bacteria. Summarizing the results, *S. aureus* was most hydrophobic, followed by *E. faecalis*, while *S.* Enteritidis was most hydrophilic. The fluorescence of HS-167 in the presence of different bacteria correlated well with their hydrophobicity. Indeed, at acidic pH, when the hydrophobicity of *E. faecalis* was highest, HS-167 bound to this bacterium. Results from fluorescence spectroscopy were corroborated by microscopy, as we could visualize the binding of HS-167 to both gram-positive bacteria tested at pH 5.0, while at neutral pH, only *S. aureus* could be visualized and the fluorescence was lower. These experiments suggested that HS-167 binds bacteria predominantly via hydrophobic interactions, however other types of non-covalent interactions cannot be excluded.

In summary, HS-167 is the first optotracer reported to bind gram-positive bacteria, as we showed for *S. aureus* in this study. We found that the optotracer can be used for fluorescence spectroscopy and microscopy. The high-throughput optotracing assay facilitated our work tremendously, but the data analysis is relatively crude at this time and will be improved in the future. Importantly, the interval for the exponential growth phase was pre-determined, which is something that worked for our setup, but would not work for very slow or very fast growing strains. In future studies, it would be useful to incorporate an algorithm where the exponential phase would be determined in a more flexible way, so that a wider selection of bacteria could be tested. The transposon screen has provided us with valuable insight, but there are some control experiments we have not performed that would be of value. Beyond simple optical microscopy, we have not examined the phenotypes of transposon mutants in detail. If any of the mutations would result in increased cell size, for example, the relationship between volume and surface would change, which would affect the slope. Moreover, the mutations were confirmed with PCR, but we have not tested for off-target effects. Complementing the mutants with a plasmid-encoded gene that was disrupted, would be a good control to perform to ensure that the observed phenotype is due to the predicted mutation only.

To apply optotracers for research in microbiology, it is of crucial importance to understand how they bind. Our observations, that binding to gram-positive bacteria changes depending on the different pH and salt concentration were expected and have been shown for several other dyes[300,301]. This is a double-edged sword; on one side the subtle changes in hydrophobicity of different species or even strains, might enable their discrimination with HS-167, while on the other, this requires tight control of environmental parameters, which limits the experimental setups in which this optotracer can be used. As our knowledge advances, we can hopefully use both sides of the sword by designing optotracers for the desired application.

5.3 PAPER III

This study was performed to advance our understanding of the structural requirements for optotracer detection of *S. aureus*. A selection of optotracers (**Figure 8**) with varying *i)* lengths of the oligothiophene backbone, *ii)* total charge, and *iii)* charge distribution along the conjugated backbone was screened to determine which of these characteristics are important for fluorescence spectroscopy based detection of *S. aureus*. Detection is possible when the spectral signatures and/or the fluorescence intensity of the optotracers is altered. Typically, a red-shifted excitation spectrum and an increased fluorescence are observed upon binding[302].

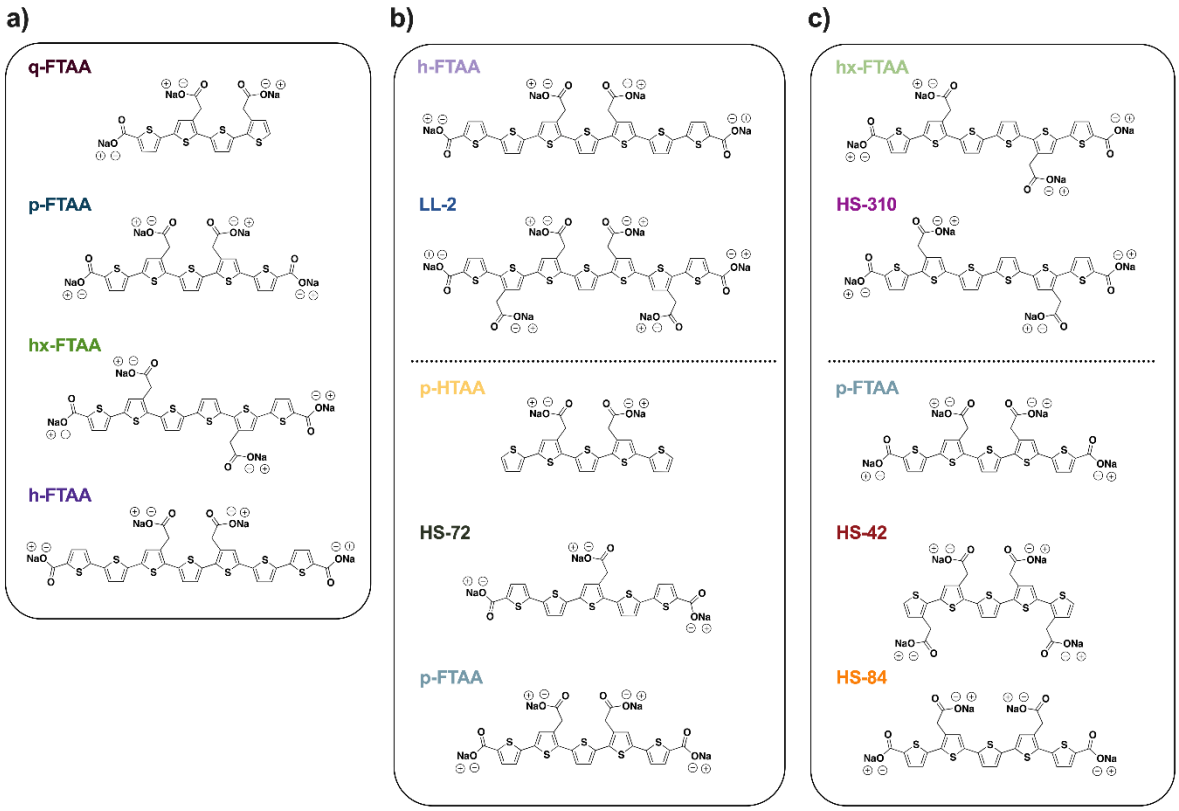

Figure 8: Chemical structures of optotracers. Optotracers with different **a)** length of the conjugated backbone (*i.e.*, number of thiophene rings), **b)** total charge, and **c)** charge distribution along the conjugated backbone. The colour-coded names of optotracers correspond to the colour codes in the following figures.

To determine whether binding occurs, the spectral signatures of free optotracers were compared to those of optotracers in the presence of bacteria. *S. aureus* overnight cultures were washed and resuspended in PBS and adjusted to OD_{600} approximately 2. Thereafter, sample aliquots were added 1 µM of each optotracer. The excitation and emission spectra (spec-plots) of these samples were compared to those of the free optotracer in PBS. As a control, we used *S.* Enteritidis, a gram-negative bacterium, whose spectra were also compared to those of the free optotracers. To objectively analyze the optotracer signals, we developed an algorithm to *i)* extract peak wavelengths, *ii*) determine the spectral shift, and *iii*) quantify relative fluorescence intensity. The spectral shift was determined by cross-correlation, a measure of similarity between two signals at different lag positions that determines the lag (i.e., shift) at which the best overlap is reached. To quantify relative fluorescence intensity, we first aligned the spectra of the free optotracer with those of the optotracer in the presence of either *S. aureus* or *S.* Enteritidis, according to the shift determined by cross-correlation. Next, the integrated fluorescence of the overlapping spectra was calculated. The relative fluorescence was presented as the quotient of the integrated fluorescence (i.e., area under the curve, AUC) of the optotracer in the presence of bacteria (AUC_{sample}) and that of the free optotracer ($AUC_{optotracer}$).

Previous work on optotracers has shown that the number of thiophene rings, i.e., the length of an optotracer, is an important property influencing detection as well as binding to protein aggregates[205] and polysaccharides[210]. To investigate the effect of the length of optotracers on *S. aureus* detection, we screened a small panel containing tetra-, penta-, hexa- and heptameric optotracers, namely q-FTAA, p-FTAA, hx-FTAA and h-FTAA

(**Figure 8a**), by characterizing their photophysical properties in the presence and absence of bacteria (**Figure 9a-d**). We first determined the peak excitation (Ex. λ_{max}) and emission (Em. λ_{max}) wavelengths. No changes in Ex. λ_{max} or Em. λ_{max} were observed for q-FTAA and p-FTAA in the presence of *S. aureus* (**Figure 9a,b**). Red-shifted Ex. λ_{max} were observed for hx-FTAA and h-FTAA, a minor blue shift (i.e., towards shorter wavelengths) in Em. λ_{max} was observed for h-FTAA (**Figure 9c,d**). Interestingly, a second emission peak appeared for hx-FTAA in the presence of *S. aureus* (**Figure 9c**), as has previously been observed for hx-FTAA bound to amyloids[204]. For *S.* Enteritidis, no shifts in Ex. λ_{max} were observed for any of the optotracers, while h-FTAA exhibited a blue shifted Em. λ_{max} (**Figure 9a-d**).

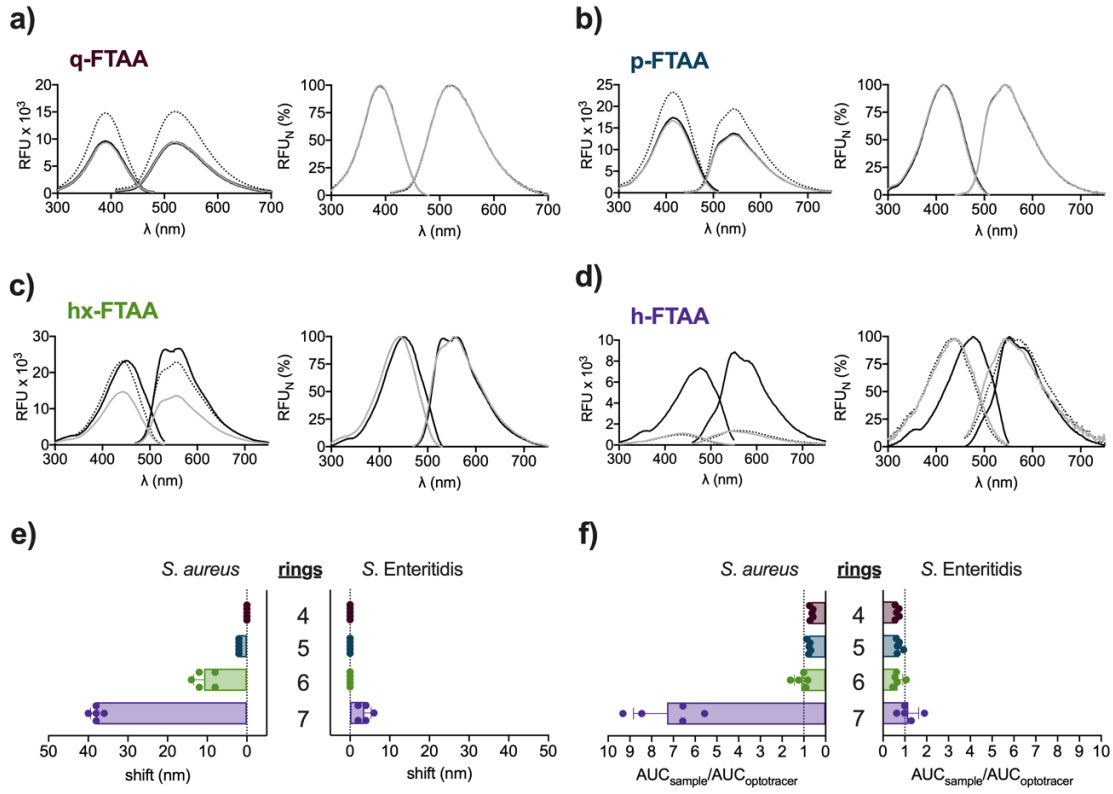

Figure 9: Optotracer length (= number of thiophene rings) influences binding. (a-d) Spec-plots (left) and normalized spec-plots (right) of **a)** q-FTAA, **b)** p-FTAA, **c)** hx-FTAA and **d)** h-FTAA. Dotted line = optotracer, grey line = *S.* Enteritidis + optotracer, black line = *S. aureus* + optotracer. Lines show mean of n = 5. **e, f)** Shift (**e**) and fold increase in fluorescence intensity (**f**) for excitation spectra of q-FTAA (4 rings), p-FTAA (5 rings), hx-FTAA (6 rings) and h-FTAA (7 rings) in the presence of *S. aureus* and *S.* Enteritidis. Colour codes of spec-plot titles correspond to bars. Bars show mean values, dots show individual experimental points, error bars show + SD.

Excitation and absorption spectra were previously identified to reflect the binding and planarization of optotracers[303] and, accordingly, our peak wavelength comparison mostly yielded shifts in Ex. λ_{max} when the different optotracers were incubated with *S. aureus*. Therefore, cross-correlation analysis was only performed on the excitation spectra. In the presence of *S. aureus*, no spectral shift was observed for q-FTAA, while a small shift (2 nm) was observed for p-FTAA, an increased shift for hx-FTAA and the largest spectral shift for h-FTAA (**Figure 9e**). In the presence of *S.* Enteritidis, a shift was only observed for h-FTAA, albeit only 1/10 of that observed with *S. aureus*. Fluorescence increase was observed only for *S. aureus* in the presence of h-FTAA, and not with any other

optotracer. No fluorescence increase was observed for *S.* Enteritidis in the presence of any of the tested optotracers (**Figure 9f**).

To determine how the spectroscopic results correlate with fluorescence staining observed under the microscope, we added optotracers to mixed samples containing *S. aureus* and *S.* Enteritidis and imaged them under the confocal microscope. At 1 μM concentration, the fluorescent *Staphylococci* could only be observed when hx-FTAA and h-FTAA were used. The small spectral shifts observed when p-FTAA was added to *S. aureus* and h-FTAA was added to *S.* Enteritidis are therefore not enough to produce a signal under the microscope at this optotracer concentration. Taken together, these results indicate that the optotracer length positively correlates with its ability to detect *S. aureus.*

Since both, the optotracers (due to the presence of carboxyl and acetate groups) and the bacteria are negatively charged, we hypothesized that some electrostatic repulsion exists between them. To investigate the effect of optotracer charge on the detection of *S. aureus,* we compared optotracers of equal length but different total charge (**Figure 8b**). h-FTAA (4 charged groups) was compared with LL-2 (6 charged groups), another heptameric optotracer containing two additional acetate groups. In the presence of *S. aureus*, a red-shifted Ex. λ_{max} was observed for LL-2 (**Figure 10a**). A spectral shift was likewise identified by cross-correlation analysis (**Figure 10b**). Peak and spectral shifts were approximately 1/3 of those observed by h-FTAA. No shifts were observed for LL-2 in the presence of *S.* Enteritidis. No fluorescence increase was observed for LL-2 in the presence of either of the two species (**Figure 10c**). Smaller spectral shifts and the absence of fluorescence increase indicate that the introduction of additional charged groups reduced the interaction of the heptameric optotracer with *S. aureus*. On the other hand, the shift was abolished also in the presence of *S.* Enteritidis, demonstrating that charges can be used to tune the selectivity of optotracers. Taking these results into account, we approached this from the opposite direction, and investigated if we could improve detection by reducing the number of charged groups on the optotracers. We had earlier only detected very small spectral shifts for p-FTAA in the presence of *S. aureus*. We compared it to HS-72 (3 charged groups) (**Figure 10d**), and p-HTAA (2 charged groups) (**Figure 10e**). The same trend appeared as with the heptameric optotracers – reducing the charge increased the spectral shift (**Figure 10f**) when the optotracers were incubated with *S. aureus*. None of the optotracers exhibited a spectral shift when incubated with *S.* Enteritidis. Fluorescence increase was only observed for p-HTAA in the presence of *S. aureus* (**Figure 10g**), and not in the presence of *S.* Enteritidis. No fluorescence increase was observed for the other pentamers in the presence of either *S. aureus* or *S.* Enteritidis. An informative comparison is that between p-FTAA and LL-2, the former having 0.8 charges/thiophene ring and the latter 0.86. The recorded spectral shift is approximately 6 x larger for LL-2 compared to p-FTAA, indicating that the length of the conjugated backbone is of greater importance for spectral detection than the charge of the molecule.

In the amyloid field, it was recently shown that the distribution of the anionic groups, i.e., the "geometry" of the molecule, plays a crucial role for the spectral separation of β-amyloid and tau[206]. We therefore compared optotracers of equal length and total charge but with varied distribution of charged groups (**Figure 8c**) to investigate if this affects their ability to detect *S. aureus*. Two hexamers, hx-FTAA and HS-310 were included and three pentamers, p-FTAA, HS-42 and HS-84. No differences in relative fluorescence intensity and in peak or spectral shifts were identified within any of the two groups. This indicates that the

distribution of the charged groups for the tested optotracers did not influence their ability to detect *S. aureus*.

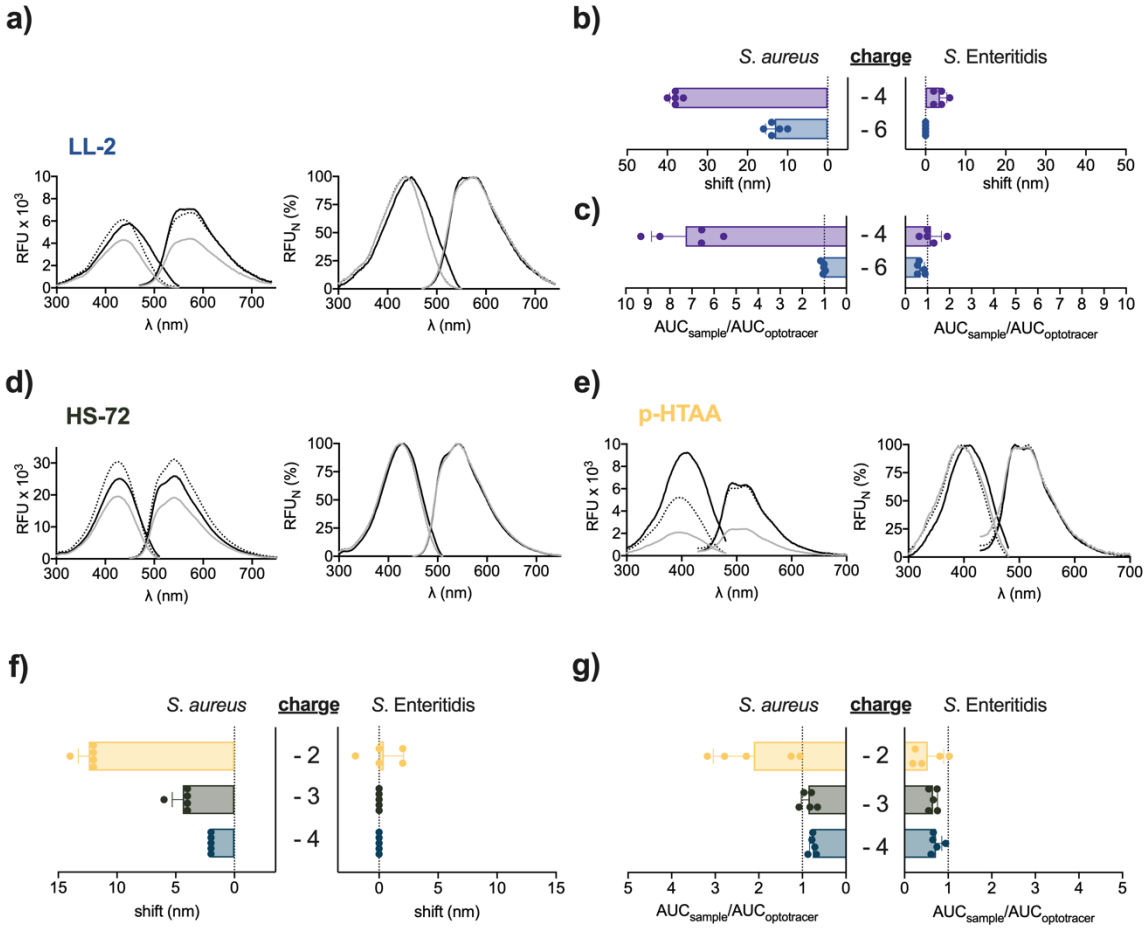

Figure 10: Optotracer charge influences binding. (a, d, e) Spec-plots (left) and normalized spec-plots (right) of **a)** LL-2, **d)** HS-72 and **e)** p-HTAA. Dotted line = optotracer, grey line = *S.* Enteritidis + optotracer, black line = *S. aureus* + optotracer. Lines show mean of n = 5. **(b, c)** Shift (**b**) and fold increase in fluorescence intensity (**c**) for excitation spectra of h-FTAA (charge = -4) and LL-2 (charge = -6) in the presence of *S. aureus* and *S.* Enteritidis. **(f, g)** Shift (**f**) and fold increase in fluorescence intensity (**g**) for excitation spectra of p-HTAA (charge = -2), HS-72 (charge = -3) and p-FTAA (charge = -4) in the presence of *S. aureus* and *S.* Enteritidis. Colour codes of spec-plot tittles correspond to bars. Bars show mean values, dots show individual experimental points, error bars show + SD.

Based on our findings presented in Paper II, we hypothesized that the optotracers bind to the cell wall of *S. aureus*. To determine whether this is the case, we tested a selection of optotracers, namely hx-FTAA, HS-310 and LL-2. Those were selected since they all exhibited a pronounced red-shifted excitation spectra when incubated with *S. aureus*, no shift when incubated with *S.* Enteritidis and did not show substantial variation in the data. We performed confocal microscopy of a red fluorescent protein FP650 expressing *S. aureus,* stained with the three different optotracers. In all cases, optotracers appeared as a "green ring" around the intracellular FP650, confirming their predominant binding in the cell envelope.

In summary, the number of thiophene rings, i.e., the length of the optotracer and its total charge were both important determinants for optotracer based detection of *S. aureus*. Within the selection of optotracers tested, the distribution of charged groups did

not appear to be an important factor. We propose that an increased number of thiophene rings leads to increased aromatic interactions between optotracers and the cell wall components. Interaction of sugars and aromatic rings is well-established[304] and aromatic interactions were shown to be crucial for Wheat Germ Agglutinin binding to PGN[305]. Moreover, we suggest that hydrophobic interactions are increased as the number of rings increases. In contrast, negatively charged groups lead to electrostatic repulsion and discourage the interaction between optotracers and bacteria. For the least charged and longest optotracer, h-FTAA, a small spectral shift was observed for *S.* Enteritidis, implying that the negatively charged groups are important for the selectivity of the optotracers, i.e., to prevent non-selective interactions. As for the distribution of charged groups, it is important to keep in mind that the selection of optotracers tested was limited and it is possible that an effect would be observed, if a wider selection of optotracers would be tested.

Several recent studies have unveiled the potential for optotracer use in microbiology. To move the field forward, however, it is necessary to understand where and how (on bacterial cells or in the biofilm matrix) the optotracers bind so that their design could be targeted for specific applications. A brute force approach to do this would be to conduct big screens with many optotracers vs many targets and find patterns that would hopefully reveal the underlying molecular mechanisms. The optotracers with and without the relevant targets should be tested at different environmental conditions, since we have previously seen that altering the pH or salt concentration can alter binding[21] – this is important not only for their applicability but also to understand the types of interactions governing binding. Moreover, different concentrations of optotracers need to be tested, since we know (from unpublished data) that optotracers can detect different targets depending on the concentration. To extract such information, however, we would need to establish approaches for data analysis that will provide us with quantifiable information that can be used to compare and rank optotracers. In the present study, we explored some options for automated data analysis with a limited set of optotracers and have demonstrated that different approaches can be taken to obtain complementary information. In the future, alternative methods will be explored and we hope to eventually establish a valid pipeline for automatic processing and visualization of spectral data.

5.4 PAPER IV

Indoor high touch surfaces are exposed to different environmental conditions, such as different humidity levels and the presence of air pollutants. A variety of substances are applied to these surfaces via touch. In this study, a systematic approach was developed to evaluate corrosion and antimicrobial properties of high-touch surfaces, using copper as an example.

To set the stage, a pilot study was performed where three people were applying fingerprint contact (5 times a week) on a copper surface exposed to daily wet/dry cycles in a climatic chamber (to mimic the atmospheric corrosion) for up to 4 weeks. Already after one week, locally occurring corrosion features were present on the copper surfaces, as determined by scanning electron microscopy (SEM). To investigate the role of sweat in the fingerprint contact induced corrosion, we simulated the fingerprint contact by applying artificial sweat (ASW), prepared as previously described[306]. The ASW was applied by an air brush, resulting in an even and reproducible surface distribution of small-sized droplets (10 – 150 μm) with the mean deposited mass of 6.88 ± 0.77 mg ASW/cm^2, corresponding to palm-surface contact of approximately 70 people[307]. ASW was sprayed daily on copper surfaces that were incubated in

a climatic chamber at cyclic wet/dry cycles. The surfaces with and without ASW deposition were compared. Using grazing incidence X-ray diffraction (GIXRD), energy dispersive X-ray spectroscopy (EDS) and Fourier transform infrared spectroscopy (FTIR), the predominant corrosion products were identified to be cupric (CuO) and cuprous (Cu_2O) oxide, with local presence of chloride-rich corrosion products, possibly $Cu_2Cl(OH)_3$ and after four weeks also $Na_2Cu(CO_3)_2$ x $3H_2O$. ASW-mediated formation of corrosion products had a profound influence on the surface appearance of copper, resulting in visible surface darkening already after the first exposure. Compared to their counterparts without ASW pre-deposition, ASW exposed, corroded surfaces exhibited increased hydrophilicity over time, as determined from the contact angle measurements. This is of interest since surface hydrophobicity is an important determinant for microbial adhesion[308,309]. Moreover, SEM showed that these surfaces had a rather different topography (e.g. surface roughness) as well, which could likewise influence the attachment of bacteria.

Understanding the profound effects of ASW on copper surface characteristics, we next investigated its effect on bacterial adhesion to and antimicrobial properties of copper. Different approaches were tested to apply bacteria on the surfaces, and we found that the most consistent was a "quasi-dry" protocol. According to this protocol, *E. coli* were resuspended in ASW and 3 μL of were applied to either copper surfaces or a glass control surface (1 x 1 cm^2). At different incubation times, the surfaces were placed in 2 mL ASW and vortexed. The ASW was plated on agar plates to determine the number of detached viable bacteria. Bacterial numbers remained stable on glass surfaces, while they declined sharply on copper. The fastest rate of killing was observed for copper surfaces aged in the presence of ASW, followed by copper aged without ASW and finally by as-received copper surfaces. To determine if some viable bacteria still adhered to the surfaces after vortexing, the copper surfaces were imprinted on agar plates. No growth was ever observed. However, when checking these surfaces with SEM (after rigorous vortexing and imprinting on agar), attached bacteria were found to be present. More bacteria were observed on surfaces that were aged with ASW, which could be a consequence of higher surface roughness and/or increased hydrophilicity of these surfaces.

To investigate the viability of bacteria on copper surfaces, a bacterial viability assay (i.e., Live/Dead stain) was performed, using a commercially available kit. The kit contains two DNA (and RNA) intercalating dyes, SYTO9 and propidium iodide (PI). The dyes are used to determine the membrane integrity of the cell, from which its viability is inferred. SYTO9 enters live and dead cells, while PI only enters cells with compromised membrane and is used to label dead cells. The fluorescence intensity of both dyes is increased upon binding to DNA[310] but the PI has a higher affinity for DNA compared to SYTO9, therefore dead cells often appear red instead of yellow[311]. For these experiments, stationary phase *E. coli* resuspended in ASW were sprayed on glass (= control) and one day aged copper surfaces (without ASW pre-deposition) and incubated for 0 and 20 min. After incubation, the surfaces were turned upside down on a drop (5 – 10 μL) of Live/Dead stain on a cover glass and sealed with nail polish. After approximately 10 – 15 min incubation, the samples were imaged under a confocal microscope. At 0 min incubation time, the majority of bacteria on glass surfaces were alive, while all bacteria on copper appeared dead (**Figure 11**). This being said, the actual time bacteria were exposed to glass/copper is incubation time on the surface + incubation time with the dye + imaging time, meaning that no bacteria were exposed for less than approximately 15 min, explaining why all appear dead on copper "already" at 0 min incubation

time. Membrane damage is one of the major mechanisms of copper toxicity towards bacteria[247], therefore it is understandable that membrane integrity is severely impaired when bacteria come in contact with copper surfaces. After 20 min incubation, many bacteria appeared dead also on glass surfaces, most likely because of desiccation. As expected, all bacteria appeared dead on copper surfaces after 20 min. Interestingly, all bacteria on copper were red, not orange or yellow, while dead bacteria on glass were more often orange or yellow, suggesting that more SYTO9 was present in the dead bacteria on glass compared to copper. We also noticed that both SYTO9 and PI gave some unspecific signal on copper surfaces since they bound to what we assumed were corrosion products. This was corroborated by the observation that no background staining was observed on polished surfaces (personal observation). Overall, Live/Dead staining has an obvious advantage over culturing approaches since it enables visualization of dead and non-culturable cells. However, there are several limitations associated with it as well. Beyond the conceptual question of how to define life and death in microbes[312], there are practical issues with using PI as a marker for dead cells. It has been previously reported that an increased membrane potential of viable cells can amplify the ion motive force for cations, such as PI, enabling its entrance into actively growing viable cells[313] and it is of value to test the strain of interest to see if it can be used with Live/Dead stain at all. To understand the killing kinetics, we would ideally like to have the results for Live/Dead stain within minutes resolution, but this was unfortunately not possible due to the incubation time

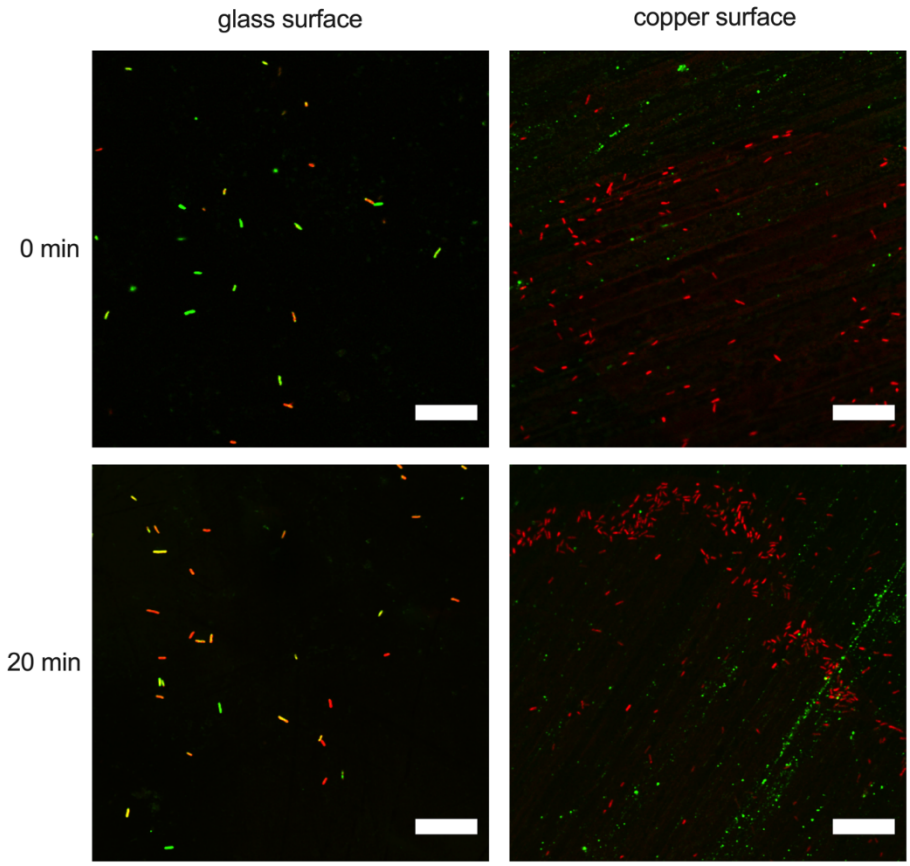

Figure 11: Live/Dead staining of *E. coli* on glass and copper surfaces. Confocal microscopy images of *E. coli* on glass (left) or copper (right) surface incubated for 0 (top row) or 20 min (bottom row). After incubation, bacteria were stained with Live/Dead stain. SYTO9 (green channel) labels all bacteria, PI (red channel) labels dead bacteria only. Scale bar = 25 μm.

for the dye and the time it took for us to focus on the samples and image. This is, however, a general limitation with microscopy-based methods and it is difficult to envision it could be improved.

It has been widely argued that the copper toxicity towards bacteria stems from copper ions[254,258,314]. To determine the amount of copper ions released from our surfaces, atomic absorption spectroscopy was employed. Surfaces aged for one day (without ASW pre-deposition) were found to release approximately 0.7 $\mu g/\mu m^2$ of copper ions when drops of 3 µL ASW were applied and incubated for 10 min. In parallel experiments, copper chloride ($CuCl_2$) was added to bacteria in ASW to determine the copper ion concentrations necessary for bactericidal effects. The results show that substantially higher concentrations of Cu^{2+} ($CuCl_2$) are needed for bacterial killing than that measured in ASW drops after 10 min contact with a copper surface. This suggests that surface contact is necessary for copper surface toxicity. Interestingly, it has previously been shown that applying $CuSO_4$ on iron surfaces leads to a bactericidal effect at concentrations of $CuSO_4$ that do not kill bacteria if applied on glass[315]. A later study by the same group showed that the reason for iron-induced copper ion toxicity is the conversion of Cu^{2+} to Cu^{+}, the latter having a more potent bactericidal effect[316]. It would therefore be of interest to investigate the redox state of copper ions released from the surfaces to understand if this might influence the concentration needed for the bactericidal effect.

In this study, a multi-angled approach to evaluate corrosion and antimicrobial surface properties has been established, using copper as a benchmark. We foresee that a similar approach can be taken to evaluate the antimicrobial properties of other types of surfaces. In this work we have, however, not evaluated the antimicrobial efficiency at different concentrations of bacteria and/or after subsequent application of bacteria over time. This would be a valuable experiment to perform in the future, since such surfaces are likely to experience a heavy load of microbes, should they be used in hospitals and similar environments. Another important aspect to consider is the diversity of microbial world, as pathogens might behave differently than model organisms. It has already been postulated that the mechanism of toxicity for copper differs between gram-positive and gram-negative bacteria[256,257] and different response systems have been identified, that need to be taken into account to fully understand the interactions between bacteria and copper[317]. Moreover, while copper can in some instances be considered as an alternative to antibiotics, copper resistance has already been demonstrated[318] and needs to be understood in order to prevent its spread.

6 CONCLUSIONS

It has been estimated that more than 95 % of scientists that ever lived are alive today. The exponential rate of knowledge growth has led to the differentiation of science into sub-disciplines that are becoming increasingly disconnected from each other[83]. Cross-disciplinary research takes advantage of the achievements from different disciplines to generate novel ideas, promoting innovation. In this thesis, we aimed to combine microbiology with electrochemistry, organic chemistry and corrosion science to answer relevant questions and design unconventional approaches for future research and diagnostics.

Paper I is based on the utilization of conjugated polymers for electrochemical detection of bacteria. Electroactivity of bacteria was previously described, and so were the electrocatalytic properties and biocompatibility of PEDOT. We combined this knowledge to demonstrate that bacteria can be detected via changes they induce in the redox state of their extracellular milieu. The two-electrode potentiometric (PEDOT:PSS)-based sensor is in some ways similar to the A_{600} measurement commonly used to determine bacterial density; it is robust but non-specific and a calibration curve is necessary to gain information about the actual number of bacteria. While the redox sensor measurement is slower (approximately 15 min) compared to the A_{600} measurement, it can measure the presence of bacteria in opaque liquids, which is not possible for $A_{600.}$ This sensor is a prototype that can be improved in the future by introducing specificity, improving the sensitivity and shortening the detection time.

In Paper II we switched gears and, while still employing conjugated thiophene based materials, went from electronic to optical detection of bacteria. For the first time, we showed that optotracing of gram-positive bacteria is possible, as we demonstrated that HS-167 can be used for spectroscopic and microscopic detection of *S. aureus.* Our experiments showed that HS-167 binds predominantly to the cell wall of *S. aureus*. This seems plausible, since PGN, the major component of the cell wall is composed of β- (1,4) linked glycans, just like cellulose, that is known to strongly bind optotracers. The binding is not restricted to PGN however, and other cell surface components likely take part. We investigated the interactions between HS-167 and *S. aureus* and showed that binding correlates with cell surface hydrophobicity. The binding induced on-switch of HS-167 fluorescence enabled us to correlate fluorescence intensity with A_{600} over time and define the slope as a quantifiable variable for comparison between species and strains. In the future, we aim to explore the possibility of establishing high-throughput screening with HS-167 for discrimination of *Staphylococcal* species.

While the use of optotracers (i.e., luminescent conjugated oligothiophenes) for amyloid detection and discrimination is well-researched, we know comparably little about the detection and binding mechanisms of optotracers to polysaccharides and even less about binding to and/or detection of gram-positive bacteria. In Paper III, we tested a set of pure oligothiophene optotracers of different length, charge and charge distribution and compared their ability to detect to *S. aureus*, using *S.* Enteritidis as a negative control. To facilitate analysis, we introduced automated peak determination and implemented cross-correlation to quantify the spectral shift. Our results have shown that the length and total charge are important

determinants for optimal spectral detection, while the distribution of charged groups did not seem to play a role within the selection of optotracers tested. Confocal microscopy of selected optotracers confirmed their localization in the cell wall. In this work, we have established a structured approach for optotracer performance evaluation and in the future, we aim to test an extended optotracer selection, in a wider range of experimental conditions, with a broader selection of bacteria to generate a comprehensive overview of interactions between the optotracers and bacteria. This will be useful to understand the interactions governing binding as well as to find new possible applications.

In Paper IV we developed a versatile approach towards evaluation of indoor high touch material properties, focusing on corrosion and antimicrobial capacity. As an example, we used copper, a well-known antimicrobial metal. Touch was simulated by deposition of artificial sweat, which led to accelerated corrosion and altered surface properties, i.e., colour change, increased hydrophilicity and surface roughness. A quasi-dry protocol for bacterial deposition to surfaces was established to improve reproducibility in antimicrobial surface testing. Viability assays and Live/Dead staining demonstrated that bacteria die within minutes after being applied on a copper surface. Corrosion seemed to promote, rather than delay the killing effect. Since it has previously been shown that copper and its alloys reduce the incidence of hospital-acquired infections[248–251], the understanding of the complex interplay between the different factors influencing its antimicrobial properties is of great relevance.

7 POINTS OF PERSPECTIVE

7.1 ORGANIC BIOELECTRONICS FOR BACTERIAL SENSING AND BEYOND

The increasing evidence of EET in bacteria opened a new venue for research and diagnostics. Employing electrochemical means of bacterial detection, rather than optical, comes with the possibility to detect bacteria in opaque solutions – this is of interest for food and beverages, such as monitoring milk quality. Moreover, since the detection occurs via redox-active soluble metabolites, bacterial metabolic products can be detected even if bacterial cells themselves are immobilized (e.g. in a biofilm) or have been removed from the solution.

Electrochemical methods can also be applied in basic microbiology, where they might enable monitoring of bacterial growth beyond the classical OD_{600} measurements. Currently, for the great majority of experiments, we follow the dynamics of bacterial populations only by monitoring the net increase in density, i.e., the multiplication of cells. For this and other reasons, the stationary phase bacteria are only poorly characterized, despite being the prevalent form in nature[319]. The transcriptional profile of bacteria changes significantly when they enter stationary phase[320] and despite the absence of net growth, stationary phase bacteria were shown to sustain protein production for several days[319]. We suggest that electrochemical monitoring of bacterial growth could enable a better insight into the growth stages of bacteria and we envision for the electrochemical growth curve to become complementary to the turbidimetric one. CPs are advantageous due to their electrocatalytic properties, enabling sensitive detection of redox-active metabolites. Moreover, they can be employed in devices such as organic electrochemical transistors, enabling sensitive monitoring of ion concentration in solution, a possible alternative to impedance microbiology. Another important phenomenon associated with electrical signalling is biofilm formation. In a seminal publication in 2015, Prindle et al. have shown that long range electrical signals within *B. subtilis* biofilms are conducted by propagating waves of potassium[321]. Moreover, it was later shown that the potassium mediated signalling attracts distant cells to the biofilm community[322]. Having ionic and electronic conductivity, PEDOT based materials could be useful to study such processes. Organic electronic ion pump, a device very similar to the sensor we used for detection of bacteria in Paper I, has previously been used for targeted ion delivery[323] and could be employed to simulate ion oscillations in a biofilm. Moreover, PEDOT (or other CP) based devices could potentially also be employed to detect such oscillations.

An interesting application for redox based detection of bacterial growth is antibiotic susceptibility testing (AST). To my knowledge, the first electrochemical AST (eAST) was reported already 20 years ago and was based on bacterial reduction of $Fe(CN)_6$. The ability of *E. coli* and *Clostridium sporogenes* to reduce $Fe(CN)_6$ was shown to decrease in the presence of antibiotics and, in most cases, the results were in good agreement with disk diffusion methods[324]. Other eASTs followed, some still based on $Fe(CN)_6$[325] or other redox-active molecules[326], while label-free eAST has been, to my knowledge, reported only for strong exoelectrogens[327]. Knowing that the electrocatalytic properties of PEDOT enable sensitive detection of weak electrogens, the electrochemical monitoring of bacterial growth could be employed to evaluate antibiotic susceptibility. This would be possible provided antibiotics would not be absorbed by or interact with PEDOT. This approach could offer testing in actual

physiological conditions (i.e., in urine or blood) and the time to result could be shortened significantly compared to disk diffusion and minimal inhibitory concentration assays.

Finally, measuring redox potentials is interesting in applications other than those directly related to monitoring bacterial growth. It is known that redox potential of body fluids is altered in stress and disease conditions. Altered blood redox status has been associated with cognitive impairment and Alzheimer disease progression[328,329] and it has been suggested that salivary redox state could likewise be used for the diagnosis and prognosis of certain neurodegenerative diseases[330]. Redox balance is of great importance also in the gut, where bacteria play an important role. Oxidative stress is associated with intestinal inflammation, an important player in inflammatory bowel disease[331] and fecal redox state is altered upon malnutrition and eating disorders[332]. A recent study based on animal models demonstrated how antibiotics alter gut redox balance by changing the microbiota[333]. With the prospect that redox diagnostics will enter clinical laboratories, cheap, disposable sensors will be needed and CPs could be the material of choice for fabrication of such devices.

7.2 FUTURE OPTOTRACING

Optotracing for microbiology is a technology in early development and at this stage, it is of critical importance to enhance the basic understanding of molecular mechanisms governing binding and fluorescence readout. For this, an interdisciplinary, systematic and well-structured approach should be adopted.

In this thesis, we have shown that environmental variables have a profound effect on the intrinsic properties of optotracers and their binding to different targets. In protein science, for example, a buffer stability screen is a common approach to understand the behaviour and optimize conditions for a given protein[334]. A similar approach would be well worth to take with optotracers, both to understand the photophysical properties of unbound optotracer in different solutions but also in the presence of different binding targets to determine if binding selectivity can be tuned by altering the environmental conditions. Ideally, this could be complemented with in silico calculations.

Currently, optotracers do not yet achieve specificities comparable to antibodies. Other strategies could possibly be employed to achieve a specific readout. An interesting approach would be to perform differential sensing[335,336]. Instead of aiming to detect one specific interaction, an array containing multiple optotracers at multiple assay conditions could be employed and the combined readout would hopefully provide a complete answer. Ideally, a combination of optotracers with different structural features can be used so that some can be aimed at positively or negatively charged analytes, others at hydrophobic moieties, etc.. Since a spectral shift, as well as a change in fluorescence intensity, can be measured, a lot of information would be extracted from each assay and appropriate data analysis procedures would need to be implemented to extract meaningful results.

Finally, since optotracers are synthesized by design, different moieties rendering them amenable for coupling to other compounds of choice can be introduced, as was demonstrated by azide functionalization of p-FTAA[337]. This means that optotracers could be bound to different surfaces or incorporated in Sephadex columns, for example, to function as a binding agent for certain bacteria or biofilm components. Due to their robustness, the sample could be washed away and the surface/column regenerated.

8 ACKNOWLEDGEMENTS

For this thesis to come true I received the help and support of many people and I am very grateful to all of you!

To my supervisor, Professor **Agneta Richter-Dahlfors** for enabling this work, for your enthusiasm and your patience during these years.
To my co-supervisor, Professor **Peter Nilsson** for teaching me so much! A coffee break conversation with you was always more fruitful than a day spent reading. Thank you for answering my numerous emails and explaining basic photo-physics to me.
To my co-supervisor, Assistant Professor **Susanne Löffler** for educating me about science, life and the great value of parafilm. I am still waiting for your book to come out! Thank you for taking me in and giving me an opportunity as an MSc student in the lab and for not giving up on me during all the years that followed.
To Professor **Mikael Rhen** – on the (unfortunately) rare occasions that we met I was always so inspired! You are the scientist I dream to be. Thank you for your valuable insight and your help with all possible *Salmonella* related questions.
Margret Wahlström, thank you for your kindness and for making me feel welcome in the lab! Your positive attitude made all the difference for me and I still remember how much better you made me feel the first days being a PhD student. **Linda Thörn,** thank you for your tireless help with all possible administrative issues I came up with!

I was truly blessed with great colleagues during these years. To be surrounded with people I admire so much – both professionally and personally, meant the world to me. Getting to know all of you made me think in new ways and expand my horizons in so many directions.
Dr. **Anette Schulz** – your friendship means SO much to me. I am grateful for all our discussions on subjects ranging from science to not-so-much-science and your input in all aspects of life. I love the way you really think about things. And I love you for being such a caring person! Your skills are amazing – I am having difficulties to find something you don't know how to do admittedly. The next big star in research, Dr. **Haris Antypas** - also a superhuman! 16 hour working days, weekends included, a perfect body, great social life, being an amazing chef and interior designer, super educated in all matters ranging from politics to history. Most importantly a person with a huge heart! Thanks for all your help in the lab, for organizing booze fikas, for taking me to Greece <3 and for the breakfasts in Bergshamra. I cannot wait to visit you and have not forgotten you promised me to go hiking!!! Dr. **Svava Steiner**, the person I aspire to be. Thank you for staying with me throughout all those years! I cannot express how much I respect you, for being so smart, thorough, and correct. Whenever I am in a dilemma, I am asking myself "what would Svava do?". I find you so interesting from so many points of view and your insight has changed my mind on many topics in life. Finally, I cannot stop being amazed over you being so modest while you are so great in everything you do and who you are! Dr. **Polyxeni Nikolakopoulou,** thank you for making me laugh so much! I am so happy that you did not stay at KTH but came to sit at KI. That made my quality of life at work way better. Next step is to convince you we do acroyoga together! Dr. **Keira Melican**, your presence in the group was so reassuring. Thank you for being so positive and always ready to

help, you made many (huge) problems seem reasonably small. I am looking so much forward to hear about all the exciting things that will come from your group. Staph is best! Big thanks to Dr. **Sara Fahlén** – it was you who told me about Sarek, which turned out to be one of the best experiences I ever had in Sweden. Thank you for being such a great colleague and friend, around you things always felt easier and we could laugh about everything. Dr. **Ben Libberton**, you are one of the most creative and imaginative people I have gotten to know. I am still hoping that some of your crazy ideas come true! Big thanks for teaching me about Staph, I would have not made it without your contribution. Dr. **Marta Veses Garcia**, thank you for being so much fun and down to earth. I will always be grateful that you literally sacrificed a part of you for my project. All for science! Also, the prank with the orange juice was genius! I am constantly hoping an opportunity arises when I can use it. Dr. **Jonatan Martin Rodriguez -** the person whose day has 34 hours! It became a challenge for me to appear at work at any crazy time and see that you are not there. I never succeeded. Thank you for your selfless help with all my microbiology questions, for your advice and for caring about my ethical dilemmas. You deserve to become the biggest of the big professors! I hope then you will take some time off. The electronic engineer Dr. **Salvador Gómez Carretero –** thank you so much for taking the time to explain basic electrochemistry to me! Assistant Professor **Onur Parlak -** the scientist who will rock the bioelectronics world! Thank you for teaching me about zeta potential and square wave voltammetry and for taking the time to answer my numerous stupid questions. Cannot wait to see the cool science coming from the Parlak Lab! Assistant Professor **Ferdinand X. Choong**, the man who makes biofilms shine. Thank you for all the advice you gave me when I started to work with optotracing. Most of all, thank you for keeping your cool even at times when I absolutely could not. **Charles Zhang**, thank you for interesting lunch discussions, for sneaking me into the gym and for the absolutely amazing tea! I wish you best of luck with your PhD, you are in great hands.

During these years I have had the honour to work with many students that made my time in the lab much more fun and taught me many new things!
A gigantic thanks go to **Ana Tomac** and **Filip Filipović**. You have shown Karolinska that best students come from Ljubljana! You both have made a great contribution to the lab and my PhD – not only in the work you did but also because it was so nice to have you around and I have really learnt a lot from you and laughed a lot with you. Without a doubt, a bright future lays ahead of you and please remember me when you are big bosses in Slovenia some day and I might need a job!
Thanks to **Charbel Kreidy**, **Christine Nylander**, **Victoria Muliadi** and **Tiit Sihukevend**. All of you are so smart and hardworking! I hope you never forget that and know that you will be great at whatever you will do. It has been such a pleasure to have you around, thank you for this time!
Finally, I would like to thank other students that I have not worked with directly but still enjoyed the good atmosphere you made in the lab – **Ana Felicita Gobec**, **Eleanor Marshall**, **Anilcan Kus**, **Johannes Eckert**, **Lisanne de Vor** and many others.

I would like to thank our collaborators, Professor **Inger Odnewall Wallinder** and Dr.**Tingru Chang**. Thank you for giving me the opportunity to work with you, it has been a great pleasure for me, and I have learnt so much. Tingru, thank you for all the fun hours by the microscope,

it was always so nice when you came over to KI! I hope you keep being excited about bacteria and am looking very much forward to the continuation of your work.

Very importantly, there have been many people who have made my life outside of work wonderful throughout these years.
Johan Lundberg, you know I could write another book of this size about the good memories I have with you. Thank you so much for being a wonderful friend, for bringing so much joy and laughter to my life and for being with me through the thick and thin. **Johan Boström**, thank you for being by my side at all times. You have introduced me to so many new and exciting things and filled my life with adventures! Thank you for all the running and climbing and burpies and wine and fiskgratäng (yes, I appreciated the gesture!) and for fixing my bike and buying me lights for winter cycling. You really have a gigantic heart! **Hannes Feyrer**, one of the most interesting people I have met. Thank you so much for all the science breakfasts, the long walks from Lappis to KI and for teaching me how to choose clementines in Hemköp. I really value your critical judgement, curiosity and independence and I wish to be more like you when I grow up! Also, I hope you will write a book one day. **Miloš Gojković,** thank you for making me feel like home even if I was 2000 km away! Your warmth and affection made all the difference. **Stelia Ntika**, I am so happy Haris invited us both for dinner so many years ago! Thank you for all the good times we had and I really hope we will keep on spending holidays together forever. **Laura Barbieri**, thank you for putting things into perspective and for making me sane. You definitely have grit and I admire you for it! It was always a pleasure to discuss things with you and am so glad that we shared love for sushi. I am really happy that we met and would wish to have you as my neighbour wherever I go! **Martina Matsson**, thank you for the numerous fantastic cakes over these years and for all the fun we had practising acro. **Jakob Schuy**, thank you for the Wednesday acroyoga sessions at KI and for teaching me how to bake! **Elizaveta Burdukova**, one of my first and best Stockholm friends! Thank you for understanding the issue of Slovenia/Slovakia, unfortunately not many people do!! Your friendship made my life here much happier and I am very grateful to have you. I admire you for being so very wise (and gorgeous!) and I hope we will be able to go for many more trips together! **Petra Gabrič Topličan** and **Gašper Topličan** – I am so glad that we all ended up here in Stockholm! Petra, I am often thinking of midsummer trips and I really hope we will manage to keep this tradition going. I miss our dinners and gin-tonics so much and cannot wait to be able to go out again. There are so many great memories I have with you in Stockholm and I hope we will never live apart (for long) again! Dr. **Mark Zupančič**, the story of success! It is so nice that we found each other here. Every time we meet I have so much fun, cannot really express my appreciation of your humour enough! **Bojana Lazović** thank you so much for joining me here in Sweden! I am really longing for this period to be over so that I can go to Gothenburg again.

Biggest thanks to my close friends who were willing to have a long distance relationship with me throughout all these years! **Nina Jazbec**, even if is is by now 10 years we are not in the same country (and no, that does NOT make us old!), it does not seem to matter at all and I know you are always there for me. You helped me so much through tough times and I am really grateful for this! **Katja Glinšek** thank you for the great Christmas dinners you were hosting, for the Viber phonecalls and for visiting me in Stockholm – I have such beautiful memories of those weekends. **Tjaša Kunavar** I know you will visit me if I move to Spain or Greece so I

will consider this for my next job! **Katja Mali**, you are my soulmate! Only that your soul is better than mine. Thank you for everything!! **Luka Schönlieb**, we still have to do the parachute jump! Thank you for the wonderful times we spent in Italy and for being so good at WhatsApp even if I was not always. **Anže Smole**, thank you for keeping overseas contact and for supporting me in so many ways. And thank you for the headphones! They have been with me throughout my PhD. Big thanks to **Pia Lucija Rotar**, **Katarina Müller Šuštar**, **Veronika Košir Firbas, Mateja Grahovac, Nejc Hočevar** and others for whom I love coming back to Slovenia.

Most importantly, I owe a great deal of gratitude to my family, the foundation of everything else. I would like to thank my parents **Mirjam Rogl Butina** and **Tomaž Butina**. I really appreciate that you have never put any pressure on me or forced me in any direction in life. I always felt full support and respect from your side and this has been of great value for me. I would also like to thank my sisters **Nika Kristina Butina** and **Ana Ariana Butina** for not hating me (at least not very obviously) even if I never wanted to dress up for Christmas photography. A big thanks to my grandmother, **Jana Rogl**, for all the tonnes of poppyseed cake I received from you throughout the years.

(soon Dr.!) **Žiga Ogorelec**, you are simply the best! Now I know that everyone, who was telling me that perfect men do not exist, was lying. I am so grateful that you are still with me despite all the craziness you had to put up with. To come home to you means the world to me and I would never have made it without your support. You made me discover a whole new world, one that I like so much! When I am done with the PhD, I will learn the names of all the trees, the bugs and the fish. Promise.

9 REFERENCES

1. Achtman, M. How old are bacterial pathogens? *Proc. R. Soc. B Biol. Sci.* **283**, 1–10 (2016).
2. 1.1B: History of Microbiology - Hooke, van Leeuwenhoek, and Cohn - Biology LibreTexts. (2020). Available at: https://bio.libretexts.org/Bookshelves/Microbiology/Book%3A_Microbiology_(Boundless)/1%3A_Introduction_to_Microbiology/1.1%3A_Introduction_to_Microbiology/1.1B%3A_History_of_Microbiology_-_Hooke_van_Leeuwenhoek_and_Cohn. (Accessed: 22nd September 2020)
3. Madigan, M. T., Martinko, J. M., Dunlap, P. V. & Clark, D. P. *Brock Biology of Microorganisms*. (Pearson Benjamin Cummings, 2009).
4. Kadar, N., Romero, R. & Papp, Z. Ignaz Semmelweis: 'The Savior of Mothers' On the 200th Anniversary of the Birth. *Am J Obs. Gynecol* **219**, 519–522 (2018).
5. Lammie, S. L. & Hughes, J. M. Antimicrobial Resistance, Food Safety, and One Health: The Need for Convergence. *Annu. Rev. Food Sci. Technol* **7**, 287–312 (2016).
6. Butler, M. S. & Paterson, D. L. Antibiotics in the clinical pipeline in October 2019. *J. Antibiot. (Tokyo).* **73**, 329–364 (2020).
7. Institute for Health Metrics and Evaluation. Global Burden of Disease Visualisations: Compare. *Global Burden of Disease 2019* (2019). Available at: https://www.thelancet.com/lancet/visualisations/gbd-compare. (Accessed: 23rd September 2020)
8. Bhutta, Z. A., Salam, R. A., Das, J. K. & Lassi, Z. S. Tackling the existing burden of infectious diseases in the developing world: Existing gaps and the way forward. *Infect. Dis. Poverty* **3**, 1–6 (2014).
9. Cassini, A. *et al.* Burden of Six Healthcare-Associated Infections on European Population Health: Estimating Incidence-Based Disability- Adjusted Life Years through a Population Prevalence-Based Modelling Study. *PLOS Med.* **13**, 1–16 (2016).
10. Cloutier, M., Mantovani, D. & Rosei, F. Special Focus on Materials Antibacterial Coatings: Challenges, Perspectives, and Opportunities. *Trends Biotechnol.* **33**, 637–652 (2015).
11. Bauer, K. A., Perez, K. K., Forrest, G. N. & Goff, D. A. Review of Rapid Diagnostic Tests Used by Antimicrobial Stewardship Programs. *Clin. Infectous Dis.* **59**, S134–S145 (2014).
12. Lee, C.-R., Cho, I., Jeong, B. & Lee, S. Strategies to Minimize Antibiotic Resistance. *Int. J. Environ. Res. Public Health* **10**, 4274–4305 (2013).
13. Berggren, M. & Richter-Dahlfors, A. Organic bioelectronics. *Adv. Mater.* **19**, 3201–3213 (2007).
14. Gomez-Carretero, S., Libberton, B., Rhen, M. & Richter-Dahlfors, A. Redox-active conducting polymers modulate Salmonella biofilm formation by controlling availability of electron acceptors. *npj Biofilms Microbiomes* **3**, 1–10 (2017).
15. Gomez-Carretero, S., Nybom, R. & Richter-Dahlfors, A. Electroenhanced Antimicrobial Coating Based on Conjugated Polymers with Covalently Coupled Silver Nanoparticles Prevents Staphylococcus aureus Biofilm Formation. *Adv. Healthc. Mater.* **6**, 1–10 (2017).
16. Löffler, S. & Richter-Dahlfors, A. Phase angle spectroscopy on transparent conducting polymer electrodes for real-time measurement of epithelial barrier integrity. *J. Mater. Chem. B* **3**, 4997–5000 (2015).
17. Löffler, S. *et al.* Organic bioelectronics in infection. *J. Mater. Chem. B* **3**, 4979–4992 (2015).
18. Butina, K., Löffler, S., Rhen, M. & Richter-Dahlfors, A. Electrochemical sensing of bacteria via secreted redox active compounds using conducting polymers. *Sensors Actuators, B Chem.* **297**, 1–8 (2019).
19. Choong, F. X. *et al.* Real-time optotracing of curli and cellulose in live Salmonella biofilms using luminescent oligothiophenes. *npj Biofilms Microbiomes* **2**, 1–11 (2016).
20. Antypas, H., Choong, F. X., Libberton, B., Brauner, A. & Richter-Dahlfors, A. Rapid diagnostic assay for detection of cellulose in urine as biomarker for biofilm-related urinary tract infections. *npj Biofilms Microbiomes* **4**, 1–7 (2018).
21. Butina, K. *et al.* Optotracing for selective fluorescence-based detection, visualization and quantification of live S. aureus in real-time. *npj Biofilms Microbiomes* **6**, 1–12 (2020).
22. Levin, P. A. & Angert, E. R. Small but mighty: Cell size and bacteria. *Cold Spring Harb. Perspect. Biol.* **7**, 1–11 (2015).
23. Todar, K. Online Textbook of Bacteriology. (2020). Available at: http://textbookofbacteriology.net/. (Accessed: 23rd September 2020)
24. Kadner, R. J. Cytoplasmic membrane. in *Escherichia coli and Salmonella: Cellular and Molecular Biology* (eds. Neidhardt, F. C. et al.) 58–87 (ASM, 1996).
25. Anraku, Y. Bacterial electron transport chains. *Ann. Rev. Biochem* **57**, 101–32 (1988).
26. Gay, N. J. & Walker, J. E. The atp operon: nucleotide sequence of the promoter and the genes for the membrane

proteins, and the 5 subunit of Escherichia coli ATP-synthase. *Nucleic Acids Res.* **9**, 3919–26 (1981).

27. Gram, H. C. Ueber die isolirte Färbung der Schizomyceten in Schnitt- und Trockenpräparaten. *DMW - Dtsch. Medizinische Wochenschrift* **10**, 234–235 (1884).

28. Bos, M. P., Robert, V. & Tommassen, J. Biogenesis of the Gram-Negative Bacterial Outer Membrane. *Annu. Rev. Microbiol* **61**, 191–214 (2007).

29. Silhavy, T. J., Kahne, D. & Walker, S. The bacterial cell envelope. *Cold Spring Harb. Perspect. Biol.* **2**, 1–16 (2010).

30. Yi, E. C. & Hackett, M. Rapid isolation method for lipopolysaccharide and lipid A from Gram-negative bacteria. *Analyst* **125**, 651–656 (2000).

31. Lerouge, I. & Vanderleyden, J. O-antigen structural variation: mechanisms and possible roles in animal/plant–microbe interactions. *FEMS Microbiol. Rev.* **26**, 17–47 (2002).

32. Aderem, A. & Ulevitch, R. J. Toll-like receptors in the induction of the innate immune response. *Nature* **406**, 782–787 (2000).

33. Wang, L., Wang, Q. & Reeves, P. R. The Variation of O Antigens in Gram-Negative Bacteria. in *Endotoxins: Structure, Function and Recognition. Subcellular Biochemistry, vol 53.* (eds. Wang, X. & Quinn, P. J.) 123–152 (Springer, Dordrecht, 2010). doi:10.1007/978-90-481-9078-2_6

34. Turner, R. D., Hurd, A. F., Cadby, A., Hobbs, J. K. & Foster, S. J. Cell wall elongation mode in Gram-negative bacteria is determined by peptidoglycan architecture. *Nat. Commun.* **4**, 1–8 (2013).

35. Rogers, H. J., Perkins, H. R. & Ward, J. B. Structure of peptidoglycan. in *Microbial Cell Walls and Membranes* 190–214 (University Press, Cambridge, 1980). doi:10.1007/978-94-011-6014-8_6

36. Vollmer, W., Blanot, D. & De Pedro, M. A. Peptidoglycan structure and architecture. *FEMS Microbiol. Rev.* **32**, 149–167 (2008).

37. Vollmer, W. & Seligman, S. J. Architecture of peptidoglycan: more data and more models. *Trends Microbiol.* **18**, 59–66 (2010).

38. Gan, L., Chen, S. & Jensen, G. J. Molecular organization of Gram-negative peptidoglycan. *PNAS* **105**, 18953–7 (2008).

39. Depuydt, M. *et al.* A Periplasmic Reducing System Protects Single Cysteine Residues from Oxidation. *Science (80-.).* **326**, 1109–11 (2009).

40. Asmar, A. T. & Collet, J.-F. Lpp, the Braun lipoprotein, turns 50-major achievements and remaining issues. *FEMS Microbiol. Lett.* **365**, 1–8 (2018).

41. Braun, V. & Wolff, H. Attachment of lipoprotein to murein (peptidoglycan) of Escherichia coli in the presence and absence of penicillin FL 1060. *J. Bacteriol.* **123**, 888–897 (1975).

42. Vollmer, W. Structural variation in the glycan strands of bacterial peptidoglycan. *FEMS Microbiol. Rev.* **32**, 287–306 (2008).

43. Pasquina-Lemonche, L. *et al.* The architecture of the Gram-positive bacterial cell wall. *Nature* **582**, 294–297 (2020).

44. Fischetti, V. A. Surface proteins on Gram-Positive bacteria. in *Gram Positive Pathogens* (eds. Fischetti, V. A., Novick, R. P., Ferretti, J. J., Portnoy, D. A. & Rood, J. I.) 12–25 (ASM press, 2006).

45. Mazmanian, S. K., Liu, G., Ton-That, H. & Schneewind, O. Staphylococcus aureus sortase, an enzyme that anchors surface proteins to the cell wall. *Science* **285**, 760–3 (1999).

46. Dramsi, S. & Bierne, H. Spatial Organization of Cell Wall-Anchored Proteins at the Surface of Gram-Positive Bacteria. in *Protein and Sugar Export and Assembly in Gram-positive Bacteria* (eds. Bagnoli, F. & Rappuoli, R.) 177–201 (Springer International Publishing, 2016). doi:10.1007/82_2016_4

47. Foster, T. J., Geoghegan, J. A., Ganesh, V. K. & Höök, M. Adhesion, invasion and evasion: the many functions of the surface proteins of Staphylococcus aureus. *Nat. Rev. Microbiol.* **12**, 49–62 (2014).

48. Brown, S., Santa Maria, J. P. J. & Walker, S. Wall Teichoic Acids of Gram-Positive Bacteria. *Annu. Rev. Microbiol* **67**, 313–336 (2013).

49. Weidenmaier, C. & Peschel, A. Teichoic acids and related cell-wall glycopolymers in Gram-positive physiology and host interactions. *Nat. Rev. Microbiol.* **6**, 276–287 (2008).

50. Xia, G., Kohler, T. & Peschel, A. The wall teichoic acid and lipoteichoic acid polymers of Staphylococcus aureus. *Int. J. Med. Microbiol.* **300**, 148–154 (2010).

51. Neuhaus, F. C. & Baddiley, J. A Continuum of Anionic Charge: Structures and Functions of D-Alanyl-Teichoic Acids in Gram-Positive Bacteria. *Microbiol. Mol. Biol. Rev.* **67**, 686–723 (2003).

52. Percy, M. G. & Grundling, A. G. Lipoteichoic Acid Synthesis and Function in Gram-Positive Bacteria. *Annu. Rev.* **68**, 81–100 (2014).

53. Schneewind, O. & Missiakas, D. Lipoteichoic Acids, Phosphate-Containing Polymers in the Envelope of Gram-Positive Bacteria. *J. Bacteriol.* **196**, 1133–1142 (2014).

54. Fedtke, I. *et al.* A Staphylococcus aureus ypfP mutant with strongly reduced lipoteichoic acid (LTA) content: LTA governs bacterial surface properties and autolysin activity. *Mol. Microbiol.* **65**, 1078–1091 (2007).

55. Bæk, K. T. *et al.* The Cell Wall Polymer Lipoteichoic Acid Becomes Nonessential in Staphylococcus aureus Cells Lacking the ClpX Chaperone. *MBio* **7**, 1–11 (2016).

56. Jordan, S., Hutchings, M. I. & Mascher, T. Cell envelope stress response in Gram-positive bacteria. *FEMS Microbiol. Rev.* **32**, 107–146 (2008).

57. O 'Riordan, K. & Lee, J. C. Staphylococcus aureus Capsular Polysaccharides. *Clin. Microbiol. Rev.* **17**, 218–234 (2004).

58. Boyle-Vavra, S. *et al.* USA300 and USA500 clonal lineages of Staphylococcus aureus do not produce a capsular polysaccharide due to conserved mutations in the cap5 locus. *MBio* **6**, 1–10 (2015).

59. Potter, M. C. Electrical effects accompanying the decomposition of organic compounds. *Proc. R. Soc. London* **84**, 260–276 (1911).

60. Watanabe, K., Manefield, M., Lee, M. & Kouzuma, A. Electron shuttles in biotechnology. *Curr. Opin. Biotechnol.* **20**, 633–641 (2009).

61. Shi, L. *et al.* Extracellular electron transfer mechanisms between microorganisms and minerals. *Nat. Rev. Microbiol.* **14**, 651–662 (2016).

62. Lovley, D. R. Dissimilatory Metal Reduction. *Annu. Rev. Microbiol.* **47**, 263–290 (1993).

63. Wang, F. *et al.* Structure of Microbial Nanowires Reveals Stacked Hemes that Transport Electrons over Micrometers. *Cell* **177**, 361–369 (2019).

64. Kotloski, C. J. & Gralnick, N. J. Flavin electron shuttles dominate extracellular electron transfer by Shewanella oneidensis. *MBio* **4**, 553–565 (2013).

65. Deng, L., Li, F., Zhou, S., Huang, D. & Ni, J. A study of electron-shuttle mechanism in Klebsiella pneumoniae based-microbial fuel cells. *Chinese Sci. Bull.* **55**, 99–104 (2010).

66. Freguia, S., Masuda, M., Tsujimura, S. & Kano, K. Lactococcus lactis catalyses electricity generation at microbial fuel cell anodes via excretion of a soluble quinone. *Bioelectrochemistry* **76**, 14–18 (2009).

67. Keck, A. *et al.* Identification of quinoide redox mediators that are formed during the degradation of naphthalene-2-sulfonate by Sphingomonas xenophaga BN6. *Appl. Environ. Microbiol.* **68**, 4341–9 (2002).

68. You, L.-X. *et al.* Flavins mediate extracellular electron transfer in Gram-positive Bacillus megaterium strain LLD-1. *Bioelectrochemistry* **119**, 196–202 (2018).

69. Keogh, D. *et al.* Extracellular Electron Transfer Powers Enterococcus faecalis Biofilm Metabolism. *MBio* **9**, 1–16 (2018).

70. Pankratova, G., Leech, N., Gorton, L. & Hederstedt, L. Extracellular Electron Transfer by the Gram-Positive Bacterium Enterococcus faecalis. *Biochemistry* **57**, 4597–4603 (2018).

71. Light, S. H. *et al.* A flavin-based extracellular electron transfer mechanism in diverse Gram-positive bacteria. *Nature* **562**, 140–144 (2018).

72. Saunders, S. H. & Newman, D. K. Extracellular Electron Transfer Transcends Microbe-Mineral Interactions. *Cell Host Microbe* **24**, 611–613 (2018).

73. Glasser, N. R., Saunders, S. H. & Newman, D. K. The Colorful World of Extracellular Electron Shuttles. *Annu. Rev. Microbiol* **71**, 731–51 (2017).

74. Ciemniecki, J. A. & Newman, D. K. The Potential for Redox-Active Metabolites To Enhance or Unlock Anaerobic Survival Metabolisms in Aerobes. *J. Appl. Polym. Sci.* **202**, 1–14 (2020).

75. Nealson, K. H. & Rowe, A. R. Electromicrobiology: realities, grand challenges, goals and predictions. *Microb. Biotechnol.* **9**, 595–600 (2016).

76. van Belkum, A. Molecular diagnostics in medical microbiology: Yesterday, today and tomorrow. *Curr. Opin. Pharmacol.* **3**, 497–501 (2003).

77. Isenberg, H. D. Clinical microbiology: Past, present, and future. *J. Clin. Microbiol.* **41**, 917–918 (2003).

78. Thomson, R. B. One Small Step for the Gram Stain, One Giant Leap for Clinical Microbiology. *J. Clin. Microbiol.* **54**, 1416–1417 (2016).

79. Devillé, W. L. J. M. *et al.* The urine dipstick test useful to rule out infections. A meta-analysis of the accuracy. *BMC Urol.* **4**, 1–14 (2004).

80. Kralik, P. & Ricchi, M. A Basic Guide to Real Time PCR in Microbial Diagnostics: Definitions, Parameters, and Everything. *Front. Microbiol.* **8**, 1–9 (2017).

81. Frickmann, H. *et al.* Fluorescence in situ hybridization (FISH) in the microbiological diagnostic routine laboratory: a review. *Crit. Rev. Microbiol.* **43**, 263–293 (2017).

82. Banada, P. P. & Bhunia, A. K. Antibodies and Immunoassays for Detection of Bacterial Pathogens. in *Principles of Bacterial Detection: Biosensors, Recognition Receptors and Microsystems* (eds. Zourob, M., Elwary, S. &

Turner, A.) 567–602 (Springer New York, 2008). doi:10.1007/978-0-387-75113-9_21

83. Stres, B. & Kronegger, L. Shift in the paradigm towards next-generation microbiology. *FEMS Microbiol. Lett.* **366**, 1–9 (2019).

84. Fournier, P.-E. *et al.* Modern clinical microbiology: new challenges and solutions. *Nat. Rev. Microbiol.* **11**, 574–585 (2013).

85. Meuzelaar, H. L. C. & Kistemaker, P. G. A Technique for Fast and Reproducible Fingerprinting of Bacteria by Pyrolysis Mass Spectrometry. *Anal. Chem.* **45**, 587–590 (1973).

86. Schulten, H. R., Beckey, H. D., Meuzelaar, H. L. C. & Boerboom, A. J. H. High Resolution Field Ionization Mass Spectrometry of Bacterial Pyrolysis Products. *Anal. Chem.* **45**, 191–195 (1973).

87. Seng, P. *et al.* Ongoing revolution in bacteriology: routine identification of bacteria by matrix-assisted laser desorption ionization time-of-flight mass spectrometry. *Clin. Infect. Dis.* **49**, 543–51 (2009).

88. Welker, M., Van Belkum, A., Girard, V., Charrier, J.-P. & Pincus, D. An update on the routine application of MALDI-TOF MS in clinical microbiology. *Expert Rev. Proteomics* **16**, 695–710 (2019).

89. Jurinke, C., Oeth, P. & van den Boom, D. MALDI-TOF Mass Spectrometry : A Versatile Tool for High-Performance DNA Analysis. *Mol. Biotechnol.* **26**, 147–164 (2004).

90. Wieser, A. & Schubert, S. MALDI-TOF MS entering the microbiological diagnostic laboratory – from fast identification to resistance testing. *TrAC - Trends Anal. Chem.* **84**, 80–87 (2016).

91. Freiwald, A. & Sauer, S. Phylogenetic classification and identification of bacteria by mass spectrometry. *Nat. Protoc.* **4**, 732–742 (2009).

92. Welker, M. & van Belkum, A. One System for All: Is Mass Spectrometry a Future Alternative for Conventional Antibiotic Susceptibility Testing? *Front. Microbiol.* **10**, 1–18 (2019).

93. Wetterstrand, K. A. DNA Sequencing Costs: Data from the NHGRI Genome Sequencing Program (GSP). (2020). Available at: https://www.genome.gov/about-genomics/fact-sheets/DNA-Sequencing-Costs-Data. (Accessed: 3rd September 2020)

94. Goodwin, S., McPherson, J. D. & McCombie, W. R. Coming of age: Ten years of next-generation sequencing technologies. *Nat. Rev. Genet.* **17**, 333–351 (2016).

95. Bragg, L. & Tyson, G. W. Metagenomics using next-generation sequencing. in *Methods in Molecular Biology* (eds. Paulsen, I. & Holmes, A. J.) **1096**, 183–201 (Humana Press Inc., 2014).

96. Staley, C. *et al.* Application of Illumina next-generation sequencing to characterize the bacterial community of the Upper Mississippi River. *J. Appl. Microbiol.* **115**, 1147–1158 (2013).

97. Goodwin, K. D. *et al.* DNA sequencing as a tool to monitor marine ecological status. *Front. Mar. Sci.* **4**, 1–14 (2017).

98. Westblade, L. F. *et al.* Role of clinicogenomics in infectious disease diagnostics and public health microbiology. *J. Clin. Microbiol.* **54**, 1686–1693 (2016).

99. Quick, J. *et al.* Real-time, portable genome sequencing for Ebola surveillance. *Nature* **530**, 228–232 (2016).

100. Ahmed, A., Rushworth, J. V, Hirst, N. A. & Millner, P. A. Biosensors for Whole-Cell Bacterial Detection. *Clin. Microbiol. Rev.* **27**, 631–646 (2014).

101. Parlak, O. & Richter-Dahlfors, A. Bacterial Sensing and Biofilm Monitoring for Infection Diagnostics. *Macromol. Biosci.* **20**, 1–17 (2020).

102. Janata, J. Introduction: Modern Topics in Chemical Sensing. *Chem. Rev.* **2**, 327–328 (2008).

103. Templier, V., Roux, A., Roupioz, Y. & Livache, T. Ligands for label-free detection of whole bacteria on biosensors: A review. *TrAC Trends Anal. Chem.* **79**, 71–79 (2015).

104. Byrne, B., Stack, E., Gilmartin, N. & O'Kennedy, R. Antibody-Based Sensors: Principles, Problems and Potential for Detection of Pathogens and Associated Toxins. *Sensors* **9**, 4407–4445 (2009).

105. Wang, W., Singh, S., Zeng, D. L., King, K. & Nema, S. Antibody Structure, Instability, and Formulation. *J. Pharm. Sci.* **96**, 1–26 (2007).

106. Huang, L., Muyldermans, S. & Saerens, D. Nanobodies® : proficient tools in diagnostics. *Expert Rev Mol Diagn.* **10**, 777–85 (2010).

107. Mannoor, M. S., Zhang, S., Link, A. J. & Mcalpine, M. C. Electrical detection of pathogenic bacteria via immobilized antimicrobial peptides. *PNAS* **107**, 19207–19212 (2010).

108. Fjell, C. D., Hiss, J. A., Hancock, R. E. W. & Schneider, G. Designing antimicrobial peptides: Form follows function. *Nat. Rev. Drug Discov.* **11**, 37–51 (2011).

109. Bobone, S. & Stella, L. Selectivity of antimicrobial peptides: A complex interplay of multiple equilibria. in *Advances in Experimental Medicine and Biology* **1117**, 175–214 (Springer New York LLC, 2019).

110. Wang, Y., Ye, Z., Si, C. & Ying, Y. Monitoring of Escherichia coli O157:H7 in food samples using lectin based surface plasmon resonance biosensor. *Food Chem.* **136**, 1303–1308 (2013).

111. Bulard, E. *et al.* Carbohydrates as New Probes for the Identification of Closely Related Escherichia coli Strains Using Surface Plasmon Resonance Imaging. *Anal. Chem.* **87**, 1804–1811 (2015).

112. Guo, X. *et al.* Carbohydrate-Based Label-Free Detection of Escherichia coli ORN 178 Using Electrochemical Impedance Spectroscopy. *Anal. Chem.* **84**, 241–246 (2012).

113. Richter, Ł. *et al.* Ordering of bacteriophages in the electric field: Application for bacteria detection. *Sensors Actuators B* **224**, 233–240 (2016).

114. Denyes, J. M. *et al.* Modified Bacteriophage S16 Long Tail Fiber Proteins for Rapid and Specific Immobilization and Detection of Salmonella Cells. *Appl. Environ. Microbiol.* **83**, 1–15 (2017).

115. Cao, X. *et al.* Combining use of a panel of ssDNA aptamers in the detection of Staphylococcus aureus. *Nucleic Acids Res.* **37**, 4621–4628 (2009).

116. Pan, Q. *et al.* Aptamers That Preferentially Bind Type IVB Pili and Inhibit Human Monocytic-Cell Invasion by Salmonella enterica Serovar Typhi Downloaded from. *Antimicrob. Agents Chemother.* **49**, 4052–4060 (2005).

117. Labuda, J. *et al.* Electrochemical nucleic acid-based biosensors: Concepts, terms, and methodology (IUPAC Technical Report). *Pure Appl. Chem.* **82**, 1161–1187 (2010).

118. Ellington, A. D. & Szostak, J. W. In vitro selection of RNA molecules that bind specific ligands. *Nature* **346**, 818–822 (1990).

119. Alizadeh, N., Memar, M. Y., Moaddab, S. R. & Kafil, H. S. Aptamer-assisted novel technologies for detecting bacterial pathogens. *Biomed. Pharmacother.* **93**, 737–745 (2017).

120. Zelada-Guillén, G. A., Riu, J., Düzgün, A. & Rius, F. X. Immediate Detection of Living Bacteria at Ultralow Concentrations Using a Carbon Nanotube Based Potentiometric Aptasensor. *Angew. Chemie Int. Ed.* **48**, 7334–7337 (2009).

121. Labib, M. *et al.* Aptamer-Based Viability Impedimetric Sensor for Bacteria. *Anal. Chem.* **84**, 8966–8969 (2012).

122. Cieplak, M. & Kutner, W. Artificial Biosensors: How Can Molecular Imprinting Mimic Biorecognition? *Trends Biotechnol.* **34**, 922–941 (2016).

123. Piletsky, S., Canfarotta, F., Poma, A., Bossi, A. M. & Piletsky, S. Molecularly Imprinted Polymers for Cell Recognition. *Trends Biotechnol.* **38**, 368–387 (2020).

124. Tokonami, S. *et al.* Recognition of gram-negative and gram-positive bacteria with a functionalized conducting polymer film. *Res. Chem. Intermed.* **40**, 2327–2335 (2014).

125. Qi, P., Wan, Y. & Zhang, D. Impedimetric biosensor based on cell-mediated bioimprinted films for bacterial detection. *Biosens. Bioelectron.* **39**, 282–288 (2013).

126. Golabi, M., Kuralay, F., Jager, E. W. H. H., Beni, V. & Turner, A. P. F. F. Electrochemical bacterial detection using poly(3-aminophenylboronic acid)-based imprinted polymer. *Biosens. Bioelectron.* **93**, 87–93 (2017).

127. Borisov, S. M. & Wolfbeis, O. S. Optical biosensors. *Chem. Rev.* **108**, 423–461 (2008).

128. Sharma, H. & Mutharasan, R. Review of biosensors for foodborne pathogens and toxins. *Sensors actuators B Chem.* **183**, 535–549 (2013).

129. Chen, C. & Wang, J. Optical biosensors: An exhaustive and comprehensive review. *Analyst* **145**, 1605–1628 (2020).

130. Bocková, M., Slabý, J., Špringer, T. & Homola, J. Advances in Surface Plasmon Resonance Imaging and Microscopy and Their Biological Applications. *Annu. Rev. Anal. Chem.* **12**, 151–176 (2019).

131. Li, D. *et al.* Label-free capacitive immunosensor based on quartz crystal Au electrode for rapid and sensitive detection of Escherichia coli O157:H7. *Anal. Chim. Acta* **687**, 89–96 (2011).

132. Poitras, C. & Tufenkji, N. A QCM-D-based biosensor for E. coli O157:H7 highlighting the relevance of the dissipation slope as a transduction signal. *Biosens. Bioelectron.* **24**, 2137–2142 (2009).

133. Wong, Y. Y. *et al.* Immunosensor for the differentiation and detection of Salmonella species based on a quartz crystal microbalance. *Biosens. Bioelectron.* **17**, 676–684 (2002).

134. Alvarez, M. & Lechuga, L. M. Microcantilever-based platforms as biosensing tools. *Analyst* **135**, 827–836 (2010).

135. Tamayo, J., Kosaka, P. M., Ruz, J. J., San Paulo, A. & Calleja, M. Biosensors based on nanomechanical systems. *Chem. Soc. Rev. Chem. Soc. Rev* **42**, 1287–1311 (2013).

136. Fritz, J. Cantilever biosensors. *Analyst* **133**, 855–863 (2008).

137. Bard, A. J. & Faulkner, L. R. *Electrochemical methods : fundamentals and applications*. (Wiley, 2000).

138. Orazem, M. E. & Tribollet, B. *Electrochemical Impedance Spectroscopy*. (John Wiley & Sons, Inc., 2008). doi:10.1002/9780470381588

139. Zelada-Guillén, G. A., Bhosale, S. V, Riu, J. & Rius, F. X. Real-Time Potentiometric Detection of Bacteria in Complex Samples. *Anal Chem* **82**, 9254–9260 (2010).

140. Hernández, R. *et al.* Graphene-based potentiometric biosensor for the immediate detection of living bacteria. *Biosens. Bioelectron.* **54**, 553–557 (2013).

141. Vasquez, G., Rey, A., Rivera, C., Iregui, C. & Orozco, J. Amperometric biosensor based on a single antibody of dual function for rapid detection of Streptococcus agalactiae. *Biosens. Bioelectron.* **87**, 453–458 (2017).

142. Silley, P. & Forsythe, S. Impedance microbiology-a rapid change for microbiologists. *J. Appl. Bacteriol.* **80**, 233–243 (1996).

143. Lillehoj, P. B., Kaplan, C. W., He, J., Shi, W. & Ho, C.-M. Rapid, Electrical Impedance Detection of Bacterial Pathogens Using Immobilized Antimicrobial Peptides. *J. Lab. Autom.* **19**, 42–49 (2014).

144. Couniot, N., Francis, L. A. & Flandre, D. Resonant dielectrophoresis and electrohydrodynamics for high-sensitivity impedance detection of whole-cell bacteria. *Lab Chip* **15**, 3183–3191 (2015).

145. Guimard, N. K., Gomez, N. & Schmidt, C. E. Conducting polymers in biomedical engineering. *Prog. Polym. Sci* **32**, 876–921 (2007).

146. Löffler, S., Melican, K., Nilsson, K. P. R. & Richter-Dahlfors, A. Organic bioelectronics in medicine. *J. Intern. Med.* **282**, 24–36 (2017).

147. Rivnay, J., Owens, R. M. & Malliaras, G. G. The rise of organic bioelectronics. *Chem. Mater.* **26**, 679–685 (2013).

148. Münstedt, H. Ageing of electrically conducting organic materials. *Polymer (Guildf).* **29**, 296–302 (1988).

149. Heywang, G. & Jonas, F. Poly(alkylenedioxythiophene)s - New, very stable conducting polymers. *Adv. Mater.* **4**, 116–118 (1992).

150. Jonas, F. & Morrison, J. T. 3,4-Polyethylenedioxythiophene (PEDT): Conductive coatings technical applications and properties. *Synth. Met.* **85**, 1397–1398 (1997).

151. Tybrandt, K. Ionic Circuits for Transduction of Electronic Signals into Biological Stimuli. (Linköping University, 2012).

152. Shi, W., Zhao, T., Xi, J., Wang, D. & Shuai, Z. Unravelling Doping Effects on PEDOT at the Molecular Level: From Geometry to Thermoelectric Transport Properties. *J Am Chem Soc* **137**, 12929–12938 (2015).

153. Abalyaeva, V. V & Dremova, N. N. Electrochemical Doping of Polyaniline with the Tetracyanoquinodimethane Anion. *Russ. J. Electrochem.* **52**, 746–753 (2016).

154. Hillman, A. R., Daisley, S. J. & Bruckenstein, S. Kinetics and mechanism of the electrochemical p-doping of PEDOT. *Electrochem. commun.* **9**, 1316–1322 (2007).

155. Gueye, M. N., Carella, A., Faure-Vincent, J., Demadrille, R. & Simonato, J. P. Progress in understanding structure and transport properties of PEDOT-based materials: A critical review. *Prog. Mater. Sci.* **108**, 1–40 (2020).

156. Tsakova, V. & Seeber, R. Conducting polymers in electrochemical sensing: factors influencing the electroanalytical signal. *Anal. Bioanal. Chem.* **408**, 7231–7241 (2016).

157. Skotheim, T. A. & Reynolds, J. R. *Handbook of conducting polymers.* (CRC, 2007).

158. Reyes-Reyes, M., Cruz-Cruz, I. & López-Sandoval, R. Enhancement of the Electrical Conductivity in PEDOT:PSS Films by the Addition of Dimethyl Sulfate. *J Phys Chem C* **114**, 20220–20224 (2010).

159. Wang, T., Qi, Y., Xu, J., Hu, X. & Chen, P. Effects of poly(ethylene glycol) on electrical conductivity of poly(3,4-ethylenedioxythiophene)–poly (styrenesulfonic acid) film. *Appl. Surf. Sci.* **250**, 188–194 (2005).

160. Shi, H., Liu, C., Jiang, Q. & Xu, J. Effective Approaches to Improve the Electrical Conductivity of PEDOT:PSS: A Review. *Adv. Electron. Mater.* **1**, 1–16 (2015).

161. Ouyang, J. *et al.* On the mechanism of conductivity enhancement in poly(3,4-ethylenedioxythiophene):poly(styrene sulfonate) film through solvent treatment. *Polymer (Guildf).* **45**, 8443–8450 (2004).

162. Song, C. *et al.* The effect of solvent treatment on the buried PEDOT:PSS layer. *Org. Electron.* **43**, 9–14 (2017).

163. Saltó, C., Jager, E. W. H., Tengvall, P., Arenas, E. & Berggren, M. Control of Neural Stem Cell Adhesion and Density by an Electronic Polymer Surface Switch. *Langmuir* **24**, 14133–14138 (2008).

164. Marzocchi, M. *et al.* Physical and Electrochemical Properties of PEDOT:PSS as a Tool for Controlling Cell Growth. *ACS Appl Mater Interfaces* **7**, 17993–18003 (2015).

165. Gualandi, I. *et al.* A simple all-PEDOT: PSS electrochemical transistor for ascorbic acid sensing. *J. Mater. Chem. B* **3**, 6753–6762 (2015).

166. Vasantha, V. S. & Chen, S.-M. Electrocatalysis and simultaneous detection of dopamine and ascorbic acid using poly (3, 4-ethylenedioxy) thiophene film modified electrodes. *J. Electroanal. Chem.* **592**, 77–87 (2006).

167. Su, W.-Y. & Cheng, S.-H. Electrocatalysis and sensitive determination of cysteine at poly (3, 4-ethylenedioxythiophene)-modified screen-printed electrodes. *Electrochem. commun.* **10**, 899–902 (2008).

168. Balamurugan, A. & Chen, S.-M. Voltammetric oxidation of NADH at phenyl azo aniline/PEDOT modified electrode. *Sensors Actuators B* **129**, 850–858 (2008).

169. Liao, C. *et al.* Flexible Organic Electronics in Biology: Materials and Devices. *Adv. Mater.* **27**, 7493–7527 (2015).

170. Stavrinidou, E. *et al.* Direct measurement of ion mobility in a conducting polymer. *Adv. Mater.* **25**, 4488–4493 (2013).

171. Lang, U., Naujoks, N. & Dual, J. Mechanical characterization of PEDOT:PSS thin films. *Synth. Met.* **159**, 473–479 (2009).

172. Aygun, A. *et al.* Electrochemically controlled swelling properties of nanoporous templated polypyrrole and layer by layer polypyrrole. *J. Electroanal. Chem.* **684**, 47–52 (2012).

173. Machida, S., Miyata, S. & Techagumpuch, A. Chemical synthesis of highly electrically conductive polypyrrole. *Synth. Met.* **31**, 311–318 (1989).

174. Bargon, J., Mohmand, S. & Waltman, R. J. Electrochemical Synthesis of Electrically Conducting Polymers from Aromatic Compounds. *IBM J. Res. Dev.* **27**, 330–31 (1983).

175. Guo, X. & Facchetti, A. The journey of conducting polymers from discovery to application. *Nat. Mater.* **19**, 922–928 (2020).

176. Ramanavičius, A., Ramanavičien E, A. & Malinauskas, A. Electrochemical sensors based on conducting polymer—polypyrrole. *Electrochim. Acta* **51**, 6025–6037 (2006).

177. Fang, Q., Chetwynd, D. G. & Gardner, J. W. Conducting polymer films by UV-photo processing. *Sensors Actuators A* **99**, 74–77 (2002).

178. Liu, J. *et al.* Thermal Conductivity and Elastic Constants of PEDOT:PSS with High Electrical Conductivity. *Macromolecules* **48**, 585–591 (2015).

179. Xiong, Z. & Liu, C. Optimization of inkjet printed PEDOT:PSS thin films through annealing processes. *Org. Electron.* **13**, 1532–1540 (2012).

180. Park, S., Kang, Y. J. & Majd, S. A Review of Patterned Organic Bioelectronic Materials and their Biomedical Applications. *Adv. Mater.* **27**, 7583–7619 (2015).

181. Aydemir, N., Malmström, J. & Travas-Sejdic, J. Conducting polymer based electrochemical biosensors. *Phys. Chem. Chem. Phys* **18**, 8264–8277 (2016).

182. Nien, P.-C., Tung, T.-S. & Ho, K.-C. Amperometric Glucose Biosensor Based on Entrapment of Glucose Oxidase in a Poly(3,4-ethylenedioxythiophene) Film. *Electroanalysis* **18**, 1408–1415 (2006).

183. Liu, M. *et al.* Electrochemical immobilization of ascorbate oxidase in poly(3,4-ethylenedioxythiophene)/multiwalled carbon nanotubes composite films. *J. Appl. Polym. Sci.* **122**, 1142–1151 (2011).

184. Le, D. Q. *et al.* Development of an observation platform for bacterial activity using polypyrrole films doped with bacteria. *Anal Chem* **87**, 4047–4052 (2015).

185. Löffler, S., Seyock, S., Nybom, R., Jacobson, G. B. & Richter-Dahlfors, A. Electrochemically triggered release of acetylcholine from scCO 2 impregnated conductive polymer films evokes intracellular Ca 2 + signaling in neurotypic SH-SY5Y cells. *J. Control. Release* **243**, 283–290 (2016).

186. Binder, W. H. & Sachsenhofer, R. 'Click' Chemistry in Polymer and Materials Science. *Macromol. Rapid Commun.* **29**, 952–981 (2008).

187. Berezhetska, O., Liberelle, B., De Crescenzo, G. & Cicoira, F. A simple approach for protein covalent grafting on conducting polymer films. *J. Mater. Chem. B* **3**, 5087–5094 (2015).

188. Strakosas, X. *et al.* A facile biofunctionalisation route for solution processable conducting polymer devices. *J. Mater. Chem. B* **2**, 2537–2545 (2014).

189. Hai, W. *et al.* Human influenza virus detection using sialyllactose-functionalized organic electrochemical transistors. *Sensors Actuators, B Chem.* **260**, 635–641 (2018).

190. Leclerc, M. Optical and Electrochemical Transducers Based on Functionalized Conjugated Polymers. *Sensors Updat.* **8**, 21–38 (2000).

191. Wang, B., Queenan, B. N., Wang, S., Nilsson, K. P. R. & Bazan, G. C. Precisely Defined Conjugated Oligoelectrolytes for Biosensing and Therapeutics. *Adv. Mater.* **31**, 1–21 (2019).

192. Phillips, R. L., Miranda, O. R., You, C.-C., Rotello, V. M. & Bunz, U. H. F. Rapid and Efficient Identification of Bacteria Using Gold-Nanoparticle–Poly(para-phenyleneethynylene) Constructs. *Angew. Chemie Int. Ed.* **47**, 2590–2594 (2008).

193. Yan, W. *et al.* Conjugated Polythiophene/Porphyrin Complex for Rapid and Simple Detection of Bacteria in Drinking Water. *Macromol. Chem. Phys.* **216**, 1603–1608 (2015).

194. Yuan, H. *et al.* Cationic Conjugated Polymers for Discrimination of Microbial Pathogens. *Adv. Mater.* **26**, 4333–4338 (2014).

195. Klingstedt, T. Fluorescent thiophene-based ligands for detection and characterization of disease-associated protein aggregates. (Linköping University, 2013).

196. Nilsson, K. P. R. & Inganäs, O. Chip and solution detection of DNA hybridization using a luminescent zwitterionic polythiophene derivative. *Nat. Mater.* **2**, 419–424 (2003).

197. Nilsson, K. P. R. *et al.* Self-assembly of synthetic peptides control conformation and optical properties of a zwitterionic polythiophene derivative. *PNAS* **100**, 10170–10174 (2003).

198. Nilsson, K. P. R., Herland, A., Hammarström, P. & Inganäs, O. Conjugated Polyelectrolytes: Conformation-Sensitive Optical Probes for Detection of Amyloid Fibril Formation. *Biochemistry* **44**, 3718–3724 (2005).

199. Nilsson, K. P. R. *et al.* Conjugated polyelectrolytes - Conformation-sensitive optical probes for staining and characterization of amyloid deposits. *ChemBioChem* **7**, 1096–1104 (2006).

200. Herland, A. *et al.* Synthesis of a Regioregular Zwitterionic Conjugated Oligoelectrolyte, Usable as an Optical Probe for Detection of Amyloid Fibril Formation at Acidic pH. *J. Am. Chem. Soc.* **127**, 2317–2323 (2005).

201. Åslund, A. *et al.* Studies of luminescent conjugated polythiophene derivatives: Enhanced spectral discrimination of protein conformational states. *Bioconjug. Chem.* **18**, 1860–1868 (2007).

202. Nilsson, K. P. R. *et al.* Imaging Distinct Conformational States of Amyloid-Fibrils in Alzheimer's Disease Using Novel Luminescent Probes. *ACS Chem. Biol.* **2**, 553–560 (2007).

203. Åslund, A. *et al.* Novel Pentameric Thiophene Derivatives for in Vitro and in Vivo Optical Imaging of a Plethora of Protein Aggregates in Cerebral Amyloidoses. *ACS Chem. Biol.* **4**, 673–684 (2009).

204. Klingstedt, T. *et al.* Synthesis of a library of oligothiophenes and their utilization as fluorescent ligands for spectral assignment of protein aggregates. *Org. Biomol. Chem.* **9**, 8356–8370 (2011).

205. Klingstedt, T. *et al.* The Structural Basis for Optimal Performance of Oligothiophene-Based Fluorescent Amyloid Ligands: Conformational Flexibility is Essential for Spectral Assignment of a Diversity of Protein Aggregates. *Chem. Eur. J.* **19**, 10179–10192 (2013).

206. Klingstedt, T. *et al.* Distinct Spacing Between Anionic Groups: An Essential Chemical Determinant for Achieving Thiophene-Based Ligands to Distinguish β-Amyloid or Tau Polymorphic Aggregates. *Chem. Eur. J.* **21**, 9072–9082 (2015).

207. Shirani, H. *et al.* A Palette of Fluorescent Thiophene-Based Ligands for the Identification of Protein Aggregates. *Chem. Eur. J.* **21**, 15133 –15137 (2015).

208. Lantz, L., Shirani, H., Klingstedt, T. & Nilsson, K. P. R. Synthesis and Characterization of Thiophene-based Donor–Acceptor–Donor Heptameric Ligands for Spectral Assignment of Polymorphic Amyloid-β Deposits. *Chem. Eur. J.* **26**, 7425–7432 (2020).

209. Choong, F. X. *et al.* Stereochemical identification of glucans by a donor-acceptor-donor conjugated pentamer enables multi-carbohydrate anatomical mapping in plant tissues. *Cellulose* **26**, 4253–4264 (2019).

210. Wahlström, N. *et al.* Cellulose from the green macroalgae Ulva lactuca: isolation, characterization, optotracing, and production of cellulose nanofibrils. *Cellulose* **27**, 3707–3725 (2020).

211. Choong, F. X. *et al.* Nondestructive, real-time determination and visualization of cellulose, hemicellulose and lignin by luminescent oligothiophenes. *Sci. Rep.* **6**, 1–12 (2016).

212. Lakowicz, J. R. *Principles of fluorescence spectroscopy*. (Springer US, 1999).

213. Burroughes, J. H. *et al.* Light-emitting diodes based on conjugated polymers. *Nature* **347**, 539–541 (1990).

214. Bhuvana, K. P., Bensingh, R. J., Abdul Kader, M. & Nayak, & S. K. Polymer Light Emitting Diodes: Materials, Technology and Device. *Polym. Plast. Technol. Eng.* **57**, 1784–1800 (2018).

215. Geffroy, B., le Roy, P. & Prat, C. Organic light-emitting diode (OLED) technology: materials, devices and display technologies. *Polym. Int.* **55**, 572–582 (2006).

216. Kraft, A., Grimsdale, A. C. & Holmes, A. B. Electroluminescent Conjugated Polymers—Seeing Polymers in a New Light. *Angew. Chemie Int. Ed.* **37**, 402–428 (1998).

217. Jaffe, H. H. & Miller, A. L. The fates of electronic excitation energy. *J. Chem. Educ.* **43**, 469–473 (1966).

218. Holliday, S., Li, Y. & Luscombe, C. K. Recent advances in high performance donor-acceptor polymers for organic photovoltaics. *Prog. Polym. Sci.* **70**, 34–51 (2017).

219. Campoccia, D., Montanaro, L. & Arciola, C. R. A review of the biomaterials technologies for infection-resistant surfaces. *Biomaterials* **34**, 8533–8554 (2013).

220. Zarie, E. S. *et al.* Solvent Free Fabrication of Micro and Nanostructured Drug Coatings by Thermal Evaporation for Controlled Release and Increased Effects. *PLoS One* **7**, 1–11 (2012).

221. Qi, R. *et al.* Controlled release and antibacterial activity of antibiotic-loaded electrospun halloysite/poly(lactic-co-glycolic acid) composite nanofibers. *Colloids Surfaces B Biointerfaces* **110**, 148–155 (2013).

222. Wang, B. *et al.* A self-defensive antibacterial coating acting through the bacteria-triggered release of a hydrophobic antibiotic from layer-by-layer films. *J. Mater. Chem. B* **5**, 1498–1506 (2017).

223. Traba, C. & Liang, J. F. Bacteria responsive antibacterial surfaces for indwelling device infections. *J. Control. Release* **198**, 18–25 (2015).

224. Kalia, V. C. Quorum sensing inhibitors: An overview. *Biotechnol. Adv.* **31**, 224–245 (2013).

225. Bahar, A. A. & Ren, D. Antimicrobial peptides. *Pharmaceuticals (Basel).* **6**, 1543–75 (2013).

226. Pál, C., Papp, B. & Lázár, V. Collateral sensitivity of antibiotic-resistant microbes. *Trends Microbiol.* **23**, 401–407 (2015).

227. Zou, F. *et al.* Wrinkled Surface-Mediated Antibacterial Activity of Graphene Oxide Nanosheets. *ACS Appl Mater Interfaces* **9**, 1343–1351 (2017).

228. Bixler, G. D. & Bhushan, B. Rice and Butterfly Wing Effect Inspired Low Drag and Antifouling Surfaces: A Review. *Crit. Rev. Solid State Mater. Sci.* **40**, 1–37 (2015).

229. Nir, S. & Reches, M. Bio-inspired antifouling approaches: the quest towards non-toxic and non-biocidal materials. *Curr. Opin. Biotechnol.* **39**, 48–55 (2016).

230. Sakamoto, A. *et al.* Antibacterial effects of protruding and recessed shark skin micropatterned surfaces of polyacrylate plate with a shallow groove. *FEMS Microbiol. Lett.* **361**, 10–16 (2014).

231. Yang, H. *et al.* Preparation of lotus-leaf-like antibacterial film based on mesoporous silica microcapsule- supported Ag nanoparticles. *RSC Adv.* **4**, 2793–2796 (2014).

232. Watson, G. S. *et al.* A gecko skin micro/nano structure – A low adhesion, superhydrophobic, anti-wetting, self-cleaning, biocompatible, antibacterial surface. *Acta Biomater.* **21**, 109–122 (2015).

233. Zhang, G., Zhang, J., Xie, G., Liu, Z. & Shao, H. Cicada Wings: A Stamp from Nature for Nanoimprint Lithography. *Small* **2**, 1440–1443 (2006).

234. Ji, H., Sun, H. & Qu, X. Antibacterial applications of graphene-based nanomaterials: Recent achievements and challenges ☆. *Adv. Drug Deliv. Rev.* **105**, 176–189 (2016).

235. Hegab, H. M. *et al.* The controversial antibacterial activity of graphene-based materials. *Carbon N. Y.* **105**, 362–376 (2016).

236. Mi, L. & Jiang, S. Integrated Antimicrobial and Nonfouling Zwitterionic Polymers. *Angew. Chemie Int. Ed.* **53**, 1746–1754 (2014).

237. Rzhepishevska, O. *et al.* The surface charge of anti-bacterial coatings alters motility and biofilm architecture. *Biomater. Sci* **1**, 589–602 (2013).

238. Tiller, J. C., Liao, C.-J., Lewis, K. & Klibanov, A. M. Designing surfaces that kill bacteria on contact. *PNAS* **98**, 5981–5985 (2001).

239. Alves, D. & Pereira, M. O. Mini-review: Antimicrobial peptides and enzymes as promising candidates to functionalize biomaterial surfaces. *Biofouling* **30**, 483–499 (2014).

240. Green, J.-B. D., Fulghum, T. & Nordhaus, M. A. Review of immobilized antimicrobial agents and methods for testing. *Biointerphases* **6**, MR13–MR28 (2011).

241. Costa, F. *et al.* Covalent immobilization of antimicrobial peptides (AMPs) onto biomaterial surfaces. *Acta Biomater.* **7**, 1431–1440 (2011).

242. Onaizi, S. A. & Leong, S. S. J. Tethering antimicrobial peptides: Current status and potential challenges. *Biotechnol. Adv.* **29**, 67–74 (2010).

243. Héquet, A., Humblot, V., Berjeaud, J.-M. & Pradier, C.-M. Optimized grafting of antimicrobial peptides on stainless steel surface and biofilm resistance tests. *Colloids Surfaces B Biointerfaces* **84**, 301–309 (2011).

244. Veluchamy, P., Sivakumar, P. M. & Doble, M. Immobilization of Subtilisin on Polycaprolactam for Antimicrobial Food Packaging Applications. *J. Agric. Food Chem* **59**, 10869–10878 (2011).

245. Thallinger, B., Prasetyo, E. N., Nyanhongo, G. S. & Guebitz, G. M. Antimicrobial enzymes: An emerging strategy to fight microbes and microbial biofilms. *Biotechnol. J.* **8**, 97–109 (2013).

246. Kim, M. K. *et al.* Surface-attached molecules control Staphylococcus aureus quorum sensing and biofilm development. *Nat. Microbiol.* **2**, 1–12 (2017).

247. Lemire, J. A., Harrison, J. J. & Turner, R. J. Antimicrobial activity of metals: Mechanisms, molecular targets and applications. *Nat. Rev. Microbiol.* **11**, 371–384 (2013).

248. O'Gorman, J. & Humphreys, H. Application of copper to prevent and control infection. Where are we now? *J. Hosp. Infect.* **81**, 217–223 (2012).

249. Salgado, C. D. *et al.* Copper Surfaces Reduce the Rate of Healthcare-Acquired Infections in the Intensive Care Unit. *Infect. Control Hosp. Epidemiol.* **34**, 479–486 (2013).

250. Michels, H. T., Keevil, C. W., Salgado, C. D. & Schmidt, M. G. From laboratory research to a clinical trial: copper alloy surfaces kill bacteria and reduce hospital-acquired infections. *Heal. Environ. Res. Des. J.* **9**, 64–79 (2015).

251. Colin, M. *et al.* Copper Alloy Touch Surfaces in Healthcare Facilities: An Effective Solution to Prevent Bacterial Spreading. *Materials (Basel).* **11**, 1–12 (2018).

252. Arendsen, L. P., Thakar, R. & Sultan, A. H. The use of copper as an antimicrobial agent in health care, including obstetrics and gynecology. *Clin. Microbiol. Rev.* **32**, 1–28 (2019).

253. Pinkes, M. E., White, C. & Wong, C. S. Native-valve Enterococcus hirae endocarditis: A case report and review of the literature. *BMC Infect. Dis.* **19**, 1–5 (2019).

254. Molteni, C., Abicht, H. K. & Solioz, M. Killing of Bacteria by Copper Surfaces Involves Dissolved Copper. *Appl. Environ. Microbiol.* **76**, 4099–4101 (2010).

255. Santo, C. E., Taudte, N., Nies, D. H. & Grass, G. Contribution of copper ion resistance to survival of Escherichia coli on metallic copper surfaces. *Appl. Environ. Microbiol.* **74**, 977–986 (2008).

256. Warnes, S. L., Caves, V. & Keevil, C. W. Mechanism of copper surface toxicity in Escherichia coli O157:H7 and Salmonella involves immediate membrane depolarization followed by slower rate of DNA destruction which differs from that observed for Gram-positive bacteria. *Environ. Microbiol.* **14**, 1730–1743 (2012).

257. Warnes, S. L. & Keevil, C. W. Mechanism of Copper Surface Toxicity in Vancomycin-Resistant Enterococci following Wet or Dry Surface Contact. *Appl. Environ. Microbiol.* **77**, 6049–6059 (2011).

258. Hans, M. *et al.* Role of Copper Oxides in Contact Killing of Bacteria. *Langmuir* **29**, 16160–16166 (2013).

259. Platzman, I., Brener, R., Haick, H. & Tannenbaum, R. Oxidation of Polycrystalline Copper Thin Films at Ambient Conditions. *J. Phys. Chem. C* **112**, 1101–1108 (2008).

260. Peters, K. *et al.* Copper inhibits peptidoglycan LD-transpeptidases suppressing β-lactam resistance due to bypass of penicillin-binding proteins. *PNAS* **115**, 10786–10791 (2018).

261. Huff, J. The Airyscan detector from ZEISS: confocal imaging with improved signal-to-noise ratio and super-resolution. *Nat. Methods* **12**, i–ii (2015).

262. Rodriguez, M. D., Paul, Z., Wood, C. E., Rice, K. C. & Triplett, E. W. Construction of Stable Fluorescent Reporter Plasmids for Use in Staphylococcus aureus. *Front. Microbiol.* **8**, 1–7 (2017).

263. Krute, C. N. *et al.* Generation of a Stable Plasmid for In Vitro and In Vivo Studies of Staphylococcus Species. *Appl. Environ. Microbiol.* **82**, 6859–6869 (2016).

264. Horsburgh, M. J. *et al.* sigmaB modulates virulence determinant expression and stress resistance: characterization of a functional rsbU strain derived from Staphylococcus aureus 8325-4. *J Bacteriol* **184**, 5457–5467 (2002).

265. Bose, J. L. *The Genetic Manipulation of Staphylococci*. **1373**, (Springer New York, 2016).

266. Fey, P. D. *et al.* A Genetic Resource for Rapid and Comprehensive Phenotype Screening of Nonessential Staphylococcus aureus Genes. *MBio* **4**, 1–8 (2013).

267. Rosenberg, M. Bacterial adherence to hydrocarbons: a useful technique for studying cell surface hydrophobicity. *FEMS Microbiol. Lett.* **22**, 289–295 (1984).

268. Mirceski, V., Skrzypek, S. & Stojanov, L. Square-wave voltammetry. *ChemTexts* **4**, 1–14 (2018).

269. Savitzky, A. & Golay, M. J. E. Smoothing and Differentiation of Data by Simplified Least Squares Procedures. *Anal. Chem.* **36**, 1627–1639 (1964).

270. Virtanen, P. *et al.* SciPy 1.0: fundamental algorithms for scientific computing in Python. *Nat. Methods* **17**, 261–272 (2020).

271. Hunter, J. D. Matplotlib: A 2D Graphics Environment. *Comput. Sci. Eng.* **9**, 90–95 (2007).

272. Nasybulin, E. *et al.* Electrocatalytic properties of poly(3,4-ethylenedioxythiophene) (PEDOT) in Li-O 2 battery. *Electrochem. commun.* **29**, 63–66 (2013).

273. Rodríguez-Calero, G. G., Lowe, M. A., Kiya, Y. & Abruña, H. D. Electrochemical and computational studies on the electrocatalytic effect of conducting polymers toward the redox reactions of thiadiazole-based thiolate compounds. *J. Phys. Chem. C* **114**, 6169–6176 (2010).

274. Rodríguez-Calero, G. G., Lowe, M. A., Burkhardt, S. E. & Abruña, H. D. Electrocatalysis of 2, 5-dimercapto-1, 3, 5-thiadiazole by 3, 4-ethylenedioxy-substituted conducting polymers. *Langmuir* **27**, 13904–13909 (2011).

275. McNaught, A. D. & Wilkinson, A. *IUPAC. Compendium of Chemical Terminology*. (Blackwell Scientific Publications, 1997). doi:10.1351/goldbook.L03540

276. Michalska, A., Gałuszkiewicz, A., Ogonowska, M., Ocypa, M. & Maksymiuk, K. PEDOT films: multifunctional membranes for electrochemical ion sensing. *J. Solid State Electrochem.* **8**, 381–389 (2004).

277. Rivnay, J. *et al.* Organic electrochemical transistors. *Nat. Rev. Mater.* **3**, 1–14 (2018).

278. Smirnova, G. V. & Oktyabrsky, O. N. Glutathione in Bacteria. *Biochem.* **70**, 1199–1211 (2005).

279. García-Angulo, V. A. Overlapping riboflavin supply pathways in bacteria. *Crit. Rev. Microbiol.* **43**, 196–209 (2017).

280. Wos, M. & Pollard, P. Sensitive and meaningful measures of bacterial metabolic activity using NADH fluorescence. *Water Res.* **40**, 2084–2092 (2006).

281. Marsili, E. *et al.* Shewanella secretes flavins that mediate extracellular electron transfer. *PNAS* **105**, 3968–73 (2008).

282. Flores-Mireles, A. L., Walker, J. N., Caparon, M. & Hultgren, S. J. Urinary tract infections: epidemiology, mechanisms of infection and treatment options. *Nat. Rev. Microbiol.* **13**, 269–284 (2015).

283. Qiao, Y. *et al.* Direct electrochemistry and electrocatalytic mechanism of evolved Escherichia coli cells in microbial fuel cells. *RSC ChemComm /*, 1290–1292 (2008).

284. Xiang, K., Qiao, Y., Ching, C. B. & Li, C. M. GldA overexpressing-engineered E. coli as superior electrocatalyst for microbial fuel cells. *Electrochem. commun.* **11**, 1593–1595 (2009).

285. Olukanni, O. D., Osuntoki, A. A., Kalyani, D. C., Gbenle, G. O. & Govindwar, S. P. Decolorization and biodegradation of Reactive Blue 13 by Proteus mirabilis LAG. *J. Hazard. Mater.* **184**, 290–298 (2010).

286. Abdollah, M. R. A. *et al.* Prolonging the circulatory retention of SPIONs using dextran sulfate: in vivo tracking achieved by functionalisation with near-infrared dyes. *Faraday Discuss.* **175**, 41–58 (2014).

287. Moscoso, M., Garcia, P., Cabral, M. P., Rumbo, C. & Bou, G. A D-Alanine auxotrophic live vaccine is effective against lethal infection caused by Staphylococcus aureus. *Virulence* **9**, 604–620 (2018).

288. Said-Salim, B. *et al.* Global Regulation of Staphylococcus aureus Genes by Rot. *J. Bacteriol.* **185**, 610–619 (2003).

289. Hsieh, H.-Y., Wen Tseng, C. & Stewart, G. C. Regulation of Rot Expression in Staphylococcus aureus. *J. Bacteriol.* **190**, 546–554 (2008).

290. Geisinger, E., Adhikari, R. P., Jin, R., Ross, H. F. & Novick, R. P. Inhibition of rot translation by RNAIII, a key feature of agr function. *Mol. Microbiol.* **61**, 1038–1048 (2006).

291. Wanner, S. *et al.* Wall teichoic acids mediate increased virulence in Staphylococcus aureus. *Nat. Microbiol.* **2**, 1–11 (2017).

292. Pensinger, D. A., Schaenzer, A. J. & Sauer, J.-D. Do Shoot the Messenger: PASTA Kinases as Virulence Determinants and Antibiotic Targets Phosphorylation in Bacterial Pathogens. *Trends Microbiol* **26**, 56–69 (2018).

293. Fridman, M. *et al.* Two Unique Phosphorylation-Driven Signaling Pathways Crosstalk in *Staphylococcus aureus* to Modulate the Cell-Wall Charge: Stk1/Stp1 Meets GraSR. *Biochemistry* **52**, 7975–7986 (2013).

294. Liebeke, M., Meyer, H., Donat, S., Ohlsen, K. & Lalk, M. A Metabolomic View of Staphylococcus aureus and Its Ser/Thr Kinase and Phosphatase Deletion Mutants: Involvement in Cell Wall Biosynthesis. *Chem. Biol.* **17**, 820–830 (2010).

295. Tamber, S., Schwartzman, J. & Cheung, A. L. Role of PknB kinase in antibiotic resistance and virulence in community-acquired methicillin-resistant Staphylococcus aureus strain USA300. *Infect. Immun.* **78**, 3637–3646 (2010).

296. Proctor, R. A. *et al.* Small colony variants: A pathogenic form of bacteria that facilitates persistent and recurrent infections. *Nat. Rev. Microbiol.* **4**, 295–305 (2006).

297. The UniProt Consortium. UniProt: a worldwide hub of protein knowledge. *Nucleic Acids Res.* **47**, D506–D515 (2019).

298. Blake, K. L. *et al.* The nature of Staphylococcus aureus MurA and MurZ and approaches for detection of peptidoglycan biosynthesis inhibitors. *Mol. Microbiol.* **72**, 335–343 (2009).

299. Bæk, K. T. *et al.* β-Lactam Resistance in Methicillin-Resistant Staphylococcus aureus USA300 Is Increased by Inactivation of the ClpXP Protease. *Antimicrob. Agents Chemother.* **58**, 4593–4603 (2014).

300. Linke, R. P. Congo Red Staining of Amyloid: Improvements and Practical Guide for a More Precise Diagnosis of Amyloid and the Different Amyloidoses. in *Protein Misfolding, Aggregation, and Conformational Diseases* (eds. Uversky, V. N. & Fink, A. L.) 239–276 (Springer, Boston, MA, 2006).

301. Khurana, R. *et al.* Mechanism of thioflavin T binding to amyloid fibrils. *J. Struct. Biol.* **151**, 229–238 (2005).

302. Löffler, S., Antypas, H., Choong, F. X., Nilsson, K. P. R. & Richter-Dahlfors, A. Conjugated Oligo- and Polymers for Bacterial Sensing. *Front. Chem.* **7**, 1–10 (2019).

303. Sjöqvist, J. *et al.* Toward a Molecular Understanding of the Detection of Amyloid Proteins with Flexible Conjugated Oligothiophenes. *Phys. Chem. A* **118**, 9820−9827 (2014).

304. Asensio, J. L., Ardá, A., Cañada, F. J. & Jiménez-Barbero, J. Carbohydrate-Aromatic Interactions. *Acc. Chem. Res.* **46**, 946–954 (2012).

305. Schwefel, D. *et al.* Structural Basis of Multivalent Binding to Wheat Germ Agglutinin. *J. Am. Chem. Soc.* **132**, 8704–8719 (2010).

306. EN 1811:2011+A1:2015 - Reference test method for release of nickel from all post assemblies which are inserted into pierced parts of the human body and articles intended to come into direct and prolonged contact with the skin. (2015).

307. Baker, L. B. Physiology of sweat gland function: The roles of sweating and sweat composition in human health. *Temperature* **6**, 211–259 (2019).

308. Kochkodan, V., Tsarenko, S., Potapchenko, N., Kosinova, V. & Goncharuk, V. Adhesion of microorganisms to polymer membranes: a photobactericidal effect of surface treatment with TiO2. *Desalination* **220**, 380–385 (2008).

309. Giaouris, E., Chapot-Chartier, M. P. & Briandet, R. Surface physicochemical analysis of natural Lactococcus lactis strains reveals the existence of hydrophobic and low charged strains with altered adhesive properties. *Int. J. Food Microbiol.* **131**, 2–9 (2009).

310. Stiefel, P., Schmidt-Emrich, S., Maniura-Weber, K. & Ren, Q. Critical aspects of using bacterial cell viability assays with the fluorophores SYTO9 and propidium iodide. *BMC Microbiol.* **15**, 1–9 (2015).

311. Stocks, S. M. Mechanism and use of the commercially available viability stain, BacLight. *Cytom. A* **61**, 189–195 (2004).

312. Davey, H. M. Life, death, and in-between: meanings and methods in microbiology. *Appl. Environ. Microbiol.* **77**, 5571–6 (2011).

313. Kirchhoff, C. & Cypionka, H. Propidium ion enters viable cells with high membrane potential during live-dead staining. *J. Microbiol. Methods* **142**, 79–82 (2017).

314. Zeiger, M., Solioz, M., Edongué, H., Arzt, E. & Schneider, A. S. Surface structure influences contact killing of bacteria by copper. *Microbiologyopen* **3**, 327–332 (2014).

315. Mathews, S., Hans, M., Mücklich, F. & Solioz, M. Contact killing of bacteria on copper is suppressed if bacterial-metal contact is prevented and is induced on iron by copper ions. *Appl. Environ. Microbiol.* **79**, 2605–2611 (2013).

316. Mathews, S., Kumar, R. & Solioz, M. Copper Reduction and Contact Killing of Bacteria by Iron Surfaces. *Appl. Environ. Microbiol.* **81**, 6399–403 (2015).

317. Rademacher, C. & Masepohl, B. Copper-responsive gene regulation in bacteria. *Microbiology* **158**, 2451–2464 (2012).

318. Santo, C. E., Morais, P. V. & Grass, G. Isolation and Characterization of Bacteria Resistant to Metallic Copper Surfaces. *Appl. Environ. Microbiol.* **76**, 1341–1348 (2010).

319. Gefen, O., Fridman, O., Ronin, I. & Balaban, N. Q. Direct observation of single stationary-phase bacteria reveals a surprisingly long period of constant protein production activity. *PNAS* **111**, 556–561 (2014).

320. Jaishankar, J. & Srivastava, P. Molecular Basis of Stationary Phase Survival and Applications. *Front. Microbiol.* **8**, 1–12 (2017).

321. Prindle, A. *et al.* Ion channels enable electrical communication in bacterial communities. *Nature* **527**, 59–63 (2015).

322. Humphries, J. *et al.* Species-Independent Attraction to Biofilms through Electrical Signaling. *Cell* **168**, 200–209 (2017).

323. Isaksson, J. *et al.* Electronic control of Ca2+ signalling in neuronal cells using an organic electronic ion pump. *Nat. Mater.* **6**, 673–679 (2007).

324. Ertl, P., Robello, E., Battaglini, F. & Mikkelsen, S. R. Rapid antibiotic susceptibility testing via electrochemical measurement of ferricyanide reduction by Escherichia coli and Clostridium sporogenes. *Anal. Chem.* **72**, 4957–4964 (2000).

325. Mann, T. S. & Mikkelsen, S. R. Antibiotic susceptibility testing at a screen-printed carbon electrode array. *Anal. Chem.* **80**, 843–848 (2008).

326. Besant, J. D., Sargent, E. H. & Kelley, S. O. Rapid electrochemical phenotypic profiling of antibiotic-resistant bacteria. *Lab Chip* **15**, 2799–2807 (2015).

327. Gao, Y., Ryu, J., Liu, L. & Choi, S. A simple, inexpensive, and rapid method to assess antibiotic effectiveness against exoelectrogenic bacteria. *Biosens. Bioelectron.* **168**, 1–8 (2020).

328. Perrotte, M. *et al.* Blood-based redox-signature and their association to the cognitive scores in MCI and Alzheimer's disease patients. *Free Radic. Biol. Med.* **130**, 499–511 (2019).

329. Schrag, M. *et al.* Oxidative stress in blood in Alzheimer's disease and mild cognitive impairment: A meta-analysis. *Neurobiol. Dis.* **59**, 100–110 (2013).

330. Maciejczyk, M., Zalewska, A. & Gerreth, K. Salivary Redox Biomarkers in Selected Neurodegenerative Diseases. *J. Clin. Med.* **9**, 1–27 (2020).

331. Bourgonje, A. R. *et al.* Oxidative Stress and Redox-Modulating Therapeutics in Inflammatory Bowel Disease. *Trends Mol. Med.* **26**, 1034–1046 (2020).

332. Million, M. & Raoult, D. Linking gut redox to human microbiome. *Hum. Microbiome J.* **10**, 27–32 (2018).

333. Reese, A. T. *et al.* Antibiotic-induced changes in the microbiota disrupt redox dynamics in the gut. *Elife* **7**, 1–22 (2018).

334. Huynh, K. & Partch, C. L. Analysis of protein stability and ligand interactions by thermal shift assay. *Curr. Protoc. protein Sci.* **79**, 28.9.1-28.9.14 (2015).

335. Lavigne, J. J. & Anslyn, E. V. Sensing a paradigm shift in the field of molecular recognition: From selective to differential receptors. *Angew. Chemie - Int. Ed.* **40**, 3118–3130 (2001).

336. Wong, S. F. & Khor, S. M. State-of-the-art of differential sensing techniques in analytical sciences. *TrAC - Trends Anal. Chem.* **114**, 108–125 (2019).

337. Johansson, L. B. G. *et al.* An azide functionalized oligothiophene ligand--a versatile tool for multimodal detection of disease associated protein aggregates. *Biosens. Bioelectron.* **63**, 204–211 (2015).